Neutron Oscillations into Hidden Dimensions & Topological Defects of the Quark Condensate

Anja Wachowitz

München 2025

Neutron Oscillations into Hidden Dimensions & Topological Defects of the Quark Condensate

Anja Wachowitz

Dissertation
der Fakultät für Physik
der Ludwig-Maximilians-Universität
München

vorgelegt von
Anja Wachowitz
aus Neuwied

München, den 15. Oktober 2025

Erstgutachter: Prof. Dr. Gia Dvali
Zweitgutachter: PD Dr. Lasha Berezhiani
Tag der mündlichen Prüfung: 1. Dezember 2025

Zusammenfassung

Diese Arbeit besteht aus zwei Teilen:

Der erste Teil untersucht die Oszillationen von Neutronen in verborgene Dimensionen. Da Neutronen und Neutrinos keine erhaltenen Eichladungen tragen, sind sie natürliche Kandidaten um mit verborgenen Sektoren zu interagieren. Insbesondere können sie sich mit Bulk-Fermionen mischen, die in großen Extradimensionen propagieren. Da Bulk-Felder in großen Extradimensionen einen fein gestuften Kaluza-Klein-Turm besitzen, finden sowohl gebundene als auch freie Neutronen mit unterschiedlichen Energieniveaus jeweils einen nächsten Oszillationspartner im Turm. Möglicherweise beobachtbare Effekte sind das Verschwinden von gebundenen Neutronen in Atomkernen sowie ein wiederholendes Resonanzmuster in der Verschwindensamplitude freier Neutronen. Die charakteristische Signatur dieser Resonanzen korrespondieren mit bestimmten Magnetfeldstärken, die mit den Kaluza-Klein-Zuständen korrelieren. Auf diese Weise können Experimente mit freien Neutronen den Kaluza-Klein-Turm scannen und einen Parameterbereich der Theorie testen, der durch das Hierarchyproblem motiviert ist.

Der zweite Teil befasst sich mit topologischen Defekten des Quark-Kondensats der Quantenchromodynamik. Durch die spontane Brechung der chiralen Symmetrie entstehen 2π-Domänenwände der η' und π^0-Mesonen, deren Rand kosmische Strings sind. Im Falle einer starken Epoche im frühen Universum können diese Defekte der Quantenchromodynamik eine wichtige Rolle für Kosmologie gespielt haben. Wird ein verborgenes Axion in die Theorie eingefügt, so werden die axionischen Strings von Windungen in den Phasen des Quark-Kondensats begleitet. Diese gleichzeitigen Windungen können bedeutende astrophysikalische Konsequenzen haben, etwa Veränderungen der Supraleitungs- und Anomalieinfluss-Eigenschaften axionischer Strings.

Abstract

This thesis is split into two parts:

The first part explores the oscillations of neutrons into hidden dimensions. Since neutrons and neutrinos carry no conserved gauge charges, they are natural candidates to interact with hidden sectors. In particular, they can mix with bulk fermions propagating in large extra dimensions. Because bulk fields in large extra dimensions have a finely spaced Kaluza-Klein tower, both bound and free neutrons with different energy levels all find a closest oscillation partner in the tower. Potentially observable effects are the disappearance of bound neutrons in nuclei and a repetitive pattern of resonances in the neutron disappearance amplitude in free neutron experiments. The unique signature of resonances in the neutron disappearance amplitude correspond to magnetic field values which are correlated with the Kaluza-Klein states. In this way, free neutron experiments can perform a scanning of the Kaluza-Klein tower and test a parameter space of the theory motivated by the hierarchy problem.

The second part investigates topological defects of the quark condensate of Quantum Chromodynamics. The spontaneous breaking of the chiral symmetry gives rise to 2π-domain walls bounded by cosmic strings of the η' and the π^0-mesons. In case of a strong epoch in the early universe, these defects of Quantum Chromodynamics can play an important role in cosmology. When including a hidden axion in the theory, the axionic strings are accompanied by windings in the phases of the quark condensate. This simultaneous winding can have important astrophysical consequences, such as changing the superconductivity and anomaly inflow properties of axionic strings.

Publications

This thesis is based on two papers to which I have contributed during my research at the Ludwig-Maximilian-University and the Max Planck Institute for Physics. The authors are listed alphabetically and share first authorship. I have added some new aspects and rephrased many parts for better understanding.
Chapter 2 is based on

[1] G. Dvali, M. Ettengruber, and A. Stuhlfauth, "Kaluza-Klein spectroscopy from neutron oscillations into hidden dimensions", Phys. Rev. D **109**, 055046 (2024), arXiv:2312.13278 [hep-ph].

Chapter 3 is based on

[2] G. Dvali, L. Komisel, and A. Stuhlfauth, "Cosmic strings and domain walls of the QCD quark condensate with and without a hidden axion", (2025), arXiv:2505.03542 [hep-ph], to be published.

The following paper is not included in this thesis because it has been already used in my Master's thesis

[3] G. Dvali, O. Sakhelashvili, and A. Stuhlfauth, "TeV Window to Grand Unification: Higgs's Light Color Triplet Partner", (2024), arXiv:2411.14051 [hep-ph], accepted to be published in Phys. Rev. D.

Several other ongoing projects have not been included in this thesis

[4] A. Alexandre, G. Dvali, and A. Stuhlfauth, in progress,

[5] G. Dvali, L. Komisel, and A. Stuhlfauth, in progress,

[6] M. Bachmaier, G. Dvali, L. Komisel, and A. Stuhlfauth, in progress.

Contents

Chapter 1

Introduction

Since the formulation of the Standard Model of particle physics in the 70s, lots of ideas of how to go beyond have been proposed. The Standard Model has to be extended for many reasons, some of which are the origin of the neutrino mass, quantum gravity, the hierarchy problem, the strong CP puzzle and the nature of dark matter.

The hierarchy problem asks the question why the Higgs boson is so light. If we only look at the Standard Model, it being a renormalizable theory, there is no issue with the Higgs mass. However, we should consider the Standard Model an effective field theory. New physics will become important at some high energy scale. Even if there is a desert and no new physics comes in until the Planck scale, by this scale the quantum effects of gravity will set in. Thus, the physical cutoff of the theory cannot be larger than the Planck scale.

The problem with the Higgs mass is that it is very sensitive to the quantum corrections from a physical cutoff of the theory. Using the quantum gravity scale as the physical cutoff, we would expect the Higgs mass to be of the order of the Planck scale, but, clearly, it is not.

One possible explanation is supersymmetry, which is a symmetry between bosons and fermions: For each fermion in the Standard Model, supersymmetry introduces a new bosonic superpartner and vice versa. This extra symmetry explains the cancellation of the quantum corrections to the Higgs mass. However, no supersymmetric particles have been found at the Large Hadron Collider (LHC).

Another solution is the model of large extra dimensions, also called the ADD model [7, 8], after its creators Arkani-Hamed, Dimopoulos and Dvali. This model loweres the scale of quantum gravity down to 10 TeV. By lowering the cutoff of the Standard Model, the Higgs mass is now sensitive to a much lower scale than the Planck mass.

But how can the ADD model lower the scale of quantum gravity? By introducing a number of extra compact spatial dimensions, the strength of gravity gets diluted in the extra dimensions. The larger the size of these compact dimensions compared to the inverse Planck scale, the smaller the cutoff from quantum gravity. The Standard Model fields are confined to a brane embedded in higher-dimensional spacetime.

As for signatures of the ADD model in experiments, there are only few model-independent constraints. One bound comes from torsion balance experiments, testing Newton's inverse square law at small distances. Another bound stems from the search for producing black holes or gravitons at high-energy colliders.

In the first part of this thesis, we will suggest a new way to look for signatures of the ADD model in low-energy neutron experiments [1]. This project was motivated by the explanation of neutrino mass in the ADD model [9, 10].

The origin of the neutrino mass and its smallness are open question in particle physics. The neutrino could have a Dirac mass and/or a Majorana mass. For a Dirac mass, we have to include a right-handed neutrino to the Standard Model. The Seesaw mechanism, which generates a small Majorana mass, also introduces a right-handed neutrino and requires the Majorana mass of the right-handed neutrino to be much larger than the Dirac mass.

In the ADD model, a small Dirac mass for the neutrino can be naturally incorporated [9, 10]: The right-handed neutrino does not carry any charges of the Standard Model gauge group, i.e., it is a Standard Model singlet. This property allows the right-handed neutrino to travel away from the brane into the extra dimensions. So, the right-handed neutrino can be an extra-dimensional field. A general property of extra-dimensional fields is that their interactions with Standard Model fields are suppressed by the volume of the extra dimensions. Thus, the Dirac mass in the ADD model is naturally small.

With this in mind, we ask the following question: Now that our model has an extra-dimensional fermion, is it possible for other Standard Model fermions, besides the left-handed neutrino, to interact with it? The most promising candidate for interacting with an extra-dimensional fermion, since this fermion is a Standard Model singlet, is the neutron. The neutron also carries no charges of the Standard Model gauge groups. Since it is composed of Standard Model fields, it is confined to the brane.

Under the assumption that the neutron mixes with an extra-dimensional fermion, neutron experiments can put bounds on the mixing and, therefore, on the parameters of the model. Remarkably, we found that, in free neutron experiments, it is possible to perform a scanning of the Kaluza-Klein tower of the extra-dimensional fermion by increasing the magnetic field in the experiment in small steps. For a certain parameter range, this enforces a resonance in the neutron disappearance amplitude. In fact, a recent experiment [11] is already testing this setup in an interesting parameter range.

The second part of this thesis is about topological defects from the phase transition of Quantum Chromodynamics (QCD). When a symmetry is spontaneously broken, a field gets a non-zero vacuum expectation value (VEV). The structure of the vacuum manifold determines if topological defects are produced in the corresponding phase transition.

As an example, if the vacuum has disconnected parts, domain walls interpolate between two regions of space that are in two disconnected vacua. Other examples of topological defects are cosmic strings and magnetic monopoles. Around the cosmic string, the phase of the field with a VEV winds with an integer number.

In our project in chapter 3, we consider topological defects of the QCD quark condensate, i.e., domain walls that are bounded by strings. Around these objects, the phases of the quark condensate, in the form of the η' or π^0 mesons, wind. After they get produced in the QCD phase transition, the string-walls are unstable and can be the source for gravitational waves and electromagnetic radiation. They can play an important role in cosmology of the early universe.

We also investigate their interplay with axionic strings. The axion [12, 13] is a pseudoscalar particle that was introduced to solve the strong CP puzzle, which is the question of why we live in a sector with tiny or zero $\bar{\theta}$. For this solution, first proposed by Peccei and Quinn [14, 15], a new anomalous symmetry is spontaneously broken. The axion being the Nambu-Goldstone boson of the anomalous symmetry, can give rise to axionic cosmic strings in the phase transition.

We have found that when the QCD chiral symmetry is broken, the axionic strings experience additional windings by the phases of the quark condensate. This changes the superconductivity [16] and anomaly inflow [17, 18] properties of axionic strings.

The outline of this thesis is as follows: Chapter 2 is dedicated to the project in large extra dimensions [1]. We first introduce the ADD model, discuss neutrino mass in this framework and then start with neutron oscillations with an extra-dimensional fermion. At the end of the chapter, we discuss several phenomenological constraints from cosmology and collider physics on our setup.

Chapter 3 discusses the project on string-walls of the QCD quark condensate [2]. We start with an overview of chiral symmetry breaking, the strong CP puzzle, and the QCD axion. Then, we discuss the strings and walls of the QCD quark condensate in a coupled system with the axion. Also, the existance of the pure QCD defects follows from there. We emphasize their potentially extraordinary meaning for cosmology of the early universe.

An overall summary is given in chapter 4.

Chapter 2

Kaluza-Klein Spectroscopy from Neutron Oscillations into Hidden Dimensions

In this chapter, we discuss the interactions of a neutron with an extra-dimensional fermion. For this, we use the framework of large extra dimensions, i.e., the ADD model. In the ADD model, the Standard Model fields are confined to a brane that is embedded in a higher-dimensional spacetime.

In this model, the smallness of the neutrino mass has a natural explanation: The right-handed neutrino is a Standard Model singlet and, thus, propagates in the extra dimensions.

The neutron, because it also carries no charges of the Standard Model gauge group, can couple to the same extra-dimensional fermion. This mixing can have very interesting signatures for bound and free neutron experiments. We will show that neutrons oscillating with an extra-dimensional fermion opens up the novel possibility to search for signals of large extra dimensions in low-energy neutron experiments.

2.1 Large Extra Dimensions Framework

The ADD model [7, 8] was put forward by Arkani–Hamed, Dimopoulos and Dvali in 1998 as a solution to the hierarchy problem. To the usual $3+1$ dimensions, the model adds N extra spatial dimensions, also called the "bulk".

The presence of the extra dimensions changes the inverse square law for gravity. Since we know that Newton's law holds up for macroscopic distances, the extra dimensions have to be compact. Then, Newton's law changes only at distances shorter than the radii of the extra dimensions.

Usually, one assumes that the effects of gravity on our Quantum Field Theory become important at the Planck scale $M_P \sim 10^{19}\,\mathrm{GeV}$, or at distances as short as the Planck length, $l_P \sim 10^{-35}\mathrm{cm}$. However, since gravity has been tested only to distances of at least $30\mu\mathrm{m}$ [19–21], it is reasonable to question the assumption that

Newton's law holds up to distances of the order of the Planck scale.

We consider any extra dimension with size much larger than Planck length to be large. However, in our project we are especially interested in the parameter space that is motivated by the hierarchy problem, which favors extra dimensions as large as the current bound of μm size. Thus, the ADD model is also known as the model of large extra dimensions (LED).

In LED, the Standard Model (SM) particles are localized on a 4-dimensional brane embedded in the extra dimensions, see Figure 2.1. From the localization of the Standard Model gauge fields it follows that no particles charged under the Standard Model can freely propagate in the bulk [22].

Gravitons carry no Standard Model charge, which allows them to propagate in the extra dimensions. This construction offers a solution to the hierarchy problem: The ADD model explains the weakness of gravity compared to the other forces by the dilution of the strength of gravity in the extra dimensions. The Planck scale is an effective scale which is related to the actual fundamental scale of Quantum Gravity M_f by the master formula:

$$M_P = M_f \sqrt{M_f^N V_N}, \tag{2.1}$$

where V_N is the volume of the extra dimensions. Assuming compactification on an N-dimensional torus $T^N = S^1 \times \cdots \times S^1$, the volume of the extra dimensions is given by $V_N = (2\pi R_1) \dots (2\pi R_N)$. Notice that the fundamental scale of quantum gravity M_f can be much lower than the Planck scale M_P. Thus, the cutoff from gravity is now at $M_f \ll M_P$.

To solve the hierarchy problem we need M_f to be close to the electroweak scale. Originally, M_f was assumed to be at TeV scale, however, collider bounds have pushed this limit to $M_f \gtrsim 10$TeV [23, 24]. The UV-sensitivity of the Higgs mass is cutoff at the fundamental scale of quantum gravity M_f.

The extra dimensions are compactified on a torus, which means that coordinates y_i, $i = 1, \dots, N$, of the extra dimensions are identified with

$$y_i \sim y_i + 2\pi R_i, \tag{2.2}$$

where R_i are the radii of the extra dimensions. The coordinates of the 4-dimensional brane, x_μ, $\mu = 0, \dots, 3$, are not compact. A picture of one compact dimension is shown in Figure 2.3. Because of this compactification, fields that propagate in the extra dimensions give rise to a tower of massive states in the 4-dimensional effective theory, called the Kaluza-Klein (KK) tower [25, 26]. For one extra dimension, the states in the tower are characterized by an integer k and have masses

$$m_k = \frac{|k|}{R}. \tag{2.3}$$

The KK tower for one extra dimension is shown in Figure 2.2.

Besides the graviton, there can also be other fields propagating in the extra dimensions. The only requirement is that the extra-dimensional field has no SM

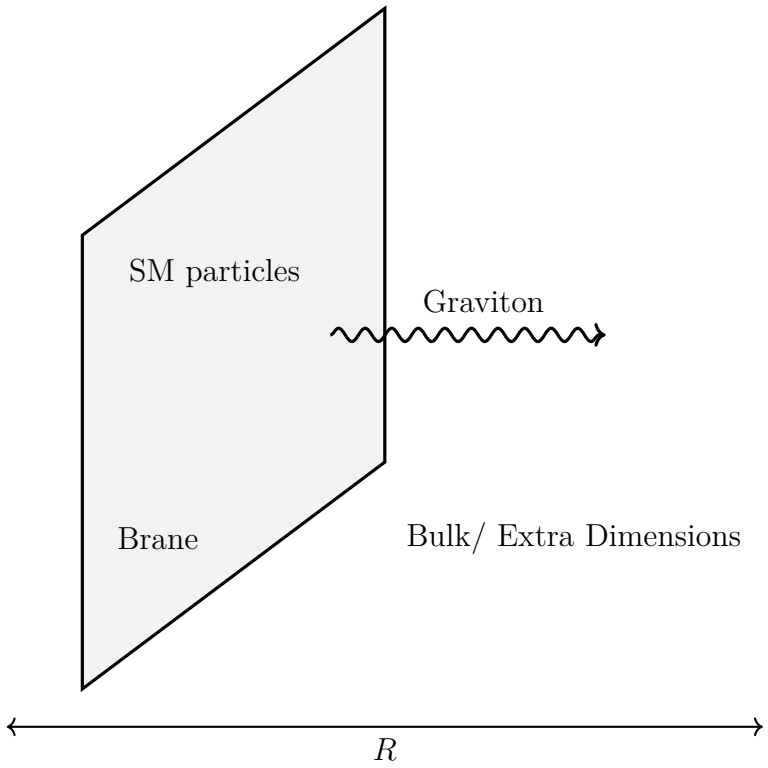

Figure 2.1: Schematic figure of the ADD model. The SM particles are confined to a 4-dimensional brane. Only gravity can propagate in the extra dimensions.

charge. If there are fields of the SM that interact with an extra dimensional field, they can act as a portal into the hidden dimension[1]. Two interesting low-energy candidates of SM fields that can interact with fields in the extra dimensions are the neutrino and the neutron since they are electrically neutral. The interaction between SM fields on the brane and fields propagating in the extra dimensions is suppressed by the volume of the extra dimensions.

For example, the right-handed partner of the Standard Model neutrino can propagate in the extra dimensions. The interaction between the left-handed neutrino and a massless bulk fermion gives a Dirac mass to the neutrino [9, 10, 27]. In this case, the right-handed $k = 0$ mode of the KK tower of the bulk fermion acts as the right-handed neutrino. Since the interaction will be suppressed by the volume of the extra dimensions, the neutrino mass predicted in the ADD model is naturally small.

Another good candidate to interact with a bulk fermion is the neutron. Even though it is composed of SM particles and thus confined to the brane, it has no SM charge and it can couple to an extra-dimensional fermion. In our project, we describe potential signatures in and constraints from low-energy neutron experiments, such as the disappearance of a bound neutron in a nucleus or oscillations of neutrons with the bulk fermion.

[1]In general, because they are SM singlets, the neutrino and the neutron are good candidates to interact with any hidden section and hence probe new physics.

Previously, neutrons in the ADD model were considered to potentially carry away global charges like baryon number from the SM brane [28]. This can happen if quantum fluctuations on the brane can produce "baby branes" which can carry a neutron into the bulk. The production of baby branes is exponentially suppressed in the low-energy theory but can have significance at higher energies, potentially explaining the baryon asymmetry in the universe.

The ADD model can be embedded in string theory [29] and survives constraints from astrophysics and cosmology [8]. For more information on the localization of fermions [30–32], scalars [7] and gauge fields [22] and the stabilization of the radii of the extra dimensions [8] the reader is referred to the literature. Before ADD, the first mention of large extra dimensions in the context of string theory was discussed in [33] and the idea of localizing fields on a domain wall has been discussed in [34]. A historic introduction to the framework of large extra dimensions is given in [35].

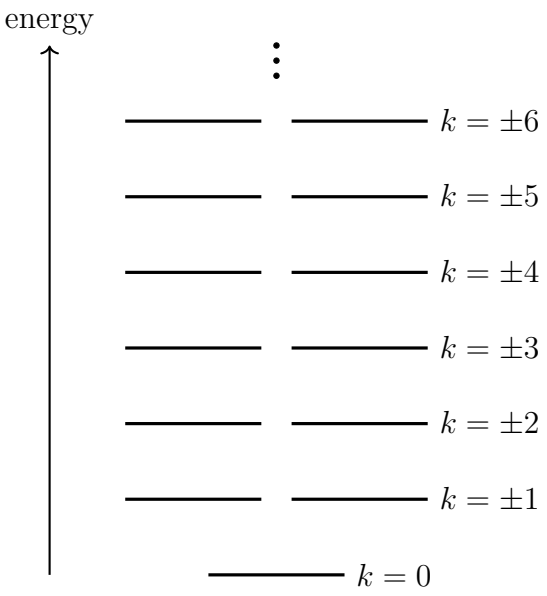

Figure 2.2: Kaluza-Klein tower for one extra dimension. The energy states correspond to $m_k = |k|/R$. The mass splitting is $1/R$.

2.1.1 The Fundamental Scale of Quantum Gravity

In the ADD model, the Planck scale, $M_P = 10^{19}\,\text{GeV}$, is an effective scale that comes from gravity diluting in the extra dimensions. The actual fundamental scale where the gravitational interaction becomes strong is much lower than the Planck scale. This scale is the fundamental scale of quantum gravity which we denote by M_f. It can also be thought of as a higher-dimensional Planck scale.

The master formula relates the Planck scale M_P and the fundamental scale of quantum gravity M_f,

$$M_P = M_f \sqrt{M_f^N V_N}, \tag{2.4}$$

where $V_N = 2\pi R_1 \cdots 2\pi R_N$ is the volume of the extra dimensions. If the factor in the square root is large, $M_f^N V_N \gg 1$, the fundamental scale of quantum gravity is much smaller than the Planck scale, $M_f \ll M_P$. The fundamental scale corresponds to the cutoff of gravity.

To solve the hierarchy problem, we want to lower the fundamental scale to its current experimental bound, $M_f \sim 10\,\text{TeV}$ [23, 24]. Thus, we are particularly interested in models with large extra dimensions, $2\pi R \gg M_f^{-1}$. Each extra dimension that is larger than the inverse fundamental scale contributes to lowering the fundamental scale.

As an example, consider two equal size extra dimensions, $N = 2$ and $R = R_1 = R_2$. The radii of the extra dimensions have to be $R \sim \mu\text{m}$ to lower the Planck scale $M_P \sim 10^{19}\,\text{GeV}$ down to $M_f \sim 10\,\text{TeV}$.

There is also a second interpretation of the master formula (2.4) by the many species formalism [36–38]. In a theory with N_{sp} particle species, the cutoff of gravity is lowered from the Planck scale to the species scale M_f,

$$M_f = \frac{M_P}{\sqrt{N_{\text{sp}}}}. \tag{2.5}$$

Already in the SM, we have $N_{\text{sp}} \sim 100$ so that the cutoff of gravity is lowered by one order of magnitude.

In the ADD model, the graviton has a whole tower of KK states because gravity propagates in the bulk. To relate the species scale with the fundamental scale, we need to know the number of species in the KK tower. In our discussion on the KK tower in section 2.1.2 we explain that the number of states in the tower up to some mass m is given by volume of an N-dimensional sphere with radius mR. So, the number of states up to the cutoff of gravity M_f is proportional to $N_{\text{sp}} = (M_f R)^N \sim M_f^N V_N$. Then the formula for the species scale (2.5) reproduces the master formula (2.4).

In [8], the relationship between the Planck scale and the string scale was discussed. For this, they used the implementation of the ADD model in type I string theory which was first discussed in [29].

In this section, we will first derive the master formula from Newton's law and then explain its phenomenological consequences.

Relating Planck Scales via Newton's Law

The master formula (2.4) can be derived from comparing the gravitational interaction at different length scales. When probing distances shorter than the radii of the extra dimensions, the ADD model predicts a modification of Newton's inverse square law.

In 3 spatial dimensions, the gravitational potential is proportional to $1/r$ and the gravitational strength is given by $1/M_P^2$, so that

$$V(r) \sim \frac{1}{M_P^2}\frac{1}{r}. \tag{2.6}$$

This leads to the famous inverse square law for the gravitational force.

The fundamental scale of quantum gravity sets the strength of gravity at distances smaller than the extra dimensions, where we have to take into account all $4+N$ dimensions. In this way, fundamental scale M_f is interpreted as the $4+N$-dimensional Planck scale. The gravitational potential in $4+N$ dimensions changes to a $1/r^{1+N}$ dependence,

$$V(r) \overset{r\ll R}{\sim} \frac{1}{M_f^{2+N}} \frac{1}{r^{1+N}}. \tag{2.7}$$

This form of the gravitational potential holds at distances r smaller than the radii of all extra dimensions R. At these distances, gravity feels the impact of the compact extra dimensions.

At distances larger than the size of the extra dimensions, $r \gg R$, space is effectively 3-dimensional and the gravitational potential has to be proportional to $1/r$. By dimensional analysis, the $4+N$-dimensional potential changes to

$$V(r) \overset{r\gg R}{\sim} \frac{1}{M_f^{2+N} V_N} \frac{1}{r}, \tag{2.8}$$

where V_N is the volume of the extra dimensions.

Comparing the gravitational potential in 3 spatial dimensions, (2.6), with the effective potential for including the extra dimension, (2.8), we arrive at the master formula (2.4).

The relation between M_P and M_f can also be derived from the KK modes of the graviton. These are 4-dimensional fields, so we know their gravitational potential: Only the massless KK mode has a potential $1/r$ and the others will have a Yukawa-type potential $e^{-m_{\boldsymbol{k}} r}/r$. In the 4-dimensional gravitational potential, we sum over the contributions from each KK mode

$$V(r) \sim \frac{1}{M_P^2} \sum_{\boldsymbol{k}} \frac{e^{-m_{\boldsymbol{k}} r}}{r}, \tag{2.9}$$

where the sum over $\boldsymbol{k} = (k_1, \ldots, k_N)$ stands for the sum over each integer k_i, $i = 1, \ldots, N$. The mass of the KK modes for N extra dimensions is explained later in detail and is given by (2.14).

The contribution of the KK modes with higher masses is exponentially suppressed. Thus, we can approximate the contribution of the modes that satisfy $m_{\boldsymbol{k}} r < 1$ with a $1/r$ potential and neglect all higher-modes in the sum. That means we treat all the lower KK modes equally and we can replace the sum over $\boldsymbol{k}$ with the multiplicity of the modes with $m_{\boldsymbol{k}} r < 1$. For $r \ll R$, the multiplicity of these modes is related to the volume of a sphere with radius R/r. Thus, we replace the sum by a factor $(2\pi R/r)^N$, where we have assumed equal size extra dimensions for simplicity. The gravitational potential at distances smaller than the radii of the extra dimensions, $r \ll R$, is

$$V(r) \sim \frac{(2\pi R)^N}{M_P^2} \frac{1}{r^{1+N}}. \tag{2.10}$$

The first fraction is the coupling of gravity in $4+N$ dimensions . We compare this potential with the $4+N$ potential in (2.7) and again reproduce the master formula (2.4).

Of course, for $r \gg R$, the multiplicity is one, as only the $\boldsymbol{k}=0$ fulfills $m_{\boldsymbol{k}} r < 1$. Thus, we reproduce the usual $1/r$ potential for the 4 dimensional theory from (2.6) for $r \gg R$.

Phenomenological Constraints

There exist several phenomenological bounds on Large Extra Dimensions from colliders, tests of gravity, Cosmology, Astrophysics and more. First, we discuss bounds on the fundamental scale of quantum gravity from the LHC. Second, we explain how experiments of gravity at small distances constrain the size of the extra dimensions. Then we analyze constraints on the radii coming from the ADD model itself. Last but not least we comment on other bounds, for example, Cosmology and Astrophysics.

From the master formula (2.4) follows one very important thing: The fundamental scale of quantum gravity can be much lower than the 4-dimensional Planck scale, so $M_f \ll M_P$. In fact, M_f can be as low as its experimentally allowed value,

$$M_f \gtrsim 10\,\mathrm{TeV}, \tag{2.11}$$

which comes from collider experiments ATLAS [23] and CMS [24].

The Higgs mass is sensitive not to the effective 4-dimensional Planck mass M_P but to the fundamental scale of quantum gravity M_f. Thus, if the fundamental scale of quantum gravity is close to its allowed experimental value, it can serve as a solution to the hierarchy problem. This makes $M_f \sim 10\,\mathrm{TeV}$ a very interesting parameter range of the model of Large Extra Dimensions.

The radii of the extra dimensions are also experimentally bounded. The constraint comes from torsion balance experiments testing Newton's law at small distances. As explained above, if extra dimensions with size R exist, Newton's inverse square law gets modified to $1/r^{2+N}$ at smaller distances $r \ll R$. The current experimental limit from these experiments on the size of the extra dimensions is $R < 30\mu\mathrm{m}$ [19–21].

Assuming that there is one extra dimension which lowers the Planck scale to 10 TeV, the master formula (2.4) for $N=1$ requires the extra dimensional radius to be of order 10^9m. This is of course excluded experimentally because Newton's law holds at these distances. Therefore, we require at least two extra dimensions. Already for $N=2$ the size of the extra dimension is phenomenologically viable: The radius for two equal size extra dimensions required to lower the Planck scale to 10 TeV is of order μm. In Table 2.1 we show the size of the extra dimensions assuming that they all have the same size and lower the Planck scale to 10 TeV.

It is important to notice that the extra dimensions do not have to have the same size. For example, it is perfectly fine to have one extra dimension of size $R_1 = 30\mu\mathrm{m}$ and further extra dimensions which are smaller. Since all phenomenological

constraints are most sensitive to the largest extra dimensions, only the largest ones are relevant. The number of relevant dimensions we call N_R.

In general, in addition to the N_R relevant extra dimensions with radius R, there are $N - N_R$ smaller ones whose radius we call $\tilde{R}$. Since $1/M_f$ is the smallest distance scale in the theory, even the smallest extra dimensions must at least as large as $2\pi\tilde{R} > 1/M_f$. Because the total volume of the extra dimensions can be split into relevant and smaller dimensions, the dimensionless factor in the master formula (2.4) can be rewritten as

$$M_f^N V_N = (2\pi R M_f)^{N_R} (2\pi \tilde{R} M_f)^{N-N_R} > (2\pi R M_f)^{N_R}. \tag{2.12}$$

It is the dimensionless product $2\pi R M_f$ that contributes to lowering the fundamental scale. Since this product is always bigger than 1, the presence of additional smaller dimensions can only further lower the fundamental scale.

From the master formula (2.4) we get an upper bound on the size of the largest dimensions,

$$R \leq \frac{1}{2\pi M_f} \left(\frac{M_P}{M_f}\right)^{\frac{2}{N_R}}. \tag{2.13}$$

This upper bound is saturated when there are no smaller extra dimensions, so $N = N_R$, with order of magnitude estimations for R shown in Table 2.1.

In the scenario with different sizes for the extra dimensions, there will be effective intermediate Planck scales that arise when integrating out only the smallest extra dimensions. For example, if there are two extra dimensions with radii $R_1 \gg R_2$, there will be three regimes where the gravitational potential is proportional to $1/r$, $1/r^2$ and $1/r^3$ for $r > R_1$, $R_1 > r > R_2$ and $r < R_2$ respectively. At $R_1 > r > R_2$, there will be an effective Planck scale M_P' with $M_P' = M_f \sqrt{M_f\, 2\pi R_2}$. This is from integrating out only the smallest extra dimension, R_2.

A long list of phenomenological constraints on the ADD model, including cosmological and astrophysical bounds, have been discussed in [8]. However, many of these constraints are model dependent: the star cooling bound on M_f [8] can be softened if the radii have different sizes [10]. Bounds coming from the diffuse gamma-ray spectrum, i.e. [39], can also be avoided by changing some details of the model [8], for example, compactifying on a different manifold or other branes besides ours in the bulk. We will discuss some cosmological and astrophysical bounds of our scenario, in which a bulk fermion interacts with the neutron, later in section 2.9.

We also want to refer to an incomplete list of references concerning radius stabilization [40], collider signals [41–43] and the production of black holes in colliders [44, 45].

2.1.2 Kaluza-Klein Tower

The Kaluza-Klein (KK) tower is a general feature of models with compact extra dimensions. From a 4-dimensional perspective, fields that live in the extra dimensions

N	R
1	10^9m
2	1μm
3	$10^{-5}\mu$m
4	$10^{-7}\mu$m
5	$10^{-8}\mu$m
6	$10^{-9}\mu$m

Table 2.1: Bound on the size of the extra dimensions R assuming that all extra dimensions have the same size $R_1 = \cdots = R_N$ and $M_f = 10\,\text{TeV}$. The values are only order of magnitude estimates, so the radii can be larger by some order one number.

acquire a tower of KK states with masses

$$m_{\boldsymbol{k}} = \sqrt{\frac{k_1^2}{R_1^2} + \cdots + \frac{k_N^2}{R_N^2}}, \tag{2.14}$$

where $R_1, \ldots, R_N$ are the radii of the N extra dimensions and $k_1, \ldots, k_N$ are integers labeling the KK state. In this section, we derive this KK mass formula for the case of a bulk scalar field. We will discuss the fermion case later.

We use coordinates x_μ, $\mu = 0, 1, 2, 3$, for the 4-dimensional brane and y_i, $i = 1, \ldots, N$, for the extra dimensions. Compact extra dimensions are periodic in the coordinates y_i, Eq. (2.2), as already explained in the introduction. Figure 2.3 shows the compactification of one extra dimension on a circle of radius R.

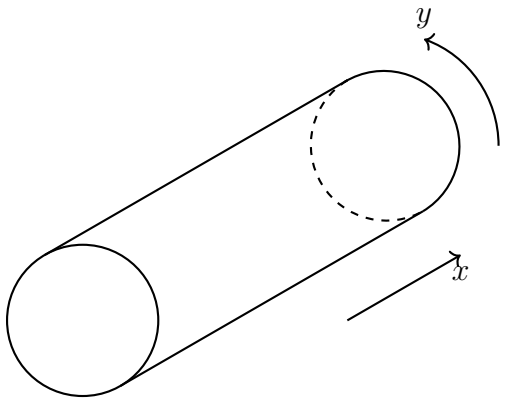

Figure 2.3: The x-direction stands for the 4 non-compact spacetime dimensions. The extra dimension with coordinate y is compactified on a circle with radius R.

Fields that live in compact extra dimensions can be expressed as a Fourier sum because of the periodicity of the extra dimension. A bulk scalar field ϕ can be written as

$$\phi(x, y) = \frac{1}{\sqrt{V_N}} \sum_{\boldsymbol{k}} e^{\mathrm{i}\frac{\boldsymbol{k}\boldsymbol{y}}{R}} \phi_{\boldsymbol{k}}(x). \tag{2.15}$$

All the dependence on the coordinates of the extra dimensions y is in the exponential. The sum over $\boldsymbol{k} = (k_1, \ldots, k_N)$ stands for summing each integer k_i from $-\infty$ to ∞. The index $\boldsymbol{k}$ labels the mode $\phi_{\boldsymbol{k}}$ which is now a 4-dimensional field only depending on x. The $\phi_{\boldsymbol{k}}$-modes are often referred to as KK modes.

For simplicity, in this derivation, we take all radii to be of the same size $R = R_1, \ldots, R_N$. This simplifies the notation, but the same derivation works for different radii as well. The normalization $1/\sqrt{V_N}$ is needed so that the KK modes are canonically normalized. To be more specific, let us consider the action for a massless bulk scalar,

$$S = \int d^4x d^N y \partial_M \phi^\dagger(x,y) \partial^M \phi(x,y), \tag{2.16}$$

where M runs over the usual 4-dimensional Lorentz index μ and the N extra dimensions. Notice that from here we can read off the mass dimension of the scalar field, which is $1 + N/2$.

We split the partial derivatives in the ones over x- and y-coordinates,

$$S = \int d^4x d^N y \Big(\partial_\mu \phi^\dagger(x,y) \partial^\mu \phi(x,y) + \partial_{y_i} \phi^\dagger(x,y) \partial^{y_i} \phi(x,y) \Big). \tag{2.17}$$

Eventually, we want to integrate out the extra dimensions y to get a simple expression for the $\phi_{\boldsymbol{k}}$-modes. In the first step, plugging in the Fourier sum of the scalar bulk field from Eq. (2.15) we find

$$S = \frac{1}{V_N} \int d^4x d^N y \sum_{\boldsymbol{k},\boldsymbol{l}} e^{\mathrm{i}(\boldsymbol{k}-\boldsymbol{l})\boldsymbol{y}/R} \Big(\partial_\mu \phi_{\boldsymbol{l}}^\dagger(x) \partial^\mu \phi_{\boldsymbol{k}}(x) + \frac{\boldsymbol{k}\boldsymbol{l}}{R^2} \phi_{\boldsymbol{l}}^\dagger(x) \phi_{\boldsymbol{k}}(x) \Big). \tag{2.18}$$

We can already see that the left term looks like a kinetic term for the KK modes, while the right term gives the KK modes a mass. The dependence on the extra dimensions is only in the exponential factor. In the following, we use the identity

$$\int d^N y \; e^{\mathrm{i}(\boldsymbol{k}-\boldsymbol{l})\boldsymbol{y}/R} = (2\pi R)^N \delta^{(N)}(\boldsymbol{k} - \boldsymbol{l}). \tag{2.19}$$

The prefactor $(2\pi R)^N$ is exactly the volume of the extra dimensions V_N and cancels the normalization in Eq. (2.15) for the scalar field. Thus, we see that the kinetic terms for the KK modes are canonically normalized.

We can perform the same integral over y for the right term in Eq. (2.18). For the entire 4-dimensional action we find

$$S = \int d^4x \sum_{\boldsymbol{k}} \Big(\partial_\mu \phi_{\boldsymbol{k}}^\dagger(x) \partial^\mu \phi_{\boldsymbol{k}}(x) + \frac{\boldsymbol{k}^2}{R^2} \phi_{\boldsymbol{k}}^\dagger(x) \phi_{\boldsymbol{k}}(x) \Big). \tag{2.20}$$

This action clearly shows the mass term for the KK modes. Also reintroducing different radii for the extra dimensions, the mass of the KK modes is given by Eq. (2.14). For one extra dimension, $N = 1$, we arrive at Eq. (2.3).

This shows that by dimensionally reducing a massless scalar bulk field, we find KK states labeled by $\boldsymbol{k}$ that have masses that depend on the integers $\boldsymbol{k} = (k_1, \ldots, k_N)$.

Here we started with a massless bulk scalar field. The lowest mass state, when $(k_1, \ldots, k_N) = (0, \ldots, 0)$, is also massless in 4 dimensions. Increasing the integers step by step we find a whole tower of massive states.

If we start with a massive bulk scalar field with mass μ, the mass of the KK modes is

$$m_{\boldsymbol{k}} = \sqrt{\mu^2 + \frac{k_1^2}{R_1^2} + \cdots + \frac{k_N^2}{R_N^2}}. \tag{2.21}$$

So, for a massive bulk field the lowest energy KK mode has a mass μ and the tower increases from there in the same way as discussed before.

Mass Splitting in the KK Tower

In this section, we will calculate the mass splitting between two nearest states in the KK tower. For one dominant extra dimension, the mass splitting is $1/R$, while for multiple dominant extra dimensions of the same size it is proportional to $1/R^2$. So, the tower splitting can be much smaller in the case of multiple dominant extra dimensions. This will be important later in the discussion, because this level splitting is directly related to the oscillation probability of the neutron with a KK state of the bulk fermion. Also, for experiments scanning the KK tower, this level splitting determines their optimal magnetic field values.

With "dominant" we mean those extra dimensions which are largest in size. The splitting between nearest tower states is dominated by the largest extra dimensions because the KK mass goes as inverse radius. The smaller extra dimensions have a much larger inverse radius so that their effect on the mass splitting is negligible.

If we have several extra dimensions but only a single dominant one, so $R_1 \gg R_2, \ldots, R_N$, the mass splitting is the same as for only one dimension. For two dominant extra dimensions, $R_1 \approx R_2 \gg R_3, \ldots, R_N$, we can again ignore the smaller extra dimensions and treat this case as two extra dimensions with equal radii. We denote the number of relevant dimensions N_R. Clearly, the number of relevant dimensions cannot be larger than the number of extra dimensions $N_R \leq N$.

For one dominant extra dimension, the masses of the tower states are given by Eq. (2.3). Then the mass splitting in the tower, denoted by δm, is

$$\delta m = m_{k+1} - m_k = \frac{k+1}{R} - \frac{k}{R} = \frac{1}{R}. \tag{2.22}$$

This shows that the level splitting is the same, no matter how far up in the tower we look. The largest radius possible is 30μm, which corresponds to a level splitting in the tower of $\delta m \sim 10^{-2}$eV. This is a lower bound on the tower splitting because for a smaller radius the splitting is even bigger.

However, for at least two dominant dimensions, the mass splitting can be much smaller. This is because there is a tupel of integers $\boldsymbol{k} = (k_1, \ldots, k_{N_R})$ which gives more freedom to choose the levels: We can at the same time increase one integer and lower another integer, for example $(k_1, k_2, k_3, \ldots, k_{N_R}) \to (k_1 + 1, k_2 - 1, k_3 \ldots, k_{N_R})$.

The mass splitting between those two states is smaller than in the one dimensional case in Eq. (2.22).

We can also understand this from a number theory perspective: For equal radii of the extra dimensions, the formula for the KK mass from Eq. (2.14) can be rewritten as

$$k_1^2 + \cdots + k_{N_R}^2 = m_{\boldsymbol{k}}^2 R^2, \tag{2.23}$$

where we set $R_1 = \cdots = R_{N_R} = R$ as we are only interested in multiple dominant dimensions with equal radius R. In this form, Eq. (2.23) shows that the KK mass is determined by a sum of integer squares.

To get some intuition, consider only one extra dimension. Then the left-hand side is just the square of integers, $0, 1, 4, 9, 16, \ldots$. However, for two dimensions, there are a lot more possibilities: $0, 1, 2, 4, 5, 8, 9, 10, \ldots$. This already shows that the energy levels can be much smaller for more than one dimension.

The sum of squares function that shows up in the energy levels in Eq. (2.23) has been studied extensively in number theory. For more than 3 dimensions, all integers can be expressed as the sum of squares. This is a theorem from number theory called Lagrange's four-square theorem [46]. For 3 extra dimensions, almost all integers are hit.

For 4 or more dominant dimensions, we can make use of Lagrange's four-square theorem in the following way: In Eq. (2.23), if the LHS is some integer $x = k_1^2 + \cdots + k_{N_R}^2$, then the next integer $x + 1$ is also hit by some other integers, $x + 1 = k_1'^2 + \cdots + k_{N_R}'^2$. This defines the mass states of two nearest neighbors in the tower and their mass splitting is

$$\delta m = \frac{\sqrt{x+1}}{R} - \frac{\sqrt{x}}{R} \approx \frac{1}{2\sqrt{x}R} = \frac{1}{2m_{\boldsymbol{k}}R^2}, \tag{2.24}$$

where we have assumed that $x \gg 1$ and Taylor expanded the square root.

This means that the splitting changes for different parts of the tower. The higher we are in the tower, the smaller the mass splitting. For the neutron mass, which is around 1 GeV, the splitting is $\delta m \approx 1/(2\text{GeV}R^2)$. For two extra dimensions with $R \sim 30\mu$m this corresponds to a level splitting $\delta m \sim 10^{-13} - 10^{-14}$eV. This is much smaller than for one dominant extra dimension, where we found $\delta m \sim 10^{-2}$eV.

The mass splitting in Eq. (2.24) is also a good approximation for 3 dominant dimensions because the sum of three squares can express almost all integers. For completeness, we also derive the average mass splitting for two dominant dimensions in the appendix. Since the sum of two squares does not reproduce every integer, there will be some gaps in the tower. Still, the average will be of the same order of magnitude as the higher-dimensional case. The derivation shown in the appendix can also be used for the higher-dimensional case and reproduces Eq. (2.24).

Degeneracy of States in the KK Tower

In the KK tower, there are always multiple states with the same energy. The number of states with the same energy level is important as it directly affects the amplitude of

the oscillation probability. If the number of degenerate states is larger, the oscillation probability is higher.

For one dominant extra dimension $N_R = 1$, because the KK mass in Eq. (2.3) is the same for $\pm k$, the degeneracy is $Z = 2$ for each energy level (see also Figure 2.2). This factor stays the same for all energy regimes. However, for multiple extra dimensions with the same size the number of states with the same energy can get large. Moreover, the degeneracy varies across energy levels in the KK tower, meaning different energy states can have different numbers of degenerate states.

In Figure 2.4, we show the degeneracies of the lowest KK modes for two dominant extra dimensions. For $N_R \geq 2$ relevant extra dimensions, the average number of degenerate states Z at some energy state m is given by

$$Z(m) \approx \frac{N_R}{2} v_{N_R} (mR)^{N_R - 2}, \tag{2.25}$$

where v_{N_R} is the volume of an N_R-dimensional unit ball. We will now derive this formula from number theory and then give another, more intuitive explanation.

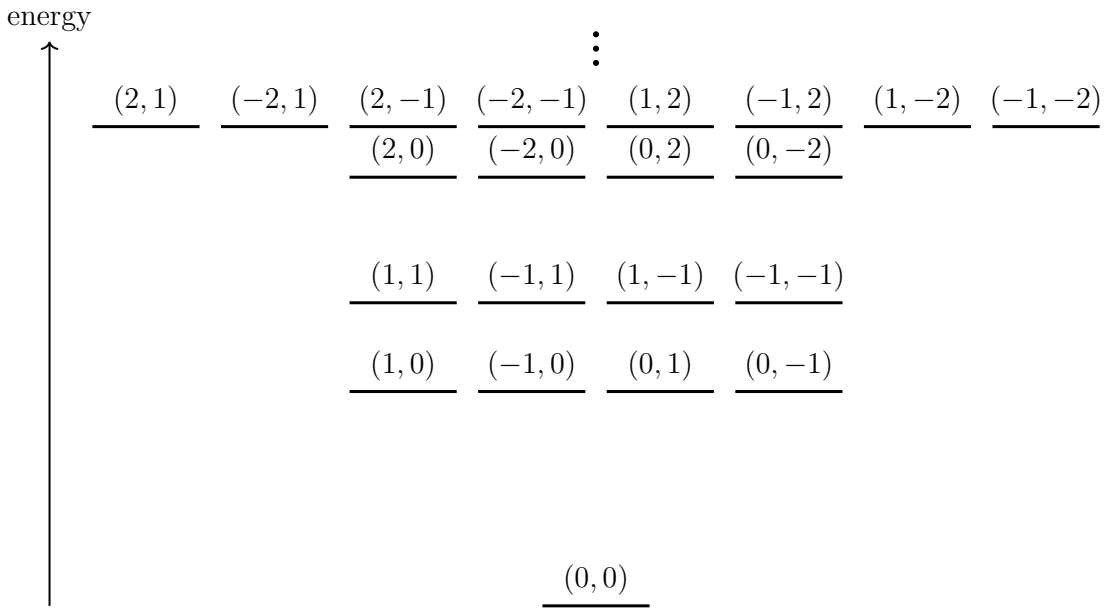

Figure 2.4: Kaluza-Klein tower for two extra dimensions. The energy states are labeled by the tupel (k_1, k_2) and have corresponding mass states $m_{(k_1,k_2)} = \sqrt{k_1^2 + k_2^2}/R$. The mass splitting for $k_1^2 + k_2^2 \gg 1$ is proportional to $1/R^2$.

In number theory, this problem is well known: The number of different integers $k_1, \ldots, k_{N_R}$ that solve $n = k_1^2 + \cdots + k_{N_R}^2$ is called $r_{N_R}(n)$. For our case, we set $n = (m_{\boldsymbol{k}} R)^2$ so that the sum of squares reproduces the KK mass in Eq. (2.14). We can take the sum over n of $r_{N_R}(n)$ up to some integer x, which corresponds to the number of different integers $k_1, \ldots, k_{N_R}$ that solve $k_1^2 + \cdots + k_{N_R}^2 \leq x$. This problem can also be addressed geometrically, as shown in Figure 2.5: Thinking of

the $k_1^2 + \cdots + k_{N_R}^2$ as a lattice of integer combinations which are bounded by an N_R-dimensional sphere with radius $\sqrt{x}$, the number of lattice points is just the volume of the sphere v_{N_R},

$$\sum_{n=0}^{x} r_{N_R}(n) = v_{N_R} x^{\frac{N_R}{2}}. \tag{2.26}$$

If we now want to know the number of states in a small region between two spheres with radii $\sqrt{x}$ and $\sqrt{x-a}$, where a is an integer with $a \ll x$, we can just take the difference of the two sums,

$$\sum_{n=x-a+1}^{x} r_{N_R}(n) = v_{N_R}\left(x^{\frac{N_R}{2}} - (x-a)^{\frac{N_R}{2}}\right) \approx \frac{N_R}{2} v_N x^{\frac{N_R}{2}-1} a. \tag{2.27}$$

This is summing up the number of possible $k_1, \ldots, k_{N_R}$ that solve $x - a < k_1^2 + \cdots + k_{N_R}^2 \leq x$, so the sum over a different states. We get the average number of states in one energy level by dividing with a,

$$Z(x) = \frac{N_R}{2} v_{N_R} x^{\frac{N_R}{2}-1}. \tag{2.28}$$

To arrive at the final result Eq. (2.25), we just have to plug in $x = (mR)^2$.

For the more intuitive way to get to this result, we take the number of states with mass $\leq m$ as a function of m, from Eq. (2.26) this is $v_{N_R}(mR)^{N_R}$, and differentiate this with respect to m. This gives us the number of states in an interval m to $m + \Delta m$,

$$Z(m) = N_R v_{N_R} (mR)^{N_R-1} \Delta m R. \tag{2.29}$$

Now we choose the Δm to be the energy difference between two states, which we calculated in Eq. (2.24), $\Delta m = 1/(2mR^2)$. Plugging this in, we again find Eq. (2.25).

Notice that for two dominant extra dimensions $N_R = 2$, the number of states stays the same for different parts of the tower, it is constant $Z \sim \pi$. But for $N_R \geq 3$, the number of states becomes more when going to higher energies in the tower. For example, if we take $N_R = 3$, $m \sim$ GeV and $R \sim 10^{-5}\mu$m from Table 2.1 and and plug it into Eq. (2.25), we find the average degeneracy of states around the GeV energy level, $Z(\text{GeV}) \sim 10^5$. Therefore, this large degeneracy can significantly enhance the oscillation probability, potentially by several orders of magnitude.

The degeneracy factor divided by the mass splitting in the KK tower, $Z/\delta m$, has a generic formula valid for all number of relevant dimensions. In the previous section we showed that for more than one relevant extra dimension $N_R \geq 2$, the mass splitting is $\delta m \sim 1/(mR^2)$. The degeneracy of the KK states is proportional to $Z \sim (mR)^{N_R-2}$, which leads to

$$\frac{Z}{\delta m} \sim (mR)^{N_R-1} R. \tag{2.30}$$

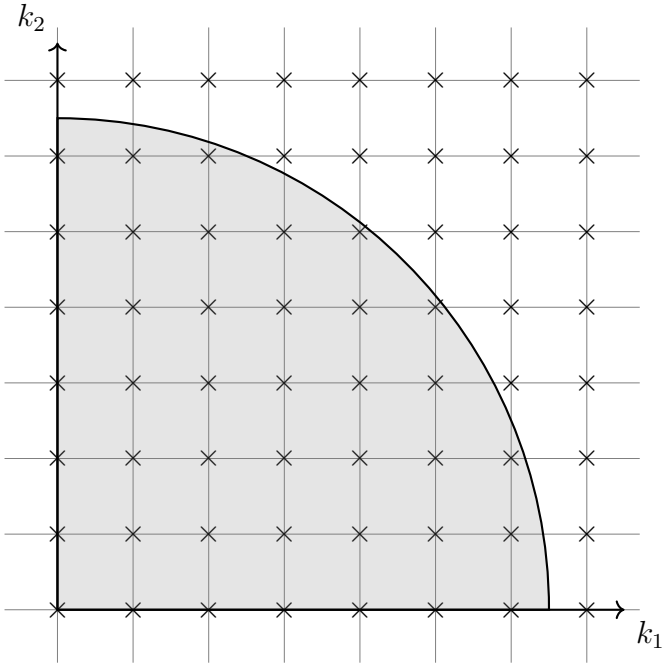

Figure 2.5: Geometric interpretation of the sum of squares function in two dimensions, $N = 2$. Each cross corresponds to one combination of integers k_1, k_2. The arc is a sphere with radius $\sqrt{x}$. The states inside the circle solve $k_1^2 + k_2^2 \leq x$. There is exactly one state per unit square in the (k_1, k_2)-plane. Thus the area inside the circle corresponds to the number of states.

This equation holds also for one dominant extra dimension with $N_R = 1$: The mass splitting for one dominant extra dimension is $\delta m \sim 1/R$ and the degeneracy factor is exactly $Z = 2$, so that $Z/\delta m \sim R$. Hence, the number of states in the region of the tower between m and $m + 1/R$ is proportional to an N_R-dimensional sphere with radius R.

2.2 Neutrino Mass in ADD

2.2.1 Dimensional Reduction of Bulk Fermion Fields

The Poincaré group, which includes translations and Lorentz transformations, is a very important symmetry in particle physics. Relativistic particles are defined as states that "transform under irreducible unitary representations of the Poincaré group" [47]. Particles are classified by their mass and spin (Wigner's theorem) which are defined as eigenvalues of the Casimir operators of the Poincaré algebra[2].

Fermions are particles with spin 1/2 and they transform under the irreducible spinor representation of the Lorentz group. In 4 dimensions, the Lorentz group is

[2]We also label them by their quantum numbers with respect to the internal symmetries of a theory.

$SO(1,3)$. However, when describing fermions that propagate in the extra dimensions we need them to transform under the higher-dimensional spinor representation of the group $SO(1,3+N)$.

In this subsection, we show how to reduce the action for a fermion field that lives in the extra dimensions to the 4-dimensional effective theory. We have already seen dimensional reduction for scalar fields in subsection 2.1.2. Since fermions are in the higher-dimensional spinor representation, the story is more complicated.

Spinor representation of $SO(1,2n-1)$

Let us first do a quick recap of what spinors are, mostly from [48–50]. For more detailed explanations, the reader can check out standard textbooks of Quantum Field Theory, e.g., Schwartz [47], Weinberg [48], Zee [50].

The Lorentz group consists of spatial rotations and boosts. Since in particle physics we have the metric $\eta_{\mu\nu}$, the Lorentz group is $SO(1,3)$. We will now work in $3+N$ spatial dimensions, so $SO(1,3+N)$.

We denote the generators of Lorentz transformation as J_{MN}, with indices $M,N = 0,\dots,3+N$. From now on, we always write the indices for higher dimensions as capital letters. They fulfill the commutation relations

$$\mathrm{i}[J^{MN},J^{PQ}] = \eta^{MP}J^{NQ} + \eta^{NQ}J^{MP} - \eta^{NP}J^{MQ} - \eta^{MQ}J^{NP}, \tag{2.31}$$

which define the Lie algebra of the Lorentz group. These commutation relations have to be fulfilled for every representation of the group.

For the 4-dimensional theory, there is a simple way to define the generators of boosts $K_i = J_{i0}$ and of rotations $J_i = \epsilon_{ijk}J_{jk}$, with $i,j = 1,2,3$. This means that the rotations are a vector of $SO(3)$. For higher dimensions, the boosts are similarly given by J_{i0} but the rotations J_{ij} are not a vector of $SO(N-1)$, with $i,j = 1,\dots,N-1$.

Elements of the Lorentz group are generated by the exponent of the generators J_{MN}, $\Lambda = \exp(\mathrm{i}\omega_{MN}J^{MN})$. A field X_M in the vector representation transforms as

$$X^M \to \Lambda^M{}_N X^N. \tag{2.32}$$

For the construction of the spinor representation of the Lorentz group we need an even number of dimensions, so we consider $SO(1,2n-1)$. It can be shown that there exist $2n$ hermitian matrices γ_i, $i = 1,\dots,2n$ that have dimensionality $2^n \times 2^n$ and satisfy the anticommutation relations

$$\{\gamma^M,\gamma^N\} = 2\eta^{MN}. \tag{2.33}$$

The proof can be found in [48–50][3]. The γ^M are called the gamma matrices or the Dirac matrices. Together with the commutation relation, the Dirac matrices form the Clifford algebra.

[3]For the proof, they use the Euclidean signature δ^{MN} instead of the η^{MN}. Since using the Euclidean signature this changes only some factors of i in the definition of the matrices, it is quite simple to go from $SO(1,N-1)$ to $SO(N)$ and vice versa.

From the Dirac matrices we can define the $2^n \times 2^n$ hermitian matrices

$$S^{MN} = \frac{\mathrm{i}}{4}[\gamma^M, \gamma^N]. \tag{2.34}$$

These matrices are special because they satisfy the commutation relations of the Lorentz algebra (2.31). This follows from using the anti-commutation relations of the Clifford algebra from Eq. (2.33). Hence, the S^{MN} are generators of $SO(1, 2n-1)$ and they define the 2^n-dimensional Dirac representation.

The Lorentz group elements are generated by the exponential of S

$$\Lambda_S = \exp(\mathrm{i}\omega_{MN} S^{MN}), \tag{2.35}$$

where ω is antisymmetric and real. The map $\Lambda \to \Lambda_S$ defines a representation with dimension 2^n. The Λ_S are matrices in spinor space, just like the Dirac matrices.

A Dirac spinor ψ with 2^n components transforms as

$$\psi \to \Lambda_S \psi. \tag{2.36}$$

Using properties of the Dirac matrices, one can show that $\overline{\psi} = \psi^\dagger \gamma^0$ transforms as $\overline{\psi}\Lambda_S^{-1}$ [47]. Thus, $\overline{\psi}\psi$ is Lorentz invariant.

The vector and spinor representation are related [47, 49] which can be seen from

$$\Lambda_S^{-1} \gamma^M \Lambda_S = \Lambda^M{}_N \gamma^N. \tag{2.37}$$

With this one can show that $\overline{\psi}\gamma^\mu\psi$ transforms as a Lorentz vector. Hence, $\overline{\psi}\gamma^\mu\partial_\mu\psi$ and $\overline{\psi}\psi$ is Lorentz invariant.

For this entire discussion, we left out the spinor indices $a, b = 1, \ldots, 2^n$ for simplicity. These are the indices that label the rows and columns of the Dirac matrices $(\gamma^M)_{ab}$ and the components of the Dirac spinor ψ^a.

The 2^n-dimensional spinor representation is reducible [50]. To see this, we define the hermitian matrix

$$\gamma_{\mathrm{FIVE}} \equiv (\mathrm{i})^{n-1} \gamma_1 \cdots \gamma_{2n}. \tag{2.38}$$

This matrix anticommutes with the other Dirac matrices, $\{\gamma_{\mathrm{FIVE}}, \gamma^\mu\} = 0$. With the definition of γ_{FIVE} we can define left- and right-handed fields: First, we define the projection matrices $P_L = \frac{1}{2}(1 - \gamma_{\mathrm{FIVE}})$ and $P_R = \frac{1}{2}(1 + \gamma_{\mathrm{FIVE}})$. Then, the left- and right-handed spinors are $\psi_L = P_L\psi$ and $\psi_R = P_R\psi$.

The left- and right-handed spinors transform separately under the Lorentz group, i.e. $\psi_L \to \Lambda_S\psi_L$ and $\psi_R \to \Lambda_S\psi_R$. Thus, the Dirac ψ spinor is reducible to two Weyl spinors ψ_L and ψ_R. The Weyl spinors are irreducible and have dimensionality 2^{n-1}.

From now on, we label the higher-dimensional Weyl spinors with their γ_{FIVE} eigenvalue, $\psi_\pm$. The left- and right-handed notation is only used for spinors of the 4-dimensional theory.

Notice that γ_{FIVE} is the key to understanding the Clifford algebra in odd dimensions: If we start with the gamma matrices in $SO(1, 2n-1)$, we need to include one more matrix to get a Clifford algebra in $SO(1, 2n)$. This matrix has to anticommute

with all other gamma matrices, so that the Clifford algebra is fulfilled. It also has to be antihermitian. So in $SO(1,2n)$, we can take the $2n$ gamma matrices of $SO(1,2n-1)$ and add $\mathrm{i}\gamma_{\mathrm{FIVE}}$ to form the Clifford algebra. That also means that there is no notion of chirality in odd dimensions. The $\mathrm{i}\gamma_{\mathrm{FIVE}}$ is part of the Clifford algebra and therefore does not split the 2^n dimensional Dirac representation in two 2^{n-1} irreducible spinor representations. Instead the irreducible spinor representation in odd dimensions is 2^n dimensional.

Dimensional reduction

To understand how to relate spinors from different dimensions, we need to understand the construction of gamma matrices for $SO(1,2n-1)$. This can be done iteratively: Knowing the Dirac matrices in $2n$ dimensions, we can construct the $2n+2$ matrices from the lower dimensional matrices [49, 50].

Before we start with the details, let us first understand a simple example: The reduction of a 5-dimensional spinor to 4 dimensions. As explained above, the irreducible spinor in 5 dimensions is the Dirac spinor. If we include only one extra dimension, there is an additional gamma matrix, which is $\mathrm{i}\gamma_{\mathrm{FIVE}}$. Similar to the scalar case, we want to reduce the higher-dimensional action to an effective 4-dimensional one.

The action for a massless spinor in 5 dimensions, where x^μ are the coordinates of our four dimensions and y is the extra-dimensional coordinate, is

$$S = \int d^4x\, dy\, \mathrm{i}\overline{\psi}\gamma^M\partial_M\psi, \tag{2.39}$$

where $M = 0,\ldots,4$ are indices for all 5 dimensions. We can split the 4-dimensional and the extra-dimensional part of the action

$$S = \int d^4x\, dy\, \left(\mathrm{i}\overline{\psi}\gamma^\mu\partial_\mu\psi + \mathrm{i}\overline{\psi}(\mathrm{i}\gamma_{\mathrm{FIVE}})\partial_y\psi\right), \tag{2.40}$$

where the left term already looks like the usual kinetic term in 4 dimensions. To integrate out the compact extra dimension, the higher-dimensional field ψ is expressed as a Fourier sum,

$$\psi(x^\mu, y) = \frac{1}{\sqrt{2\pi R}}\sum_k \psi_k(x) e^{\frac{\mathrm{i}ky}{R}}. \tag{2.41}$$

This is the same procedure as in Eq. (2.15) for the scalar. The first term in the action reduces to the kinetic terms for the 4-dimensional Dirac spinors ψ_k.

Using the Dirac matrices in the Weyl basis is a very convenient choice. We take as the Dirac matrices in 5 dimensions

$$\gamma^\mu = \begin{pmatrix} 0 & \sigma^\mu \\ \overline{\sigma}^\mu & 0 \end{pmatrix}\ ,\ \ \mathrm{i}\gamma_{\mathrm{FIVE}} = \begin{pmatrix} -\mathrm{i} & 0 \\ 0 & \mathrm{i} \end{pmatrix}, \tag{2.42}$$

where $\sigma^\mu \equiv (1,\sigma^i)$, $\overline{\sigma}^\mu \equiv (1,-\sigma^i)$ and σ^i, $i = 1,2,3$, are the three Pauli matrices. In the Weyl basis, the Dirac spinor decomposes into two irreducible Weyl spinors,

$$\psi_k = \begin{pmatrix} \psi_{Lk} \\ \psi_{Rk} \end{pmatrix}. \tag{2.43}$$

We can now rewrite everything in terms of the Weyl spinors,

$$S = \int d^4x \sum_k \mathrm{i}\psi^\dagger_{Rk}\sigma^\mu\partial_\mu\psi_{Rk} + \mathrm{i}\psi^\dagger_{Lk}\overline{\sigma}^\mu\partial_\mu\psi_{Lk} + \frac{\mathrm{i}k}{R}\Big(\psi^\dagger_{Rk}\psi_{Lk} - \psi^\dagger_{Lk}\psi_{Rk}\Big). \tag{2.44}$$

The i in the mass term of the KK modes is just a phase and can be rotated away by a field redefinition. The physical mass of the KK modes is the absolute value, which reproduces the KK mass from Eq. (2.3).

Let us now show how an irreducible spinor from $SO(1,5)$ gets reduced to two Weyl spinors from $SO(1,3)$. The dimensionality of the $SO(1,5)$ spinor is $2^2 = 4$. To perform the dimensional reduction on the level of the action, we first need to know the Dirac matrices for $SO(1,5)$.

In general, we can construct the higher-dimensional Dirac matrices of $SO(2n+2)$ from those of $SO(2n)$ [49]. So, the Dirac matrices of $SO(1,5)$ are constructed from the usual $SO(1,3)$ Dirac matrices. We use the Dirac matrices of $SO(1,3)$ and the chirality matrix γ_{FIVE} in the Weyl basis, so we take our definition of Eq. (2.42).

Then, the Dirac matrices of $SO(1,5)$, which we denote as Γ^M, are constructed from the $SO(1,3)$ matrices

$$\begin{gathered}\Gamma_0 = \begin{pmatrix} & \mathrm{i}\gamma_0 \\ -\mathrm{i}\gamma_0 & \end{pmatrix},\ \Gamma_i = \begin{pmatrix} & \mathrm{i}\gamma_i \\ -\mathrm{i}\gamma_i & \end{pmatrix}, \\ \Gamma_4 = \begin{pmatrix} & -\mathrm{i}\mathbb{1} \\ -\mathrm{i}\mathbb{1} & \end{pmatrix},\ \Gamma_5 = \begin{pmatrix} & \gamma_{\mathrm{FIVE}} \\ -\gamma_{\mathrm{FIVE}} & \end{pmatrix},\ \Gamma_{\mathrm{FIVE}} = \begin{pmatrix} -\mathbb{1} & \\ & \mathbb{1} \end{pmatrix},\end{gathered} \tag{2.45}$$

where we have also written the chirality matrix Γ_{FIVE} of $SO(1,5)$. These matrices solve the Clifford algebra. Here, it is important to choose Γ_0 as the matrix containing the γ_0 matrix so that the structure of $SO(1,5)$ keeps the correct metric in $SO(1,3)$. The factors of i are needed to define Γ_0 as an hermitian matrix and the others as antihermitian. The construction from Eq. (2.45) can also be used for the Dirac matrices of $SO(1,2n+1)$ by replacing the γ^μ matrices with the $SO(1,2n-1)$ analogues.

To single out the irreducible $SO(1,5)$ spinor with eigenvalue + with respect to the chirality matrix Γ_{FIVE}, we can introduce a projector $P_+ = (1+\Gamma_{\mathrm{FIVE}})/2$. The action for the $SO(1,5)$ spinor is the analogue of the Weyl equation,

$$S = \int d^4x d^2y\ \mathrm{i}\overline{\psi}\Gamma^M\partial_M P_+\psi = \int d^4x d^2y\ \mathrm{i}\psi^\dagger_+\mathrm{i}\gamma_0\gamma^M\partial_M\psi_+, \tag{2.46}$$

where $M = 0,\ldots,5$ and $\gamma^M = (\mathrm{i}\gamma_0, \mathrm{i}\gamma_i, -\mathrm{i}\mathbb{1}, \gamma_{\mathrm{FIVE}})$ come from the top-right blocks in the $SO(1,5)$ Dirac matrices. We have already called the coordinates of the two extra dimensions y and they belong to the $M = 4,5$ indices.

We can expand the $\gamma^M\partial_M$ in a 4-dimensional and an extra dimensional part,

$$S = \int d^4x d^2y\ \mathrm{i}\psi^\dagger_+\mathrm{i}\gamma_0\Big(\mathrm{i}\gamma^\mu\partial_\mu - \mathrm{i}\mathbb{1}\partial_4 + \gamma_{\mathrm{FIVE}}\partial_5\Big)\psi_+, \tag{2.47}$$

where the $\mu = 0,\ldots,3$ are the usual 4-dimensional indices.

Now we express ψ_+ in its KK mode expansion, as we did in Eq. (2.41),

$$\psi_+(x,y) = \frac{1}{\sqrt{V_N}} \sum_{k_1,k_2} e^{\mathrm{i}(\frac{k_1 y_1}{R_1} + \frac{k_2 y_2}{R_2})} \psi_{+(k_1,k_2)}(x). \tag{2.48}$$

The partial derivatives ∂_4, ∂_5 are equivalent with derivatives with respect to y_1, y_2.

Now we integrate out the extra dimensions and find

$$\begin{aligned} S &= \int d^4x \sum_{k_1,k_2} \left(\mathrm{i}\overline{\psi}_{+(k_1,k_2)} \gamma^\mu \partial_\mu \psi_{+(k_1,k_2)} + \left(\frac{k_1}{R_1} \mathbb{1} + \mathrm{i} \frac{k_2}{R_2} \gamma_{\mathrm{FIVE}} \right) \overline{\psi}_{+(k_1,k_2)} \psi_{+(k_1,k_2)} \right) \\ &= \int d^4x \sum_{k_1,k_2} \Bigg(\mathrm{i}\psi^\dagger_{+L(k_1,k_2)} \overline{\sigma}^\mu \partial_\mu \psi_{+L(k_1,k_2)} + \mathrm{i}\psi^\dagger_{+R(k_1,k_2)} \sigma^\mu \partial_\mu \psi_{+R(k_1,k_2)} \\ &\qquad + \left(\frac{k_1}{R_1} - \mathrm{i}\frac{k_2}{R_2} \right) \psi^\dagger_{+L(k_1,k_2)} \psi_{-R(k_1,k_2)} + h.c. \Bigg), \end{aligned} \tag{2.49}$$

where we explicitly wrote out the left- and right-handed Weyl spinors of $SO(1,3)$ in the last step. The mass of the KK modes is the absolute value of the bracket, so we get Eq. (2.14).

For more extra dimensions, we want to reduce the spinor from $SO(1,3+N)$ to spinors in $SO(1,3) \times SO(N)$. We assume $N = 2n$ is even such that the dimensionality of the $SO(1,3+N)$ spinor is 2^{n+1}. The $SO(1,3+N)$ spinor is decomposed into 2^{n-1} left-handed and 2^{n-1} right-handed $SO(1,3)$ spinors [49, 50],

$$2^{n+1}_+ \to 2_R \cdot 2^{n-1}_+ + 2_L \cdot 2^{n-1}_- \tag{2.50}$$

$$2^{n+1}_- \to 2_R \cdot 2^{n-1}_- + 2_L \cdot 2^{n-1}_+. \tag{2.51}$$

Here, we label the irreducible $SO(1,3)$ spinors explicitly with L and R. The $SO(1,3+N)$ spinors have same parts left- and right-handed fields in $SO(1,3)$. The chirality of the $SO(1,3+N)$ spinor $\pm$ is determined by the eigenvalue of γ_{FIVE} of $SO(1,3+N)$. This sign of the $SO(1,3+N)$ spinor determines the chirality with respect to the γ_{FIVE} of $SO(N)$.

A bulk fermion ψ is a field in the spinor representation of $SO(1,3+N)$. It decomposes into

$$\psi = \sum_A \psi^{(A)}_L + \sum_{\overline{A}} \psi^{(\overline{A})}_R \tag{2.52}$$

where the $A, \overline{A}$ label a basis of spinors of $SO(N)$. The A and $\overline{A}$ spinors have opposite chirality $\pm$. Which one has which is determined by the chirality of the original $4+N$-dimensional spinor.

The mass matrix of the $\psi^{(A)}_L$ and $\psi^{(\overline{A})}_R$ is $2^{n-1} \times 2^{n-1}$-dimensional. After diagonalization, we find the usual mass of the KK modes (2.14) and 2^{n-1} massive Dirac fermions.

2.2.2 Neutrino Mass in ADD

Large extra dimensions offer a natural way to explain the smallness of neutrino masses [9, 10, 27]. The right-handed or sterile neutrino is a perfect candidate for an extra-dimensional fermion. Since it carries no SM charge, i.e., it is a singlet under the SM gauge group, it is not confined on the brane and can propagate in the bulk. If there is a bulk sterile neutrino the Dirac mass of the neutrino is suppressed by the volume factor of the extra dimensions. This suppression is the reason why the neutrino is naturally small in the ADD model, which predicts neutrino masses of around $m_\nu \sim 10^{-4}$eV. Although the current experimental value for the heaviest neutrino is a couple of orders of magnitude bigger, the neutrino mass is an example of how to generate small quantities with large extra dimensions.

Yukawa Interaction Active Neutrino and Bulk Fermion

We follow the derivation in [10]. First, we introduce a new bulk fermion, ψ which ends up playing the role of a sterile neutrino. This bulk fermion is massless, so its action is given by Eq. (2.39). The bulk fermion interacts with the neutrino in a Yukawa type interaction

$$S = \int d^4x \frac{1}{M_*^{N/2}} \overline{L}(x) H(x) \psi(x, y = 0), \tag{2.53}$$

where $L = (e_L, \nu_L)^T$ is the SM Lepton doublet and H is the SM Higgs doublet. This operator breaks $4 + N$ dimensional Poincare invariance. This is expected, since the brane already breaks the higher-dimensional Poincare symmetry. We choose the brane to be at $y = 0$, so for the local interaction the sterile neutrino has to be at $y = 0$ to interact with the SM particles. Notice that lepton number is conserved if we assign the bulk fermion the same lepton number as the lepton doublet.

Together, the lepton and Higgs doublets are $SU(2)$ invariant. The mass scale $M_*^{N/2}$ is needed from dimensional analysis: The mass dimension of the bulk fermion is $(3+N)/2$, such that the operator has mass dimension $4+N/2$. Since the origin of the effective operator is unknown, we keep the mass scale M_* as a parameter. However, since it describes an interaction between brane and bulk fields it is reasonable to assume that $M_* \gtrsim M_f$.

For the case with one extra dimension, we plug in ψ with its KK decomposition from (2.41) and the vacuum expectation value of the Higgs into (2.53). This gives the following interaction of the active neutrino with the KK modes of its bulk partner

$$\mathcal{L} = \alpha_\nu \overline{\nu}_L \sum_k \psi_{kR}. \tag{2.54}$$

Notice that only the right-handed components of the bulk fermion interact with the active neutrino. In the effective coupling α_ν between the active neutrino and the right-handed component of the bulk fermion we combined all factors from the Higgs

vev and volume suppression,

$$\alpha_\nu \equiv \frac{\langle H \rangle}{\sqrt{M_* \, 2\pi R}}. \tag{2.55}$$

For more than one extra dimension, the active neutrino couples to a superposition of spinors

$$\nu_{\boldsymbol{k}R} \equiv \sum_{\bar{A}} c_{\bar{A}} \Psi^{(\bar{A})}_{\boldsymbol{k},R}(x) \tag{2.56}$$

The interaction (2.54) now sums over all $\boldsymbol{k} = (k_1, \ldots, k_N)$. The coupling of the effective interaction is modified to

$$\alpha_\nu \equiv \frac{\langle H \rangle}{\sqrt{M_*^N V_N}} = \frac{\langle H \rangle M_f}{M_P} \left(\frac{M_f}{M_*} \right)^{\frac{N}{2}}, \tag{2.57}$$

where we used the master formula (2.4) in the last step. For $M_* \sim M_f \sim 10\,\text{TeV}$ and $\langle H \rangle \sim 10^2\text{GeV}$, we estimate $\alpha_\nu \sim 10^{-4}\text{eV}$. In general, $M_* \geq M_f$ so that $\alpha_\nu \leq 10^{-4}\text{eV}$ if we assume that M_f is as low as 10 TeV. For higher M_f, the coupling α_ν could be bigger.

The mass for the neutrino comes mostly from the mixing with the 0-mode in the KK tower. To see this, we need to write down the mass matrix and diagonalize it. Majorana mass terms are forbidden by lepton number conservation The active neutrino has no mass term, but only the interaction (2.54). The KK modes of the bulk fermion have masses, as explained in 2.2.1. All together, the Lagrangian includes mixing terms and mass terms

$$\mathcal{L} = \alpha_\nu \overline{\nu}_L \sum_{k=-\infty}^{\infty} \psi_{kR} + \sum_{k=-\infty}^{\infty} \frac{\mathrm{i}k}{R} \overline{\psi}_{kL} \psi_{kR} + \text{h.c.}. \tag{2.58}$$

Because the KK modes with $\pm k$ have the same physical mass and interaction with the active neutrino, we can write out the negative k's explicitly,

$$\mathcal{L} = \alpha_\nu \overline{\nu}_L \psi_{0R} + \alpha_\nu \overline{\nu}_L \sum_{k=1}^{\infty} \Big(\psi_{kR} + \psi_{-kR} \Big) + \sum_{k=1}^{\infty} \frac{\mathrm{i}k}{R} \Big(\overline{\psi}_{kL} \psi_{kR} - \overline{\psi}_{-kL} \psi_{-kR} \Big) + \text{h.c.}. \tag{2.59}$$

The active neutrino couples in the same way to the positive and negative k states. Because they also have the same mass we can simplify this Lagrangian by redefining the fields such that the active neutrino couples only to one field $\tilde{\psi}$,

$$\begin{aligned}
\tilde{\psi}_{kR} &= \frac{1}{\sqrt{2}} \Big(\psi_{kR} + \psi_{-kR} \Big), \\
\psi'_{kR} &= \frac{1}{\sqrt{2}} \Big(\psi_{kR} - \psi_{-kR} \Big), \\
\tilde{\psi}_{kL} &= \frac{\mathrm{i}}{\sqrt{2}} \Big(\psi_{kL} - \psi_{-kL} \Big), \\
\psi'_{kL} &= \frac{\mathrm{i}}{\sqrt{2}} \Big(\psi_{kL} + \psi_{-kL} \Big).
\end{aligned} \tag{2.60}$$

The second line defines the combination with is orthogonal to $\tilde{\psi}_{kR}$, ψ'_{kR}. The third and fourth line defines the same combinations for the left-handed fields. The imaginary number makes the mass term real. This field redefinition changes the Lagrangian into

$$\mathcal{L} = \alpha_\nu \overline{\nu}_L \psi_{0R} + \sqrt{2}\alpha_\nu \overline{\nu}_L \sum_{k=1}^{\infty} \tilde{\psi}_{kR} + \sum_{k=1}^{\infty} \frac{k}{R}\left(\overline{\tilde{\psi}}_{kL}\tilde{\psi}_{kR} + \overline{\psi}'_{kL}\psi'_{kR}\right) + \text{h.c.}, \tag{2.61}$$

where we can now see that the primed states decouple from any interaction with the active neutrino. This makes sense because of the two degenerate KK modes $\pm k$, the active neutrino only couples to the right-handed component. Effectively, this cuts the number of states that interact with the active neutrino in half. This also reduces the size of the mass matrix for which we only focus on the tilde states,

$$\mathcal{L} = \begin{pmatrix} \overline{\nu}_L & \overline{\tilde{\psi}}_{1L} & \overline{\tilde{\psi}}_{2L} & \dots & \overline{\tilde{\psi}}_{kL} \end{pmatrix} \begin{pmatrix} \alpha_\nu & \sqrt{2}\alpha_\nu & \sqrt{2}\alpha_\nu & \dots & \sqrt{2}\alpha_\nu \\ 0 & \frac{1}{R} & 0 & \dots & 0 \\ 0 & 0 & \frac{2}{R} & \dots & 0 \\ \dots & \dots & \dots & \dots & \dots \\ 0 & 0 & 0 & \dots & \frac{k}{R} \end{pmatrix} \begin{pmatrix} \psi_{0R} \\ \tilde{\psi}_{1R} \\ \tilde{\psi}_{2R} \\ \dots \\ \tilde{\psi}_{kR} \end{pmatrix} + \text{h.c.} \tag{2.62}$$

We call this mass matrix M.

Mass Eigenstates

We want to diagonalize the mass matrix to find the mass eigenstates. The matrix is not symmetric because the active neutrino mixes with all KK modes, while its partner, the 0-mode ψ_{0k} is massless and interacts only with the neutrino. However, we can instead diagonalize the symmetric matrices $MM^\dagger$ or $M^\dagger M$ by rotating the left- and right-handed fields independently. For the diagonalization, we choose to consider $MM^\dagger$,

$$MM^\dagger = \begin{pmatrix} (1+2k)\alpha_\nu^2 & \sqrt{2}\alpha_\nu \frac{1}{R} & \sqrt{2}\alpha_\nu \frac{2}{R} & \dots & \sqrt{2}\alpha_\nu \frac{k}{R} \\ \sqrt{2}\alpha_\nu \frac{1}{R} & \frac{1}{R^2} & 0 & \dots & 0 \\ \sqrt{2}\alpha_\nu \frac{2}{R} & 0 & \frac{4}{R^2} & \dots & 0 \\ \dots & \dots & \dots & \dots & \dots \\ \sqrt{2}\alpha_\nu \frac{k}{R} & 0 & 0 & \dots & \frac{k^2}{R^2} \end{pmatrix}. \tag{2.63}$$

This matrix is symmetric and is diagonalized by a rotation of the left-handed fields only. To simplify the notation we define a new parameter $\epsilon \equiv \sqrt{2}\alpha_\nu R$. Then $MM^\dagger$ becomes

$$MM^\dagger = \frac{1}{R^2} \begin{pmatrix} (\frac{1}{2}+k)\epsilon^2 & \epsilon & 2\epsilon & \dots & k\epsilon \\ \epsilon & 1 & 0 & \dots & 0 \\ 2\epsilon & 0 & 4 & \dots & 0 \\ \dots & \dots & \dots & \dots & \dots \\ k\epsilon & 0 & 0 & \dots & k^2 \end{pmatrix} \tag{2.64}$$

For the diagonalization we use the approximation $\epsilon \ll 1$ and expand in ϵ. We can do this because $\alpha R \sim 10^{-4}\text{eV}10^2/\text{eV} \ll 1$.

We diagonalize each 2×2 submatrix one by one, which we can write generally as a rotation between the 0-component and the k-component. The rotation angle is

$$\tan 2\theta_k = \frac{2k\epsilon}{k^2 - (1/2 + k)\epsilon^2} \approx 2\frac{\epsilon}{k}, \tag{2.65}$$

such that for small ϵ, $\cos\theta_k \approx 1$ and $\sin\theta_k \approx \epsilon/k$. The mixing angle $\theta_k \approx \epsilon/k$ is smaller for larger k. This means that the states with low k, which have the smallest mass splitting to the neutrino state, have the largest mixing angle with the active neutrino.

To find the rotation matrix S that diagonalizes $MM^\dagger$, such that $D = S^T \cdot MM^\dagger \cdot S$ is diagonal, we multiply all rotation matrices together and get

$$S = \begin{pmatrix} 1 & \epsilon & \frac{\epsilon}{2} & \dots & \frac{\epsilon}{k} \\ -\epsilon & 1 & 0 & \dots & 0 \\ -\frac{\epsilon}{2} & 0 & 1 & \dots & 0 \\ \dots & \dots & \dots & \dots & \dots \\ -\frac{\epsilon}{k} & 0 & 0 & \dots & 1 \end{pmatrix}. \tag{2.66}$$

This method of diagonalizing each 2×2 submatrix at a time works only in the limit of small $\epsilon \ll 1$. The diagonal matrix D will have off-diagonal terms of order $\mathcal{O}(\epsilon^3)$, which we neglect. After the diagonalization, the diagonal element belonging to the active neutrino determines its mass squared,

$$m_\nu^2 \sim \frac{1}{2R^2}\epsilon^2 = \alpha_\nu^2. \tag{2.67}$$

We can now check if our expansion in ϵ is reasonable by plugging in numbers. Taking the neutrino mass $m_\nu \sim 10^{-2}$eV and the radius of the extra dimension $R < 30\mu\text{m} = 150\frac{1}{\text{eV}}$, then ϵ is approximately 1. The approximation is therefore good if the radius of the extra dimensions is smaller than the current experimental bound.

Oscillation Probability into Higher KK Modes

Another consequence of this setup, apart from the neutrino getting a mass, is that the neutrino can oscillate into higher states in the KK tower [28]. Since the mass splitting with the lowest states is the smallest, these oscillations will be the dominant effect.

From the rotation matrix, we can write down the mass eigenstate of the neutrino, denoted with a prime,

$$\nu' = \frac{1}{\mathcal{N}}\left(\nu + \sum_k \frac{\epsilon}{k}\psi_k\right), \tag{2.68}$$

where $\mathcal{N}$ is a normalization factor. It is given by $\mathcal{N} = 1 + \sum_k \epsilon^2/k^2 \approx 1$.

The time evolution is described in quantum mechanics by the operator $\exp(-\text{i}Ht)$, where H is the Hamiltonian which we can replace with its eigenvalue, the energy

of the state. The neutrino is a relativistic particle, such that its energy can be approximated by $E_\nu = \sqrt{m_\nu^2 + p^2} \approx p + m_\nu^2/(2p)$. The time evolution for the lowest KK modes is described in the same way, with $E_k = \sqrt{m_k^2 + p^2} \approx p + m_k^2/(2p)$. The mass eigenstate of the neutrino evolves in time as

$$\nu'(t) = \frac{1}{\mathcal{N}} \left(\nu + \sum_k \frac{\epsilon}{k} e^{\mathrm{i}\phi_k} \psi_k \right), \tag{2.69}$$

where $\phi_k = (E_\nu - E_k)t \approx (m_\nu^2 - m_k^2)/(2E)\, t$. Here, we pulled out an overall phase $\exp(-\mathrm{i}E_\nu t)$ which does not change the quantum mechanical state. For starting with one initial neutrino, the survival probability is defined as

$$P_{\mathrm{surv}}(t) \equiv |\, \langle \nu' \,|\, \nu'(t) \rangle \,|^2 = \frac{1}{\mathcal{N}^4} \left| 1 + \sum_k \frac{\epsilon^2}{k^2} e^{\mathrm{i}\phi_k} \right|^2 . \tag{2.70}$$

Working this out and using the identity $2\cos(x) = e^{\mathrm{i}x} + e^{-\mathrm{i}x}$, the survival probability is

$$P_{\mathrm{surv}}(t) = \frac{1}{\mathcal{N}^4} \left(1 + 2 \sum_k \frac{\epsilon^2}{k^2} \cos(\phi_k) + \mathcal{O}(\epsilon^4) \right). \tag{2.71}$$

We can also rewrite it using $2\sin^2(x) = 1 - \cos(2x)$ and we find

$$P_{\mathrm{surv}}(t) = \frac{1}{\mathcal{N}^4} \left(1 + 2 \sum_k \frac{\epsilon^2}{k^2} \left(1 - 2\sin^2\left(\frac{\phi_k}{2}\right) \right) + \mathcal{O}(\epsilon^4) \right) \tag{2.72}$$

Since the amplitude in front of the $\sin^2$ term is suppressed for higher k-modes, we can average over the those modes. To single out the oscillation into ψ_1, we average over all modes with $k \geq 2$,

$$P_{\mathrm{surv}}(t) = \frac{1}{\mathcal{N}^4} \left(1 + 2\epsilon^2 - 4\epsilon^2 \sin^2\left(\frac{\phi_1}{2}\right) + \mathcal{O}(\epsilon^4) \right) \tag{2.73}$$

The term with the $\sin^2(\phi_1/2)$ is the probability of a neutrino oscillating into ψ_1. This disappearance probability into a a KK mode we can also get from the mass eigenstate of the ψ_k,

$$\psi_k' = \psi_k - \frac{\epsilon}{k} \nu. \tag{2.74}$$

This state has time evolution

$$\psi_k'(t) = \psi_k - \frac{\epsilon}{k} e^{-\mathrm{i}\phi_k} \nu, \tag{2.75}$$

so that the disappearance probability $\nu \to \psi_k$ is given by

$$P_{\mathrm{osc}} \equiv |\, \langle \nu' \,|\, \psi_k'(t) \rangle \,|^2 = \frac{\epsilon^2}{k^2} \left| 1 - e^{-\mathrm{i}\phi_k} \right|^2 = 2\frac{\epsilon^2}{k^2}(1 - \cos(\phi_k)) = \frac{4\epsilon^2}{k^2} \sin^2(\phi_k/2) \tag{2.76}$$

Finally, let us comment on the case with more than one extra dimensions. In this case, the mass of the KK modes is given by Eq. (2.14) and the mass matrix from

Eq. (2.63) includes all KK masses. However, since there is still exactly one 0-mode, the neutrino mass is unchanged. The oscillations of neutrinos into higher KK modes is dominated by the smallest masses in the KK tower, such that only the largest dimensions are relevant.

The oscillation of active neutrinos into higher KK modes and the implications for solar neutrinos was first discussed in [10]. More recent papers discussing constraints from neutrino experiments are [51, 52].

2.3 Neutron Oscillations in ADD

The neutron, besides the neutrino, is a good candidate to interact with hidden sectors, e.g. large extra dimensions. This is because it carries no SM charge and can therefore couple to particles in the extra dimensions that are also uncharged under the SM. If the neutron's energy state is nearly degenerate with a KK mode of a bulk fermion, there can be oscillations between them. In fact, we argue that due to the fine mass splitting in the KK tower, the neutron will always find a partner mode with which it can oscillate. We show that neutron oscillations into a bulk fermion open up the possibility for magnetic resonance imaging of the KK tower.

In a minimal scenario, the bulk fermion, denoted as ψ, could be the sterile neutrino. This setup generates a neutrino mass, as discussed in subsection 2.2.2, through the interaction of the active neutrino with the massless KK mode. For the neutrino mass generation, it is crucial that the bulk fermion is massless. In this case, the neutron mixes with a different state of higher energy in the same KK tower. Because the energy scales of the neutrino and the neutron are very different, their mixings with the KK tower have no influence on each other.

2.3.1 Effective Interaction between the Neutron and the Bulk Fermion

Here, we discuss the general case where the bulk fermion ψ that couples to the neutron is unrelated to the neutrino. To include the neutrino, just add the interaction terms described in the previous subsection 2.2.2. Since the neutron has no effect on the neutrino interactions and vice versa, we can ignore the neutrino for now. However, motivated by the neutrino mass generation setup, we assume that the bulk fermion is massless.

We begin with an effective four-fermi operator that mixes the neutron with the bulk fermion,

$$S_{\text{int}} = \int d^4x \frac{1}{M_*^{2+N/2}} \overline{udd}\psi + \text{h.c.}, \tag{2.77}$$

where the neutron is represented by one up-quark and two down-quarks. The scale M_* suppresses this $6 + N/2$-dimensional operator. The M_* can be of order of the fundamental scale of quantum gravity M_f. However, if its origin is more complex,

for example, due to the quark substructure of the neutron, the scale M_* could also be larger than M_f. Thus, we assume $M_* \gtrsim M_f$.

The mixing of the left- and right-handed neutron with the bulk fermion differs since they transform differently under the electroweak symmetry. To construct the neutron from the quark fields of the SM, we need to think about their SM charges. All quarks carry $SU(3)$ color charge, which we denote with indices a, b and c. The right-handed quarks are $SU(2)$ singlets, u_{aR} and d_{aR}, whereas the left-handed quarks form an $SU(2)$ doublet $Q_{\alpha aL}$. We write α, β and γ for $SU(2)$ indices. Both $SU(2)$ and $SU(3)$ have antisymmetric tensors, $\epsilon^{\alpha\beta}$ and ϵ^{abc}, which we use to construct invariant operators. For example, the combination $Q^T \epsilon\, Q$, or with $SU(2)$ indices $Q_{\alpha aL} Q_{\beta bL} \epsilon^{\alpha\beta}$, is $SU(2)$ invariant.

The neutron, composed of one up-quark and two down-quarks, is a color singlet and electrically neutral. The right-handed neutron is an $SU(2)$ singlet, which we can construct in the following two ways:

$$n_R = d_{aR}\, (u_{bR}^T\, C\, d_{cR}) \epsilon^{abc} \;\text{ and }\; n_R = d_{aR}\, (Q_{\alpha bL}^T\, C\, Q_{\beta cL}) \epsilon^{\alpha\beta} \epsilon^{abc}. \tag{2.78}$$

Since the right-handed quarks carry no $SU(2)$ charge, in the first expression, we only need to consider color indices. In the second expression, we include the antisymmetric tensor of $SU(2)$ due to the left-handed quarks with $SU(2)$ charge. Additionally, we have added the charge conjugate operator C to construct a Lorentz invariant term in the brackets.

The operator describing the interaction between the right-handed neutron and the bulk fermion ψ is given by the four-fermion effective Lagrangian

$$(\psi_R^T\, C\, d_R)\, (u_R^T\, C\, d_R), \tag{2.79}$$

where we suppress color indices for clarity. To construct this operator, we must only ensure Lorentz symmetry, as the right-handed neutron in Eq. (2.78) is already a SM singlet.

The interaction involving the left-handed neutron is slightly more intricate. In our effective theory, we treat the left-handed neutron together with the left-handed proton, p_L, as an $SU(2)$ doublet. This doublet of the proton and neutron is constructed from a left-handed quark doublet and an up- and a down-quark with constracted indices,

$$\begin{pmatrix} p \\ n \end{pmatrix}_{\alpha L} = Q_{\alpha aL}\, (u_{bR}^T\, C\, d_{cR}) \epsilon^{abc} \;\text{ and }\; \begin{pmatrix} p \\ n \end{pmatrix}_{\alpha L} = Q_{\alpha aL}\, (Q_{\beta bL}^T\, C\, Q_{\gamma cL}) \epsilon^{\alpha\beta} \epsilon^{abc}. \tag{2.80}$$

The down-quark outside the Lorentz-invariant bracket determines the chirality of the neutron. Since the left-handed neutron is part of an $SU(2)$ doublet, we require another $SU(2)$ doublet to form an $SU(2)$-invariant operator. We single out the neutron by incorporating the Higgs doublet with a vacuum expectation value in its neutral component.

Thus, the interaction Lagrangian for the left-handed neutron includes a Higgs doublet,

$$(\psi_L^T\, C\, Q_{\alpha L})\, (Q_{\gamma L}^T\, C\, Q_{\delta L})\, H_\beta\, \epsilon^{\alpha\beta} \epsilon^{\gamma\delta}, \tag{2.81}$$

again suppressing all color indices. If the interaction strength differs for left- and right-handed fields, the oscillation will be dominated by the larger coupling. However, we argue below that this asymmetry does not significantly impact our results. For simplicity, we assume equal couplings.

With the neutron construction in mind, we turn to the four-fermion effective interaction from Eq. (2.77) and reduce it further by replacing the three quarks with a neutron field and, from dimensional analysis, three powers of the QCD scale,

$$udd \to \Lambda_{\mathrm{QCD}}^3 n. \tag{2.82}$$

We also substitute the Fourier series of the bulk fermion from Eq. (2.15). Since we choose the brane with the SM particles to be located at $y = 0$ in the extra dimensions, we evaluate the Fourier sum at this position.

We now determine the coupling α for the effective interaction between the neutron and the bulk fermion,

$$\mathcal{L}_{\mathrm{int}} = \alpha \sum_{\boldsymbol{k}} \overline{n}\psi_{\boldsymbol{k}}. \tag{2.83}$$

The coupling α is determined by powers of the QCD scale from (2.82), the suppression of the effective four-fermion operator by the mass scale M_* from (2.77) and the volume of the extra dimensions from the normalization of the KK states (2.15). Combining these factors, we obtain

$$\alpha \equiv \frac{\Lambda_{\mathrm{QCD}}^3}{M_*^2\sqrt{M_*^N V_N}} = \frac{\Lambda_{\mathrm{QCD}}^3}{M_P M_f}\left(\frac{M_f}{M_*}\right)^{2+\frac{N}{2}}, \tag{2.84}$$

where we used the master formula from Eq. (2.4) in the final step. As with all interactions between SM and bulk fields, the neutron-bulk fermion interaction is highly suppressed due to the volume of the extra dimensions. In our case, there is an additional suppression from the QCD scale, $\Lambda_{\mathrm{QCD}} \sim 300\,\mathrm{MeV}$, relative to the new scale M_*. As mentioned above, it is reasonable to assume that the M_* is at least as large as the fundamental scale of quantum gravity or even higher, $M_* \gtrsim M_f \sim 10\,\mathrm{TeV}$. From this, we can estimate that the coupling α is smaller than

$$\alpha \lesssim 10^{-15}\mathrm{eV}. \tag{2.85}$$

Thus, α is smaller than any other mass scale in the theory. In particular, it is also smaller than the mass splitting in the KK tower, discussed in section 2.1.2.

From the perspective of a 4-dimensional observer on the brane, the Lagrangian for the neutron and the bulk fermion, including both their kinetic terms, mass terms, and their interaction term, is given by

$$\mathcal{L} = \overline{n}\mathrm{i}\partial\!\!\!/ n - m_n\overline{n}n + \sum_{\boldsymbol{k}}\left(\overline{\psi}_{\boldsymbol{k}}\mathrm{i}\partial\!\!\!/\psi_{\boldsymbol{k}} - m_{\boldsymbol{k}}\overline{\psi}_{\boldsymbol{k}}\psi_{\boldsymbol{k}}\right) + \alpha\sum_{\boldsymbol{k}}\overline{n}\psi_{\boldsymbol{k}} + \mathrm{h.c.}, \tag{2.86}$$

where m_n is the mass of the neutron. Since we are interested in the mass eigenstates, we drop the kinetic terms and write the mass terms and the interaction in a more

compact notation in the mass matrix

$$\mathcal{L} = \begin{pmatrix} \overline{n} & \overline{\psi}_0 & \overline{\psi}_1 & \dots & \overline{\psi}_{\boldsymbol{k}} \end{pmatrix} \begin{pmatrix} m_n & \alpha & \alpha & \dots & \alpha \\ \alpha & 0 & 0 & \dots & 0 \\ \alpha & 0 & m_{\mathbf{1}} & \dots & 0 \\ \dots & \dots & \dots & \dots & \dots \\ \alpha & 0 & 0 & \dots & m_{\boldsymbol{k}} \end{pmatrix} \begin{pmatrix} n \\ \psi_0 \\ \psi_1 \\ \dots \\ \psi_{\boldsymbol{k}} \end{pmatrix} \tag{2.87}$$

where $\boldsymbol{k} = (k_1, \dots, k_N)$ labels the KK state. The masses of the KK modes, $m_{\boldsymbol{k}}$, are given by Eq. (2.14). Due to the degeneracy of KK states, each energy level $m_{\boldsymbol{k}}$ has Z states that all couple to the neutron with strength α. For example, there will be multiple states with $m_{\mathbf{1}}$ since each k_i can take the values ± 1. Further details on the degeneracy factor Z are provided in section 2.1.2.

This degeneracy is important for the neutron but not for the neutrino, as the neutrino primarily mixes with low-energy modes. More specifically, the 0-mode, which gives the neutrino a mass, has only one KK state, $(0, \dots, 0)$. In contrast, the neutron mixes with higher energy levels, which can have a huge degeneracy.

Another difference from the neutrino case is that this mass matrix is symmetric. This is because we assumed that the interactions of the left- and right-handed neutron with the KK modes are equal. As discussed earlier, the coupling strengths of the left- and right-handed neutron to the bulk fermion could, in general, be different. In such cases, only the larger coupling would dominate the neutron's oscillation into the extra dimensions. Accounting for this, we would denote the couplings as α_L and α_R in the relevant equations. However, this does not affect the mixing angle to diagonalize this mass matrix. Consequently, only the left- or right-handed fields would predominantly mix, reducing the oscillation probability by a factor of 2. Since this factor does not impact our broader discussion, we simplify by assuming $\alpha = \alpha_L = \alpha_R$.

This simplification is not applicable to the neutrino case, as only a left-handed neutrino exists. As a result, the neutrino mass matrix is not symmetric. This explains why in the neutron case, unlike in the neutrino case, there are no combinations of ψ_k states that decouple.

2.3.2 Mass Eigenstates

To find the mass eigenstates, we diagonalize the mass matrix in 2×2 blocks, similar to the neutrino case. For each 2×2 block involving the $(n, \psi_{\boldsymbol{k}})$ components, the rotation angle is given by

$$\tan 2\theta_{\boldsymbol{k}} = \frac{2\alpha}{\Delta m_{\boldsymbol{k}}}. \tag{2.88}$$

where we have defined $\Delta m_{\boldsymbol{k}} \equiv m_n - m_{\boldsymbol{k}}$. The rotation angle is positive for $m_n > m_{\boldsymbol{k}}$ and negative for $m_n < m_{\boldsymbol{k}}$. This $\Delta m_{\boldsymbol{k}}$ is the energy difference between the neutron and a KK mode of the bulk fermion.

The mixing of the neutron with a specific KK mode is maximal when the energy splitting $\Delta m_{\boldsymbol{k}}$ is minimal. This implies that the neutron will always find its closest partner in the KK tower and dominantly mix with this nearest energy state (see

Figure 2.6). The mass splitting between the neutron and its closest partner, $\Delta m_{\boldsymbol{k}}$, is comparable to the mass splitting in the KK tower δm. More precisely, $\Delta m_{\boldsymbol{k}}$ must be smaller than half the KK tower mass splitting, which is the case when the neutron energy is exactly midway between two states. We can reasonably assume that $\Delta m_{\boldsymbol{k}}$ is of the same order as δm, as this is far more likely than the neutron being highly degenerate with a tower state.

This is another difference between the neutron and the neutrino case. The neutrino, being massless, primarily mixes with the lowest states in the KK tower. The neutron mixes with states much further up in the tower that are closest to it in energy. In fact, different neutron energy states mix with different KK modes, specifically those closest in energy. Examples of neutrons with a different energy levels include free and bound neutrons.

Next, we expand the rotation for small angles $\theta_k \ll 1$, as $\alpha/\delta m \ll 1$. This approximation holds because $\alpha \lesssim 10^{-15}\,\text{eV}$ from Eq. (2.85), and $\delta m \sim \Delta m_{\boldsymbol{k}} \sim 10^{-2}\,\text{eV}$ for one dominant extra dimension, or $\sim 10^{-13}\,\text{eV}$ for multiple dominant dimensions, as estimated in section 2.1.2. In the next section, we will see that experimental constraints on the lifetime of bound neutrons require the coupling α to be even smaller, ensuring the validity of the small-angle approximation in all relevant cases.

Then, the rotation matrix that diagonalizes the mass matrix from Eq. (2.87) is approximately given by

$$\begin{pmatrix} 1 & -\frac{\alpha}{m_n} & -\frac{\alpha}{\Delta m_{\mathbf{1}}} & \dots & -\frac{\alpha}{\Delta m_{\boldsymbol{k}}} \\ \frac{\alpha}{m_n} & 1 & 0 & \dots & 0 \\ \frac{\alpha}{m_{\mathbf{1}}} & 0 & 1 & \dots & 0 \\ \dots & \dots & \dots & \dots & \dots \\ \frac{\alpha}{\Delta m_{\boldsymbol{k}}} & 0 & 0 & \dots & 1 \end{pmatrix}. \tag{2.89}$$

This rotation matrix transforms the fermion fields $(n, \psi_0, \psi_{\mathbf{1}}, \dots, \psi_{\boldsymbol{k}})$ into their mass eigenstates. To obtain the mass eigenstates, we multiply the inverse rotation matrix (which, in this case, is equal to its transpose) by the fermion vector. The first component is the mass eigenstate of the neutron, which is

$$n' = \frac{1}{\mathcal{N}}\left(n + \sum_{\boldsymbol{k}} \frac{\alpha}{\Delta m_{\boldsymbol{k}}}\psi_{\boldsymbol{k}}\right), \tag{2.90}$$

where $\mathcal{N}$ is a normalization factor. The normalization is $\mathcal{N}^2 = 1 + \sum_{\boldsymbol{k}} \alpha^2/\Delta m_{\boldsymbol{k}}^2$. In the following, we approximate the normalization factor by $\mathcal{N} \approx 1$ because $\alpha/\Delta m_{\boldsymbol{k}} \ll 1$. The mass eigenstate of a $\psi_{\boldsymbol{k}}$ is given by

$$\psi'_{\boldsymbol{k}} = \psi_{\boldsymbol{k}} - \frac{\alpha}{\Delta m_{\boldsymbol{k}}} n. \tag{2.91}$$

We will use these mass eigenstates in the next subsection to calculate the oscillation probability for a neutron transitioning into a bulk fermion.

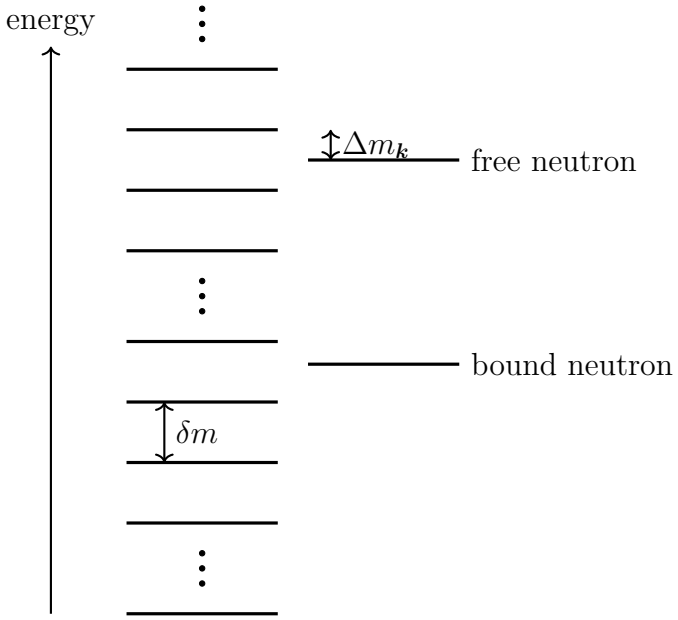

Figure 2.6: Energy states in the Kaluza-Klein tower on the left and how the free and bound neutron states always find a closest partner to oscillate with. The free neutron and the bound neutron mix with different parts of the KK tower.

2.3.3 Oscillation Probability

Using the mass eigenstates derived in the previous subsection, we can calculate the oscillation probability of a neutron oscillating into a KK mode of the bulk fermion. The time evolution of the neutron mass eigenstate is given by

$$n'(t) = \frac{1}{\mathcal{N}}\left(n - \sum_{\boldsymbol{k}} \frac{\alpha}{\Delta m_{\boldsymbol{k}}} e^{\mathrm{i}\phi_{\boldsymbol{k}}}\psi_{\boldsymbol{k}}\right), \tag{2.92}$$

where $\phi_{\boldsymbol{k}} = (E_{\boldsymbol{k}} - E_n)\,t = (m_{\boldsymbol{k}} - m_n)\,t$. This differs from the neutrino case because the neutron is non-relativistic, meaning its energy can be approximated by its mass, $E_n \approx m_n$.

The survival probability of a neutron after some time t is given by

$$P_{\text{surv}} = |\,\langle n' \,|\, n'(t)\rangle\,|^2 = \frac{1}{\mathcal{N}^4}\left|1 + \sum_{\boldsymbol{k}} \frac{\alpha^2}{\Delta m_{\boldsymbol{k}}^2} e^{\mathrm{i}\phi_{\boldsymbol{k}}}\right|^2 \tag{2.93}$$

Using the identity $2\cos(x) = e^{\mathrm{i}x} + e^{-\mathrm{i}x}$, we can rewrite the survival probability as:

$$P_{\text{surv}} = \frac{1}{\mathcal{N}^4}\left(1 + \sum_{\boldsymbol{k}} \frac{\alpha^2}{\Delta m_{\boldsymbol{k}}^2} 2\cos(\phi_{\boldsymbol{k}}) + \mathcal{O}(\alpha^4)\right) \tag{2.94}$$

Next, we group all KK modes with the same mass into a single state, ψ_k, labeled by $k = \sqrt{k_1^2 + \cdots + k_N^2}$, with degeneracy Z. The sum over $\boldsymbol{k}$ then transforms into a sum over k, which represents the square root of an integer. For $N \geq 4$, all integers

can be expressed as sums of squares, so the sum over k effectively becomes a sum over the square roots of all integers. Since $\phi_{\boldsymbol{k}}$ is identical for all states with the same mass, we replace it with ϕ_k. Using $\cos(\phi_k) = 1 - 2\sin^2(\phi_k/2)$, we read off the oscillation probability into a state ψ_k, incorporating the degeneracies of ψ_k

$$P_{\text{osc}} = \frac{Z}{\mathcal{N}^4} \frac{4\alpha^2}{\Delta m_k^2} \sin^2\left(\frac{\Delta m_k\, t}{2}\right). \tag{2.95}$$

The amplitude includes the square of the mixing parameter α divided by the mass splitting Δm_k between the oscillating states. The factor Z counts the degeneracies, as the neutron can oscillate into any of the Z states with the same mass. The normalization from the mass eigenstates is approximated as $\mathcal{N} \approx 1$.

As explained in section 2.1.2, the expression $Z/\delta m \sim (mR)^{N_R-1}R$ holds for all numbers of relevant dimensions, N_R. Since the KK tower mass splitting is related to the splitting between the neutron and its closest KK state, $\delta m \sim \Delta m_{\boldsymbol{k}}$, we can express the oscillation probability of a neutron transitioning into its nearest KK partner as

$$P_{\text{osc}} \sim (m_n R)^{N_R-1} R \frac{\alpha^2}{\Delta m_{\boldsymbol{k}}} \sin^2\left(\frac{\Delta m_k\, t}{2}\right). \tag{2.96}$$

In the following sections, we will use these approximations to derive experimental constraints on the parameters of the theory.

2.4 Neutron Disappearance in Nuclei

The oscillation amplitude derived in the previous subsection depends on a few parameters: the scales M_* and M_f, and the radius of the dominant extra dimensions R. We now analyze this setup and constrain these parameters from a phenomenological perspective.

For bound neutrons in nuclei, an oscillation with an extra-dimensional fermion leads to neutron disappearance from the nucleus. By quantum mechanics, neutrons in a nucleus occupy different discrete energy levels. If one of those energy levels is particularly close to a partner state in the KK tower, the corresponding neutron has the highest probability to oscillate into the extra dimensions. After the neutron transitions into a bulk fermion, the nucleus is left in an excited state. Now there are two options: either the bulk fermion oscillates back into the nucleus, or a neutron in a higher energy state transitions down to occupy the vacant state. In the latter case, the nucleus de-excites and emits a photon. The question is: which process is faster, the oscillation back into the nucleus or the de-excitation?

The oscillation time is given by the inverse of the KK tower mass splitting. For the following estimations we use the largest radius allowed by experiment, 30μm. For one dominant extra dimension, the oscillation time is $1/\Delta m \sim R \lesssim 10^{-13}$s, while for more dominant extra dimensions, it is $1/\Delta m \sim R^2 m \lesssim 10^{-2}$s. The timescale for de-excitation is determined by the energy splitting between the initial neutron state and the lower state it transitions to. Typical nuclear energy levels are separated by

energy scales of MeV, leading to a de-excitation time of $1/\text{MeV} \sim 10^{-21} - 10^{-22}$s. This comparison shows that, for radii around μm or smaller by nearly 10 orders of magnitude, de-excitation is significantly faster. The neutron cannot oscillate back if the de-excitation happens before because its corresponding energy state is now occupied. Thus we expect the neutron to disappear into the extra dimensions, leaving us with a nucleus missing a neutron and sending out a photon with energy of nuclear levels, i.e. a hard photon.

For a nucleus X, we can represent this process as

$$ {}^{A}_{Z}X \xrightarrow[\text{disappearance}]{\text{neutron}} {}^{A-1}_{Z}X^{*} \xrightarrow{\text{de-excitation}} {}^{A-1}_{Z}X + \gamma, \tag{2.97} $$

where Z is the atomic number (number of protons) and A is the mass number (number of protons and neutrons). The asterisk (*) denotes an excited state and the γ represents the emitted photon. During neutron disappearance, the mass number A decreases by one. After de-excitation, the resulting nucleus, now missing a neutron, may be an unstable isotope of element X and could undergo further radioactive decay.

The process of neutron disappearance is constrained by experimental limits on the lifetime of neutrons in nuclei. The KamLAND experiment [53] places a lower bound on the bound neutron lifetime

$$ \tau_n > 10^{30}\text{y} \sim 10^{62}\,\text{GeV}^{-1}. \tag{2.98} $$

This bound on the neutron lifetime translates into an upper limit on the neutron disappearance rate, $\lambda_n = 1/\tau_n$.

The neutron disappearance rate is the average transition probability per unit time. This rate is given by

$$ \lambda_n \sim \frac{Z\alpha^2}{\Delta m_k} \sim (m_n R)^{N_R-1} R\, \frac{\Lambda_{\text{QCD}}^6}{M_P^2 M_f^2} \left(\frac{M_f}{M_*}\right)^{4+N}, \tag{2.99} $$

where we used the oscillation probability (2.95) in the first step. In the second, expression we substituted $Z/\Delta m_k \sim (m_n R)^{N_R-1} R$, as explained in section 2.1.2. We also inserted the expression for the coupling α from Eq. (2.84).

Note that the degeneracy factor Z depends on the number of relevant extra dimensions N_R, while the coupling α is related to the volume of all N extra dimensions. Applying the experimental bound on the bound neutron lifetime from (2.98) we find a constraint on M_*,

$$ M_*^{4+N} > 10^{21} (\text{GeV}\, R)^{N_R} M_f^{2+N} \text{GeV}^2, \tag{2.100} $$

where we also used the master formula from Eq. (2.4) and inserted numerical values $\Lambda_{\text{QCD}} \approx 300\,\text{MeV}$, $m_n \approx \text{GeV}$ and $M_P \sim 10^{19}\,\text{GeV}$.

In the following, we distinguish between two important cases: first, the scenario with one dominant extra dimension ($N_R = 1$) and second, the case where all extra dimensions have equal radii ($N_R = N$). In both cases, we set the fundamental scale to $M_f \sim 10\,\text{TeV}$.

2.4.1 One Dominant Dimension

For the case of a single relevant extra dimension ($N_R = 1$), we choose its radius to be as large as possible, $R \sim 30\mu$m. Of course, as discussed in section 2.1.1, a scenario with only one extra dimension is already excluded. It is clear that additional, much smaller extra dimensions must exist to lower the fundamental scale of quantum gravity to $M_f \sim 10$ TeV. However, having only one additional smaller extra dimension is insufficient: From the master formula (2.4), the second smaller dimension would be of size 0.5μm, which is not significantly smaller than the larger extra dimension. Thus, the smaller dimension would still be relevant.

For $N_R = 1$, the bound on M_* from Eq. (2.100) depends only on the total number of extra dimensions and is given by

$$M_*^{4+N} > 10^{40+4N}\text{GeV}^{4+N}. \tag{2.101}$$

The explicit bounds on M_* for different numbers of extra dimensions N are summarized in Table 2.2. Depending on N, the lower bound on M_* is on the order $10^6 - 10^7$ GeV, which is approximately $2 - 3$ orders of magnitude higher than the fundamental scale M_f.

N	M_*[GeV]
3	$> 3 \cdot 10^7$
4	$> 1 \cdot 10^7$
5	$> 5 \cdot 10^6$
6	$> 3 \cdot 10^6$

Table 2.2: Bound on M_* for one dominant R with $M_f = 10$ TeV and $R = 30\mu$m

2.4.2 Equal Size Dimensions

In the case when all extra dimensions are relevant, meaning they have the same size and $N = N_R$, the bound on M_* from Eq. (2.100) becomes

$$M_*^{4+N} > 10^{29+15N}\text{GeV}^{4+N}. \tag{2.102}$$

Table 2.3 shows the bounds on M_* for different numbers of equally sized extra dimensions N and the corresponding radii required to lower the Planck scale to $M_f \sim 10$ TeV. The lower bounds on M_* range from 10^9 GeV to 10^{11} GeV. Thus, the constraints from scenarios with equal-sized extra dimensions are significantly stronger than those obtained for a single dominant extra dimension.

We also want to comment on the case with more than one dominant extra dimension ($N_R > 1$) alongside additional smaller dimensions ($N > N_R$). In this scenario, in addition to the N_R relevant extra dimensions with radius R, there are $N - N_R$ smaller ones with radius $\tilde{R}$. Since $1/M_f$ is the smallest distance scale in the theory, even the smallest extra dimensions must at least as large as $2\pi\tilde{R} > 1/M_f$.

N	$R[\mu\text{m}]$	$M_*[\text{GeV}]$
2	1.1	$> 7 \cdot 10^9$
3	$1.6 \cdot 10^{-5}$	$> 4 \cdot 10^{10}$
4	$5.5 \cdot 10^{-8}$	$> 1 \cdot 10^{11}$
5	$2 \cdot 10^{-9}$	$> 4 \cdot 10^{11}$
6	$2.2 \cdot 10^{-10}$	$> 8 \cdot 10^{11}$

Table 2.3: Bound on M_* for equal size extra dimensions.

Because the total volume of the extra dimensions can be split into relevant and smaller dimensions,

$$M_f^N V_N = (2\pi R M_f)^{N_R} (2\pi \tilde{R} M_f)^{N-N_R} > (2\pi R M_f)^{N_R}, \tag{2.103}$$

the presence of additional smaller dimensions can only further lower the fundamental scale. However, since the smaller dimensions cannot be arbitrarily small, there is an upper bound on the radius of the dominant dimensions. From the master formula (2.4), this bound is given by

$$R \leq \frac{1}{2\pi M_f} \left(\frac{M_P}{M_f} \right)^{\frac{2}{N_R}}. \tag{2.104}$$

This upper bound is saturated when there are no smaller extra dimensions, with values for R shown in Table 2.3.

For a single extra dimension ($N_R = 1$) with $M_f \sim 10\,\text{TeV}$, this bound is not very restrictive, yielding $R < 10^{15}\mu\text{m}$. Thus, we can select a smaller radius, such as $30\mu\text{m}$, and introduce additional smaller extra dimensions to lower the fundamental scale to 10 TeV. However, for $N_R = 2$, the constraint in Eq. (2.104) limits the upper bound on the radius to the μm scale. To maximize the radius of the relevant dimensions while maintaining $M_f \sim 10\,\text{TeV}$, the smaller dimensions must be at their minimum allowed size. This adjustment can relax the constraint on M_* by up to two orders of magnitude compared to the $N_R = N = 2$ case.

2.4.3 Another Scenario

Another interesting scenario arises when we set $M_* \sim M_f$, meaning the effective scale of the four-fermi operator from Eq. (2.77) is of the same order as the fundamental scale of quantum gravity M_f. In this case, the bound on M_* from Eq. (2.100) is replaced by a bound on the fundamental scale M_f,

$$M_f^2 > 10^{21} (\text{GeV}\, R)^{N_R} \text{GeV}^2. \tag{2.105}$$

This bound on the fundamental scale is more constraining than the experimental $M_f \gtrsim 10\,\text{TeV}$ bound. Thus, also the bound on R is stronger in this case. For example, plugging Eq. (2.105) into the bound on R from Eq. (2.104) we find for $N_R = 1$

$$R \leq 10^2 \text{GeV}^{-1} \sim 10^{-8} \mu\text{m}. \tag{2.106}$$

In this case, the bound on the size of the extra dimension is several orders of magnitude stronger than the experimental limit 30μm. This in turn constrains the fundamental scale as

$$M_f > 10^{12}\text{GeV}, \tag{2.107}$$

which is much stronger than the bounds on M_* as a free parameter.

To summarize, experimental constraints from bound neutron disappearance put bounds on the parameters M_*, M_f and R. The constraints on M_* can also be interpreted as an upper bound on the coupling strength α between the neutron to the bulk fermion. If we treat M_* as a free parameter, the bounds in the cases for one relevant dimension and all dimensions of the same size range from $M_* \gtrsim 10^6\,\text{GeV}$ to $M_* \gtrsim 10^{11}\,\text{GeV}$. Alternatively, assuming $M_* \sim M_f$, we put bounds on $M_f > 10^{12}\,\text{GeV}$ and $R < 10^{-8}\mu$m.

However, these bounds can be lifted if the bulk fermion has a mass μ greater than the bound neutron energy, in which case transitions into the KK tower become kinetically forbidden.

2.5 Proton Decay

With the neutron oscillating into a bulk fermion, we have to think about weather the proton is safe from decaying into the extra dimensions through a virtual neutron. The decay of a proton into a neutron, a positron and a neutrino by the weak interaction is forbidden because the neutron is heavier than the proton. However, it is not forbidden if the neutron is only an intermediate state. If the neutron can oscillate with a bulk fermion, then proton can turn into a bulk fermion, a positron and a neutrino,

$$p \to e^+ \nu_e \, \psi, \tag{2.108}$$

as shown in Figure 2.7. We still need the mass of the proton to be larger than the sum of the end products. Thus, the sum of the masses of the bulk fermion that the neutron oscillates with, of the electron, and of the neutrino has to be less than the proton mass.

Compared with the neutron disappearance rate from Eq. (2.99), the proton decay rate has additional factors from the W-boson exchange

$$\lambda_p \sim \lambda_n \left(\frac{m_n}{v}\right)^4 \sim m_p \left(\frac{m_n}{v}\right)^4 \left(\frac{\alpha}{m_n}\right)^2 (m_p R)^{N_R}, \tag{2.109}$$

where we used Eq. (2.30) and $m_n \sim m_p$. The additional factor from the weak interaction suppresses the proton decay rate by $(m_n/v)^4 \sim 10^{-9}$.

The experimental bounds on proton decay into invisible particles is $\tau_p > 10^{30}\,\text{y}$. This constraint is of the same order as the one for the disappearance of bound neutrons, Eq. (2.98). As proton decay has an additional suppression from the weak interaction, the experimental constraints on proton decay are always fulfilled and neutron disappearance bounds are stronger.

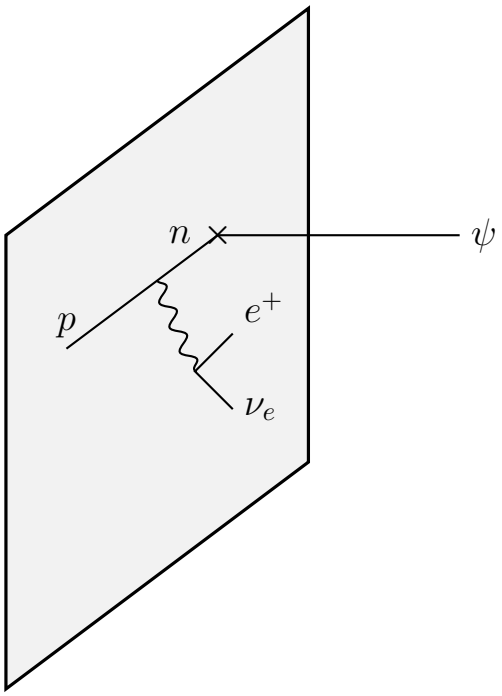

Figure 2.7: Proton decay into a positron, a neutrino and a bulk fermion. The proton turns into a virtual neutron which interacts with the fermion in the extra dimensions.

2.6 Free Neutron

In this section, we explore the parameter space where only free neutrons oscillate with the extra-dimensional fermion. This parameter space is motivated by recent experiments with ultra-cold neutrons in magnetic fields.

As mentioned earlier, the constraints on α and M_* can be lifted if the bulk fermion has a mass in the extra dimensions. The KK tower of a massive bulk particle begins at its mass μ, corresponding to its zero mode, and then includes only higher energy states. This follows from the masses of the KK modes given in Eq. (2.21). Thus, if the bulk fermion mass is larger than the energy of the bound neutron, neutron disappearance in bound nuclei is forbidden by kinematics. In this case, the bound on the coupling is $\alpha \lesssim 10^{-15}$eV from experimental constraints on the fundamental scale M_f, as explained before Eq. (2.85).

The mass of the free neutron is higher than the energy of the bound neutron. This is because of the nuclear binding energy, which is of the order of MeV. Thus, the energy difference between free and bound neutron states is $\sim$MeV. If we require the bulk fermion mass to be greater than the bound neutron energy but still below the free neutron energy, so $m_{\text{bound}\,n} < \mu < m_n$, then only the free neutron oscillates with the bulk fermion. Additionally, if the bulk fermion is heavier than the proton, there are no constraints from proton decay.

In this setup, we still expect the free neutron to oscillate with a KK state that is high up in the KK tower. This is because it is very unlikely that the mass of the

bulk fermion is so degenerate with the neutron mass that it mixes with the 0-mode. Then, the oscillation amplitude is still enhanced by the multiplicity of the KK states Z.

This setup opens up an intriguing and novel possibility: scanning the KK tower with a magnetic field in free neutron experiments. Because the neutron has a magnetic moment μ_n, an external magnetic field B shifts its energy by $\epsilon = \mu_n B$. By increasing the magnetic field in small steps, one can search for resonances in the neutron oscillation amplitude, effectively performing magnetic resonance imaging of the KK tower. For the case of two dominant extra dimensions, $N_R = 2$, the spacing in the KK tower is small enough to be scanned by current laboratory setups.

2.6.1 Magnetic Field

Since the neutron oscillates most dominantly with the KK mode closest in energy, increasing the magnetic field in steps can have several implications. If the energy shift corresponding to the magnetic field step ΔB exceeds the mass splitting in the KK tower, δm, the neutron partners up with a different KK mode. In this case, neutron oscillation resonances are unlikely to be observed. Also, nothing changes to the setup without a magnetic field except that the neutron dominantly mixes with a different tower state, not affecting any bounds.

But if the steps with which we increase the magnetic field are much smaller than the tower splitting (see Figure 2.8), we only have to take enough steps to be degenerate to a KK tower state and to observe a resonance. By selecting an appropriate magnetic field range, we can ensure coverage of at least one KK tower state. We define the range of the magnetic field as the difference between its maximum and minimum values in the experiment, $B_{\text{range}} = B_{\text{max}} - B_{\text{min}}$. Within this range, we increase the magnetic field in small steps ΔB.

This analysis highlights the significance of the level splitting in the KK tower. The magnetic field values must be carefully adjusted to match the level splitting. As explained above, we need $\Delta\epsilon = \mu_n \Delta B \ll \delta m$, and $\mu_n B_{\text{range}} \gtrsim \delta m$.

To understand which values of the magnetic field can probe which parameter space of our framework we compare some realistic values. The magnetic moment of the neutron is $\mu_n \approx -9.66 \times 10^{-27}\text{JT}^{-1}$ [54]$\approx 6 \times 10^{-14}\text{eV}/\mu\text{T}$. In Earth's magnetic field with $B_{\text{earth}} \approx 0.5\text{G} \approx 50\mu\text{T}$ this translates to an energy shift of the neutron of $\epsilon \approx 10^{-12}\text{eV}$. Using artificial magnetic fields, this energy shift can be a few orders of magnitude bigger.

The level splitting is very different for one or for more dominant extra dimensions. As explained in section 2.1.2, the level splitting for one dominant extra dimension with $R \sim 30\mu\text{m}$ is $\delta m \sim 10^{-2}\text{eV}$. This mass splitting corresponds to a magnetic field range of $B_{\text{range}} \gtrsim 10^5\text{T}$ and is too big for current experiments.

For more than one dominant extra dimension, the mass splitting is $\delta m \sim 1/(R^2 m)$. However, as discussed in section 2.1.2, the limit on the size of the extra dimensions is stronger. The smallest mass splitting we get for two dominant extra dimensions: With a radius $R \sim 1\mu\text{m}$ and at $m \sim \text{GeV}$, the level splitting is $\delta m \sim 10^{-11}\text{eV}$

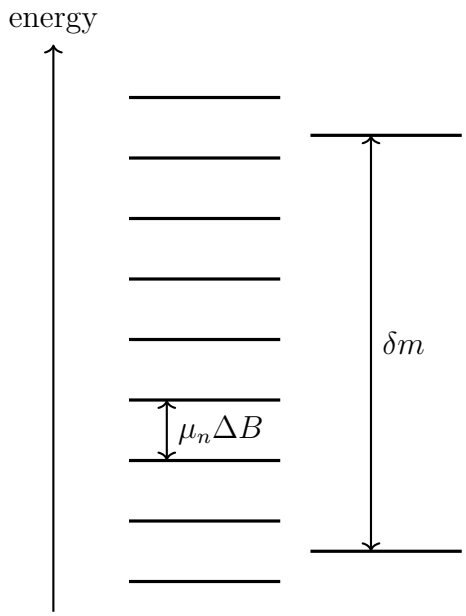

Figure 2.8: Neutron energy level on the left, is increased in small steps with the magnetic field. Two adjacent states in the KK tower on the right, level splitting δm. If the scanning is fine enough we see resonance.

corresponding to $B_{\text{range}} \gtrsim 1\text{mT}$.

Then there is also the question of how far up we are in the tower. If the fermion has a mass in the extra dimensions μ, the tower starts from there and we go up $m_n - \mu$. We suggested $\mu \sim \text{GeV}-\text{MeV}$ to evade the bound neutron constraints, then we only go up MeV in the tower and $\delta m \sim 10^{-8}\text{eV}$. However, we can also assume the tower starts at $\mu = 0$ and find constraints on α or M_* from free neutron experiments.

To summarize this last part, the mass splitting δm depends on the details of the model. The smallest mass splitting possible is for two extra dimensions, where $\delta m \sim 10^{-11}\text{eV}$. It makes sense to also test for larger splitting in the experiment, as long as this is possible for the values of the magnetic field.

2.6.2 Kaluza-Klein Spectroscopy

Experiments with magnetic fields in those ranges can constrain the oscillation amplitude. We now modify our discussion from subsection 2.3.3 to include an external magnetic field. As the neutron mixes most dominantly with the KK mode closest in energy, we simplify the problem by only looking at the 2×2 mass matrix of these two states. The energy splitting between the neutron and its closest partner in the KK tower we denote by Δm. If we put the neutron in a magnetic field, its energy will change by ϵ. If $\epsilon > \Delta m \sim \delta m$ so that the energy of the neutron is shifted by more than the tower splitting, the neutron will find a different partner in the KK

tower. Thus, in the following, we assume $\epsilon \lesssim \Delta m$. Then the 2×2 mass matrix is

$$\begin{pmatrix} m_n + \epsilon & \sqrt{Z}\alpha \\ \sqrt{Z}\alpha & m_n + \Delta m \end{pmatrix}, \tag{2.110}$$

where we included the multiplicity of the same energy states with $\sqrt{Z}$.

Compared with the oscillation amplitude without a magnetic field from Eq. (2.95), the energy difference gets an additional contribution from the shift in the magnetic field ϵ. Hence, the oscillation amplitude is

$$A \approx \frac{Z\alpha^2}{(\epsilon - \Delta m)^2}. \tag{2.111}$$

If we increase the magnetic field in small steps, $\Delta\epsilon$, then we have to hit a resonance if the following two conditions are fulfilled: 1) the steps of the magnetic field are smaller than the level splitting in the KK tower, $\Delta\epsilon \ll \delta m$, and 2) the range over which we scan with the magnetic field is larger than the level splitting, $\epsilon_{\text{range}} > \delta m$.

In this case, the increase of the magnetic field in small steps will lead us to a neutron energy that is more degenerate with the KK tower. At some point in the scanning, the neutron energy will be as close as $\Delta\epsilon$ to the KK mode. Thus, the oscillation amplitude in the resonance regime is

$$A \approx \frac{Z\alpha^2}{\Delta\epsilon^2}. \tag{2.112}$$

As long as we are not in the resonance regime, the amplitude is dominated by the level splitting

$$A \approx \frac{Z\alpha^2}{\delta m^2}. \tag{2.113}$$

There have been two recent publications of experiments with free neutrons in magnetic fields measuring the neutron disappearance rate [11, 55]. The original motivation for both experiments are oscillations of the neutron into a mirror neutron. However, their results are applicable to the neutron disappearing into any hidden species.

The first experiment is a ultracold neutron storage experiment from the nEDM collaboration at PSI [55]. They measured the neutron disappearance amplitude at two values of the magnetic field, $B_1 = (10.20 \pm 0.02)\mu\text{T}$ and $B_2 \approx (20.39 \pm 0.04)\mu\text{T}$. This corresponds to an energy shift of the neutron of $\epsilon \sim 10^{-12}\text{eV}$. For two extra dimensions with the largest radius allowed by experiment, $R_{max} \lesssim 30\mu\text{m}$, the mass splitting in the tower is smaller than the energy shift due to the magnetic field, $\mu_n \Delta B \gg \delta m$. In this case, a shift in the magnetic field would move the neutron energy to a different closest partner in the KK tower. We assume that there is no miracoulous coincidence of the neutron energy being exactly degenerate with a KK state. Then the mass splitting relevant for the oscillation amplitude is determined by the KK tower splitting. This means that we are not in the resonance regime.

This is also reasonable to assume since there are only measurements of two values of the magnetic field, so that there is no real scanning of the KK tower.

The experiment can still constrain parameters of the model. Using $R_{\max} \sim 30\mu$m, the amplitude is

$$A \sim \frac{\alpha^2}{\delta m^2} \sim 10^{27}\alpha^2 \frac{R^4}{R_{\max}^4}\text{eV}^{-2}. \tag{2.114}$$

The experiment puts bounds on the amplitude which we translate into a constraint on our parameters,

$$\alpha \frac{R^2}{R_{\max}^2} \lesssim 10^{-16}\text{eV}. \tag{2.115}$$

We can rewrite this in terms of M_* and M_f,

$$\frac{10\text{TeV}}{M_f}\left(\frac{M_f}{M_*}\right)^{2+\frac{N}{2}} \frac{R^2}{R_{\max}^2} \lesssim \frac{1}{3}. \tag{2.116}$$

When we take $M_* \sim M_f \sim 10\,\text{TeV}$, this translates into an experimental bound on the radius of the extra dimensions.

The second paper [11] is looking for neutron disappearance in an ultracold neutron beam. They start at a magnetic field $B_{min} = 50\mu$T and increase by small steps of $\Delta B = 3\mu$T until reaching the maximum magnetic field $B_{max} = 1100\mu$T. For specific values of the radius, this experiment is in the resonance regime. We need

$$\epsilon_{range} = \mu_n(B_{max} - B_{min}) = 6 \cdot 10^{-11}\text{eV} > \delta m = 10^{-13}R_{max}^2/R^2\text{eV}. \tag{2.117}$$

This is true for $R > 0.8\mu$m. We also need

$$\Delta\epsilon = \mu_n \Delta B = 10^{-13}\text{eV} \ll \delta m = 10^{-13}R_{max}^2/R^2\text{eV}. \tag{2.118}$$

This means the radius is $R < 10\mu$m.

For the values given in the experiment, they testing the resonance regime for $0.8\mu\text{m} < R < 10\mu\text{m}$. In this resonance regime the amplitude is given by

$$A \sim \frac{\alpha^2}{|\Delta\epsilon|^2} \sim \alpha^2 10^{25}\text{eV}^{-2}. \tag{2.119}$$

Thus, the bound on the amplitude does not depend on R,

$$\alpha \lesssim 10^{-14}\text{eV}. \tag{2.120}$$

Outside the resonance regime, i.e., when $R < 0.8\mu$m or $R > 10\mu$m, the experiment puts the following bound on the parameters

$$\alpha \frac{R^2}{R_{\max}^2} \lesssim 10^{-15}\text{eV}, \tag{2.121}$$

similar to the first experiment discussed above.

All in all, neutrons oscillating with bulk fermions produce a characteristic signature with recurring resonances in the neutron disappearance amplitude. The resonances occur in steps of the magnetic field, $\Delta B = \delta m/\mu_n$. Thus, the recent experiment [11] is probing the resonance regime for a specific KK level-splitting $0.8\mu\text{m} < R < 10\mu\text{m}$.

We expect the resonance pattern to look similar to the sketch in Figure 2.9. In the case for two dominant extra dimensions, the KK levels are not populated uniformly. For more than two dominant extra dimensions, the pattern will be strictly periodic. The heights of the resonances can differ because the KK levels can have different degeneracy fectors.

In the future, experiments with a finer scanning and a wider range of the magnetic field can be deeper probes of large extra dimensions. The bounds given in this section show that the recent experiments are already probing a parameter space that is motivated by the hierarchy problem.

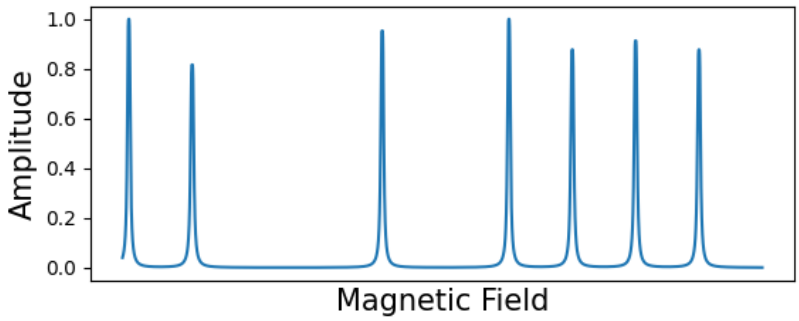

Figure 2.9: A qualitative sketch of the neutron disappearance amplitude as a function of the magnetic field. The resonance transitions take place in steps of the magnetic field $\Delta B = \Delta m/\mu_n$. The differences in the heights are due to different degeneracy factors of different KK levels. The repetitive but not strictly periodic behavior is due to the nonuniform population of KK levels.

2.6.3 Comparing with other Setups

In this section we compare our setup within the ADD model with the similar scenario of many copies of the SM with an exact permutation symmetry [36]. In this scenario, the neutron from our copy can oscillate with the neutrons in the other copies. Thus, the neutron is also mixing with multiple partners. However, the repetitive pattern of resonances in the neutron disappearance amplitude is unique to Large Extra Dimensions.

One similarity between the ADD model and the model with many copies of the SM is that both solve the hierarchy problem by lowering the fundamental scale of quantum gravity, M_f. In the ADD model, this is described by the master formula from Eq. (2.4). In the case with many species, like for example with many SM

copies, M_f is given by the species scale [37, 38]

$$M_P = \sqrt{N_{\rm sp}} M_f, \tag{2.122}$$

where $N_{\rm sp}$ is the number of species. To lower the Planck scale to 10 TeV and hence solve the hierarchy problem, we introduce $M_P^2/M_f^2 \sim 10^{30}$ copies of the SM [36][4]. However, with the SM already containing ~ 100 species, we only have to introduce 10^{28} copies of the SM to have the cutoff of gravity at 10 TeV. As this is the lowest bound on the scale for new physics, 10^{28} is also the maximal number of copies we can add to the SM.

The connection between the models is stronger than just their common motivation by the hierarchy problem. The master formula from ADD is a special case of the species scale. In the ADD model, the KK tower provides $N_{\rm sp} = M_f^N V_N$ new states with masses below the cutoff M_f, such that the species scale reproduces the master formula. In this way,the ADD model provides a geometric meaning to the fundamental scale of quantum gravity: While in the ADD model, the solution to the hierarchy problem can be viewed as a dilution of the strength of gravity in the extra dimensions, in models with many species it is a dilution in the space of species.

Because of these similarities, the models are also similar in their phenomenology. For example, both models offer a similar explanation for the smallness of neutrino masses: The volume suppression in the ADD model corresponds to a suppression in the space of species [37, 56]. Thus, in both cases the suppression of neutrino masses are related to the weakness of gravity. Also, dark matter can be made up from particles in the hidden SM copies [37, 57]. In the ADD model, the SM copies that make up dark matter can be included as copies of our SM brane [58]. These many copies of our brane are connected parallel branes that together form the manyfold universe.

In the model with many SM copies [36], the interaction between the neutrons in different copies is described by the mixing $\alpha \sum_{i\neq j} \overline{n}_i n_j$, where the sum runs over the number of copies $i, j = 1, \ldots, N$. With the exact permutation symmetry, the masses of the neutrons in different copies are equal and the couplings α between different neutrons are also equal. The coupling $\alpha < m_n/N$ is constrained by unitarity. Then the $N \times N$ mass matrix corresponding to the neutrons in different copies $(n_1, n_2, n_3, \ldots)$ is

$$\begin{pmatrix} m_n & \alpha & \alpha & \ldots \\ \alpha & m_n & \alpha & \ldots \\ \alpha & \alpha & m_n & \ldots \\ \ldots & \ldots & \ldots & \ldots \end{pmatrix}. \tag{2.123}$$

Here, we can already see that the eigenvalues of this matrix will be $m_n + (N-1)\alpha$ with eigenvector $(1, \ldots, 1)$ and all $N-1$ others $m_n - \alpha$ corresponding to $(0, \ldots, 1, 0, \ldots, -1)$.

Taking n_1 as the neutron in our SM copy, our neutron interacts only with a linear combination of other neutron fields, $n_h = \frac{1}{\sqrt{N-1}} \sum_{i\neq 1} n_i$. Then we can redefine the

[4] In [36], they lowered the cutoff to TeV, introducing 10^{32} copies.

fields so that we only need a 2×2 matrix mixing the states (n_1, n_h)

$$\begin{pmatrix} m_n & \alpha\sqrt{N-1} \\ \alpha\sqrt{N-1} & m_n + \alpha\sqrt{N-2} \end{pmatrix} \tag{2.124}$$

The other $N-2$ states, which are orthogonal to n_h decouple.

Diagonalizing this matrix and finding the mass eigenstates then gives us the disappearance probability of our neutron into a neutron copy,

$$P(t) \approx \frac{4}{N} \sin^2\left(\frac{N\alpha\, t}{2}\right). \tag{2.125}$$

Even though the neutron mixes with many neutron copies, the oscillation goes through the n_h state. The neutron has only this one single oscillation partner n_h. This is different from the neutron oscillating with KK modes of a bulk fermion, since the bulk fermion has a tower of states that each mix with the neutron.

The scanning of resonant values of the neutron disappearance amplitude with a magnetic field works only in the case with the KK tower. The neutron always finds a closest partner in the tower, no matter its energy $m_n + \epsilon$. The recurring resonances will always appear in steps of the magnetic field $\Delta B = \delta m/\mu_n$.

In the model with many SM copies, the neutron from our copy and its oscillation partner n_h have a mass splitting such that a magnetic field $B_r = \alpha\sqrt{N-2}/\mu_n$ will produce a resonance. However, there are no resonances for different values of the magnetic field.

The same happens already with one copy of the SM, the SM plus a mirror SM. The oscillations of the neutron with its mirror partner have been studied in [59, 60]. In this special case, the neutron and the mirror neutron have exactly the same mass. The energy of the (mirror) neutron is affected by a (mirror) magnetic field. Without knowing anything about the mirror magnetic field, it is difficult to make any predictions about the two states being in resonance with each other. Still, just as with many copies of the SM, there is one single value of the magnetic field that produces the resonance between the neutron and the mirror neutron. Thus, the recurring resonances in the neutron oscillation amplitude for the ADD model with a bulk fermion lead to a unique signature in neutron experiments.

2.7 Neutron Lifetime Measurements

Free neutrons decay into a proton, an electron and an antineutrino by the weak interaction. However, experiments measuring the neutron lifetime indicate a discrepancy between different types of experiments. This discrepancy has been called the neutron lifetime puzzle and may be explained by new channels of neutron disappearance.

Experiments with ultra-cold neutrons are measuring the neutron lifetime by counting how many neutrons go missing in their experiment. These "bottle" experiments store the ultra-cold neutrons in a magnetogravitational trap. They measure a neutron lifetime of $\tau_1 = (878.4 \pm 0.5)s$ [61–63].

The so called "beam" experiments are counting protons from neutrons decaying via the weak interaction. Their reported lifetime of the neutron is $\tau_2 = (887.7 \pm 2.3)s$ [64] resulting in a discrepancy of 3.8σ with the bottle experiments [64]. Taking the two results together, there seem to be more decaying neutrons than protons in the experiments.

There have been several ideas to explain the discrepancy between the two neutron lifetime measurements with new physics. The neutron could oscillate into a mirror neutron, thus disappearing from the experiment [59, 60, 65, 66]. Another idea is that the neutron has a new decay channel into new hypothetical particles. If the decay products do not include the proton, this could explain the different lifetimes [67] (this was also discussed in the context of cosmology [68]). However, there are also arguments that the bottle experiment is measuring the correct neutron lifetime and the beam experiments will shift towards that value in future experiments, thus questioning the need for new physics to explain the neutron lifetime puzzle [69].

No matter what the answer to the discrepancy is, the possibility of neutrons oscillating with a bulk fermion and thus dissapearing into the extra dimensions adds even more motivation for further measurements of the neutron lifetime with higher precision.

2.8 Baryon and Lepton Number

Since baryon and lepton number are global symmetries, they do not have to be confined to the Standard Model brane. One important ingredient for trapping the gauge charges on the brane was a gauge boson that is in the Coulomb phase on the brane and in the confinement phase in the bulk. Since there is no gauge boson associated with baryon or lepton number, extra-dimensional fields that carry baryon or lepton number can propagate in all dimensions. Hence, we can assign the extra dimensional fermion ψ a baryon and/or lepton number charge.

The interaction with the neutrino, Eq. (2.54), conserves lepton number if we assign ψ a leptonic charge of one. In the same way, the interaction with the neutron in Eq. (2.77) can preserve baryon number if the ψ carries one unit of baryon number charge.

If the ψ couples to both the neutrino and the neutron, there is only a combination of baryon and lepton number that is preserved. Taking the interactions from Eq. (2.54) and (2.77) preserves $B + L$ and breaks $B - L$. However, if the neutron or the neutrino couples the the conjugate ψ^*, the unbroken symmetry is $B - L$ while $B + L$ is broken.

Even though the global charges are conserved in $4 + N$ dimensions, in the effective 4-dimensional theory, processes like neutron disappearance take away baryon number from our brane. This is similar to the violation of global charges on the brane due to baby branes capturing global charges and taking them into the extra dimensions [28].

There is also the possibility of gauging the $B - L$ symmetry in all dimensions [8]. The exchange of a gauge boson of $B - L$ results in a gravity-competing force.

In general, the bulk fermion can also have a Majorana mass, $\mu_M \psi^T C \psi$. If we include this term, any global charge carried by ψ is broken. For example, if the ψ interacts with the neutron and thus carries baryon number charge, then baryon number is broken by two units by the Majorana mass term. This can have the interesting effect of neutron-antineutron oscillations. We expect the neutron dissappearance rate and the probability of $n - \overline{n}$ oscillations to become correlated in this case. However, this is not studied in detail in this thesis.

2.9 Phenomenological Constraints

2.9.1 Constraints from Cosmology

Bounds on the ADD model from Astrophysics and Cosmology can constrain the parameters of the model and therefore test if it is phenomenologically viable. First discussed in [9], they provide a list of constraints to check the consistency of the model, including bounds from expansion dominated cooling, big bang nucleosynthesis (BBN) and overclosure of the universe by KK gravitons and more. In the following, we will describe some of their bounds.

Gravitons

When including Large Extra Dimensions, the cosmology of the early universe is very different from the standard picture. The highest possible temperature which we can use to describe our $4 + N$-dimensional spacetime is $M_f \sim 10$ TeV. Above this temperature, gravity becomes strong and there should be a theory of quantum gravity. The mechanism for stabilizing the radii of the extra dimensions can affect the cosmology of the early universe even below temperatures of M_f.

However, since the expansion rate of the universe during BBN is well-known and correctly predicting the abundances of light elements, the stabilization of the extra-dimensional radii has to happen before BBN, which happens at a temperature ~ 1 MeV. Even though the evolution of the universe is unclear for temperatures higher than $\sim$ MeV, BBN provides important bounds on the "normalcy temperature" T_*, which is the temperature up to which the evolution of the universe is "normal". With "normal", it is meant that the stabilization of the radii has happened and the size of the extra dimensions are fixed. The evolution of the universe below T_* goes on in the usual way.

The production of KK gravitons in the early universe changes the cooling of the universe during BBN. In the normal picture, the universe cools down, i.e. reduces energy density, by expansion,

$$\left.\frac{d\rho}{dt}\right|_{\text{expansion}} \sim -3H\rho \sim -3\frac{T^2}{M_P^2}\rho. \tag{2.126}$$

However, when KK gravitons are produced in the early universe, they can take away energy from our brane into the bulk. Thus, they can also contribute to the cooling

of the universe and we need to make sure that this constribution is smaller than the one from the expansion. The cooling rate from energy loss due to KK gravitons escaping in the extra dimensions is

$$\left.\frac{d\rho}{dt}\right|_{\text{evaporation}} \sim -\frac{T^{n+7}}{M_f^{n+2}}. \tag{2.127}$$

We require the cooling of the universe to be dominated by expansion, so that we find an upper bound on the normalcy temperature T_*,

$$T_* \lesssim \left(\frac{M_f^{n+2}}{M_P}\right)^{\frac{1}{n+1}}, \tag{2.128}$$

where we also used the assumption that the universe is radiation dominated, $\rho \sim T^4$. It was checked in [9] that the KK gravitons do not change the expansion rate from radiation to matter dominated during BBN. The most stringent bound is for two extra dimensions, $n = 2$, and $M_f \sim 10\,\text{TeV}$ which gives $T_* \lesssim 100\,\text{MeV}$. So, until a temperature 100 MeV, the cooling of the universe goes in the normal, expansion dominated way. Since this is above the BBN temperature, the cooling of the universe during BBN is unaffected by KK gravitons escaping in the extra dimensions.

Since KK gravitons interact weakly with particles on the SM brane, the lifetime of those KK gravitons is very large, making them long-lived. It was estimated that KK gravitons with mass ~ 100 MeV or lower live longer than the present age of the universe [9]. For the 4-dimensional observer, the KK modes are massive particles, thus their energy density scales like that of matter. Thus, KK gravitons are candidates for dark matter [9], which has also been discussed more recently in [70].

The strongest cosmological constraint comes from the requirement that the KK gravitons do not overclose the universe. This means that the energy density of the KK gravitons due to their production in the early universe is constrained by the critical density today. Since the KK gravitons' energy density scales as matter so that ρ_{grav}/T^3 constant during the evolution of the universe, we require ρ_{grav}/T_*^3 at the time of graviton production to be smaller than today's ρ_{crit}/T_0^3.

PDG [61] puts today's critical energy at $\rho_{crit} \sim 5{\cdot}10^{-6}\frac{\text{GeV}}{\text{cm}^3}$ and today's temperature at $T_0 \sim 2.7\,\text{K}$. Then the invariant is $\rho_{crit}/T_0^3 \sim 2 \times 10^{-9}\,\text{GeV}$, as also explained in [9]. Thus, we require

$$\rho_{grav}/T_*^3 \lesssim 2 \times 10^{-9}\,\text{GeV}. \tag{2.129}$$

The number density of KK gravitons produced from photons on the SM brane was estimated to be $T_*^{n+4} M_P/M_f^{n+2}$ [9]. Since their energy is equal to the temperature at which they are produced T_*, the energy density is $\rho_{grav} \sim T_*^{n+5} M_P/M_f^{n+2}$. For $n = 2$ and $M_f \sim 10\,\text{TeV}$, this puts a bound on the temperature $T_* \lesssim 1\,\text{MeV}$. Thus, for these parameters, the normalcy temperature is of the same order as the BBN temperature.

Bulk Fermions

Cosmological bounds from a bulk fermion interacting with a neutrino are less constraining than the bounds from KK gravitons [10]. The KK modes of the bulk

fermion are produced from their interaction with the active neutrino on the brane with coupling strength m_D. The total rate of KK modes of the bulk fermion compared with the rate of neutrino production Γ_ν is

$$\frac{\Gamma_{bulk}}{\Gamma_\nu} \sim \left(\frac{m_D}{T}\right)^2 TR, \tag{2.130}$$

where the first part comes from the production of a single KK mode and TR is the multiplicity of modes with energy smaller than T.

The bulk fermion decouples when its production rate is smaller than the expansion rate $\Gamma_{exp} \sim T^2/M_P$. This relates the usual neutrino decoupling temperature $T_\nu \sim 1\,\text{MeV}$ to the decoupling of the bulk fermion temperature, $T_{bulk} \sim 200\,\text{GeV}$. Thus, the bulk fermion is not in thermal equilibrium with SM particles during BBN.

Interaction with Neutrons

With our bulk fermion interacting with a neutron, it is even less constraining than the neutrino case. This is because the mass of the KK modes that dominantly interact with the neutron is much heavier than the BBN temperature.

If the fermion has a mass μ in the extra dimensions, so that the mass of the KK modes is given by Eq. (2.21), the bulk fermion is not thermally produced by scattering with quarks below temperatures of its mass. In this case, the constraints from BBN are even weaker.

Apart from the constraints, our scenario has other cosmological implications. First, the interaction of a neutron with a bulk fermion can potentially explain baryogenesis similar to [28]. They offer a natural mechanism for explaining the baryon asymmetry in our universe: The missing baryon number charge is carried away into the bulk. The observer on the SM brane then notices that there is nonzero baryonic charge on the brane, while the missing charge is in the extra dimensions.

Thus, the first Sakharov condition, baryon number violation, can be replaced by a bulk fermion hiding the baryonic charge in the extra dimensions. To explain baryogenesis, we still need the other two Sakharov conditions, CP violation and an out-of-equilibrium state.

Thus, the bulk fermion has to be produced from SM baryons in an out-of-equilibrium process. The inverse process, a bulk fermion turning into SM particles on the brane, is highly suppressed.

Second, the bulk fermion is a dark matter candidate, similar to KK gravitons as dark matter. Since the interaction of the bulk fermion with the SM particles is suppressed, the bulk fermion is long-lived.

To estimate the lifetime of the bulk fermion we consider the decay channel $\psi \to n\pi^0$. This comes from a 4-dimensional effective operator $g\psi n\pi^0$, with coupling strength $g \sim \Lambda^2/(M_P M_f)$, where we set $M_* = M_f$. Of course, this decay requires $m_\psi \gtrsim m_n + m_\pi$, so that this is the decay of KK modes with masses of at least$\sim$ GeV. With $M_f \sim 10\,\text{TeV}$ and $\Lambda \sim \text{GeV}$, the decay rate of this process is $\Gamma \sim m_\psi 10^{-46}$. Thus the lifetime of the KK modes is $\tau_\psi \sim 10^{46}/m_\psi$. This result is not significantly changed when including other decay channels.

Thus, the KK modes with masses $m_\psi \lesssim 10^5$GeV have a longer lifetime than the universe and can be dark matter. These modes still have to be produced in the early universe in the right abundance to serve as dark matter. They can be produced in different ways, for example thermally by rescattering of SM particles into ψ or nonthermally by the decay of the inflaton. The exact production mechanism is model dependent and a viable and predictive model can be studied further.

2.9.2 Collider Constraints

The bulk fermion could potentially be produced in high energy collisions of SM particles. One possible process is $pe^- \to \psi\nu$, similar to the proton decay by the weak interaction plus an exchange of a virtual neutron.

Since the bulk fermion couples only to neutrons, the constraints coming from production of KK gravitons, which couple to all SM particles, at colliders should be more constraining.

We expect to see gravitational signatures [41–45] from the ADD model before detecting energy loss from the production of bulk fermions.

This could be studied further in the future.

2.10 Summary and Outlook

In this chapter, we showed that neutron experiments present a new way of testing large extra dimensions by a unique spectroscopy of the Kaluza-Klein tower of a bulk fermion.

In general, the neutron is a great candidate to explore new physics with ultra-feeble interactions to the Standard Model, e.g. with gravitational strength. Because of the hierarchy problem, models with a large number of species are extremely interesting, such as the ADD model [7, 8] or a model with many copies of the Standard Model [36–38]. A study of neutron oscillations with many copies of the Standard Model has been performed previously [36]. Our study is the first to consider neutron oscillations into large extra dimensions.

The bulk fermion, that the neutron oscillates with, can be the same fermion that gives a small mass to the neutrino via the mechanism proposed in [9, 10]. However, this would mean that the bulk fermion is massless in the extra dimensions, in which case the constraints from bound neutron disappearance the main effect.

If the bulk fermion has a mass in the extra dimensions that is above the bound neutron mass and below the free neutron mass, the constraints from bound neutron disappearance are lifted. Then, only the free neutron can oscillate with the bulk fermion.

In general, because of the small spacing of energy levels in the KK tower, neutrons in different energy states all find an oscillation partner. We can use this in free neutron experiments to our advantage: By increasing the magnetic field in small steps, we can make sure that the system is in resonance for a specific range of parameters.

This magnetic resonance imaging of the KK tower gives a unique signature in the neutron disappearance amplitude, with a repetitive resonance pattern corresonding to states in the KK tower.

Recent experiments [11, 55] are already testing this setup and put bounds on the parameter range of the ADD model. Especially the experiment that is increasing the magnetic field in small steps [11] is testing a resonance regime that is interesting for the mass splitting corresonding to two large extra dimensions.

In the future, neutron experiments with a wider range and smaller steps of the magnetic field have a unique opportunity to perform precision spectroscopy of the KK tower.

Chapter 3

Cosmic Strings and Domain Walls of the QCD Quark Condensate

In this chapter, we investigate the topological defects that arise in the phase transiton of Quantum Chromodynamics (QCD). QCD has an approximate global symmetry, the chiral symmetry of quarks, which is spontaneously broken when the quarks confine at the QCD scale $\Lambda_{\rm QCD}$. This gives rise to domain walls bounded by strings that wind in the phases of the QCD quark condensate. These topological defects are unstable and when they collapse, can be a source for gravitational waves and electromagnetic radiation.

Across a domain wall, the phases change by 2π, which is why we call them 2π-domain walls. The winding of the phases takes place in the direction of the uncharged pseudo-Nambu-Goldstone bosons, for example η' and π^0.

QCD with massive quarks has a small value puzzle: The effective vacuum angle, which is responsible for CP violating effects, is constrained by experiments to be tiny or even zero. This is the strong CP puzzle, which is solved by introducing a hidden axion [12, 13] that dynamically relaxes the vacuum angle to zero. It is the Goldstone boson of a spontaneously broken anomalous Peccei-Quinn symmetry [14, 15].

In the standard picture of axion cosmology, the spontaneous breaking of the Peccei-Quinn symmetry gives rise to axionic strings. When QCD confines, the strings become boundaries of domain walls. The string-wall systems of the η' are verly similar to axionic defects. This is because the η' is the axion in the massless quark solution of the strong CP puzzle and with explicit mass terms, it is a poor-quality axion.

We will show that, when taking into account the mixing of the hidden axion with the pseudo-Goldstone bosons of QCD, the axionic strings are accompanied by windings in the phases of the quark condensate. This can affect the superconductivity [16] and anomaly inflow [17, 18] properties of axionic strings.

The string-wall systems of pure QCD can exist without a hidden axion. In fact, the pure QCD defects can play an important role in the cosmology of the early universe.

We also discuss the possibility of producing the string-walls in heavy-ion colliders.

3.1 QCD and the Strong CP Puzzle

QCD is the theory of the strong interactions and is based on the gauge group $SU(3)$. Therefore, it has 8 gauge bosons, the gluons, with field strength $G^a_{\mu\nu}$. Because the gauge group is non-abelian the gluons self-interact.

The quarks of the Standard Model are charged under QCD and transform in the fundamental representation. At energies below the QCD confinement scale Λ_{QCD}, the quarks confine and they are no longer good degrees of freedom. At low energies, QCD describes the physics of baryons, e.g. protons and neutrons, and mesons, e.g. pions.

In this section, we explain how the chiral symmetry of QCD is broken by the quark condensate and how to get the low-energy theory of baryons and mesons. It is based on several reviews and books [71–73].

3.1.1 Chiral Symmetry Breaking

In this section we discuss the spontaneous breaking of the global chiral symmetry in QCD. Since the chiral symmetry is explicitly broken by quark masses, it is only an approximate symmetry for light quarks. Thus, for this discussion, we can neglect the heavy quarks: charm, bottom and top. They all have masses much higher than the QCD confinement scale Λ_{QCD}, which makes them irrelevant for the chiral symmetry. For simplicity, we will even leave out the strange-quark, as it is much heavier than the up and the down quark.

For now, we assume that the up- and the down- quark are massless. This is a good approximation, since their masses are much lower than the confinement scale, $m_u, m_d \ll \Lambda_{\text{QCD}}$. The massless quarks are denoted by ψ_i, $i = 1, 2$. This could be generalized to N_f flavors of massless quarks, but for simplicity we take $N_f = 2$. The Lagrangian of QCD with two massless quarks is

$$\mathcal{L}_{\text{QCD}} = -\frac{1}{4} G^a_{\mu\nu} G^{\mu\nu,a} + \theta \frac{g^2}{32\pi^2} G^a_{\mu\nu} \tilde{G}^{\mu\nu,a} + \mathrm{i}\overline{\psi}_i \not{D} \psi_i. \tag{3.1}$$

The first term is the kinetic term for the gluons, including the gluon field strength tensor $G^a_{\mu\nu}$. The second term is a boundary term for which we introduce the dual of the gluon field strength, $\tilde{G}^a_{\mu\nu} = \epsilon_{\mu\nu\alpha\beta} G^{\alpha\beta,a}$. This term is a boundary term, so for now we assume that it has no influence on the dynamics of the theory and we set $\theta = 0$. The third term is the kinetic term for the massless quarks.

This Lagrangian has a global flavor symmetry under which the quarks transform as

$$\psi_L \to L\psi_L \text{ with } L \in U(2)_L, \tag{3.2}$$

$$\psi_R \to R\psi_R \text{ with } R \in U(2)_R. \tag{3.3}$$

This is a chiral symmetry because the left- and right-handed fields transform differently, and thus, we call it the chiral symmetry. The chiral symmetry can also be

written with vector and axial symmetries,

$$U(2)_L \times U(2)_R \simeq SU(2)_V \times SU(2)_A \times U(1)_V \times U(1)_A. \tag{3.4}$$

For the vector symmetries $SU(2)_V$ and $U(1)_V$ we set $L = R$. The $U(1)_V$ vector symmetry is the subgroup with $L = R = e^{\mathrm{i}\alpha}\mathbb{1}$. It transforms the left- and right-handed quarks with the same phase, i.e., for a Dirac field

$$\psi \to e^{\mathrm{i}\alpha}\psi. \tag{3.5}$$

For every symmetry, there is a conserved charge. For the $U(1)_V$, this conserved charge is the quark number which is up to a factor the same as baryon number. The unbroken $SU(2)_V$ is isospin, classifying hadrons: the proton and neutron form a doublet and the pions a triplet. From experiments we know that both vector symmetries are good symmetries of nature. Thus, they are not spontaneously broken.

When we include quark masses, the vector symmtries get explicitly broken. However, since the quark masses are small compared to the QCD scale, we can treat these symmetries as approximate.

The axial symmetries are defined by setting $L = R^\dagger$. The axial $U(1)_A$ comes from setting $L = R^* = e^{\mathrm{i}\alpha}\mathbb{1}$, thus transforming left- and right-handed quarks with opposite phases, or equivalently

$$\psi \to e^{\mathrm{i}\alpha\gamma_5}\psi. \tag{3.6}$$

There are no low-energy symmetries or conserved charges corresponding to the axial symmetries. Thus, they have to be spontaneously broken in the low-energy theory.

When QCD confines, the quark condensate $\langle\overline{\psi}_L\psi_R\rangle$ gets a vacuum expectation value. The combination $\overline{\psi}_L\psi_R$ breaks $SU(2)_A$ but conserves $SU(2)_V$, which is exactly what we want. The VEV is

$$\langle\overline{\psi}_L\psi_R\rangle = -\Lambda^3_{\mathrm{QCD}}. \tag{3.7}$$

This spontaneously breaks the global symmetry down to its diagonal subgroup, the vector symmetries. So, $SU(2)_A$ and $U(1)_A$ are spontaneously broken. The origin of the VEV is nonperturbative and it is the confinement scale Λ_{QCD}.

Goldstone's theorem tells us that there will be $N_f^2 - 1$ Nambu-Goldstone bosons corresponding to the breaking $SU(N_f)_L \times SU(N_f)_R \to SU(N_f)_V$. For $N_f = 2$, these are the three pions. When we also include a third quark $N_f = 3$, the eight Goldstones are the pions, the kaons and the η-meson. There is a ninth Goldstone from the spontaneous breaking of the $U(1)_A$, called the η'.

To understand the effective theory, we expand around the VEV

$$\overline{\psi}_R\psi_L = -\Lambda^3_{\mathrm{QCD}}U(x) \tag{3.8}$$

where

$$U(x) = \exp\left(\frac{2\mathrm{i}\pi^a}{f_\pi}T^a + \mathrm{i}\frac{\pi^9}{f_9}\mathbb{1}\right) \tag{3.9}$$

The $T^a = \sigma^a/2$, with $a = 1, 2, 3$, are the three generators of $SU(2)$, σ^a being the three Pauli matrices. The Goldstone bosons are π^a and π^9 corresponding to the breaking of $SU(2)_A$ and $U(1)_A$ respectively. The f_π and f_9 are the decay constants.

We can now construct the low-energy theory by knowing the transformation properties of the field U: under the chiral symmetry from Eq. (3.2), $U \to LUR^\dagger$. The effective Lagrangian invariant under the chiral symmetry is

$$\mathcal{L} = -\frac{1}{4} f_\pi^2 \mathrm{Tr}\partial_\mu U^\dagger \partial^\mu U - \frac{1}{4} F^2 \partial_\mu (\det U^\dagger) \partial^\mu (\det U), \tag{3.10}$$

where F is a parameter that we chose to canonically normalize the fields.

After plugging in the above expression for U we see that the first term includes kinetic terms for the π^a and the π^9, while the last term only contributes to the kinetic term of η'. Thus, by choosing F^2 appropriately, we canonically normalize the π^9. Then, the Lagrangian is

$$\mathcal{L} = \frac{1}{2}\partial_\mu \pi^a \partial^\mu \pi^a + \frac{1}{2}\partial_\mu \pi^9 \partial^\mu \pi^9 + \ldots, \tag{3.11}$$

where the dots stand for an expansion in ∂_μ / f_π, so higher-derivative terms.

We can now add the quark masses of the up- and down-quarks, m_u and m_d. In a compact notation, we write them in a mass matrix $M_q = \mathrm{diag}(m_u, m_d)$, so that in the Lagrangian we have

$$\mathcal{L}_m = -\overline{\psi}_L M_q \psi_R + \text{h.c.}. \tag{3.12}$$

This term explicitly breaks the axial symmetries and thus the Goldstones get masses. In terms of $U(x)$, the Lagrangian can be expressed as

$$\mathcal{L}_m = \frac{v^3}{f_\pi^2} \mathrm{Tr}(M_q U + M_q^\dagger U^\dagger) \tag{3.13}$$

This gives a contribution to the pion masses $m_\pi^2 = 2v^3 \mathrm{Tr}(M_q)/f_\pi^2$. Since electromagnetism also explicitly breaks the axial $SU(2)_A$, only the charged pions get another mass contribution.

The η' also gets a mass from the quark mass terms. In [74] they perform the diagonalization of the mass matrix inlcuding the π^a and π^9 and show that for the physical states, $m_{\eta'} \lesssim \sqrt{3} m_\pi$. However, experimentally, the η' was nowhere to be found. The missing ninth Goldstone was called the $U(1)_A$ problem [75].

The solution is that the $U(1)_A$ symmetry is anomalous, which we discuss in the next part.

3.1.2 The Anomalous $U(1)_A$

When a symmetry is anomalous, this means it is a good symmetry on the classical level but it is broken by quantum effects. The anomaly of $U(1)_A$ can be understood in terms of the non-conservation of its current J_5^μ,

$$\partial_\mu J_5^\mu = \frac{N_f g^2}{16\pi^2} G^a_{\mu\nu} \tilde{G}^{\mu\nu,a}, \tag{3.14}$$

which is the Adler-Bell-Jackiw anomaly [76–78].

The axial $U(1)_A$ transformation on the quarks was already discussed in Eq. (3.6). Explicitly writing the left- and right-handed quarks, we see that they transform differently,

$$\psi_L \to e^{-\frac{\mathrm{i}\alpha}{2}}\psi_L \text{ and } \psi_R \to e^{\frac{\mathrm{i}\alpha}{2}}\psi_R. \tag{3.15}$$

Even though the Lagrangian of QCD with massless quarks from Eq. (3.1) looks invariant under this transformation, the measure in the path integral is not invariant. Thus, the axial tranformation effectively shifts the Lagrangian as

$$\mathcal{L}_{\mathrm{QCD}} \to \mathcal{L}_{\mathrm{QCD}} + \alpha\frac{g^2}{32\pi^2}G\tilde{G}. \tag{3.16}$$

This last term is a boundary term and it is very similar to the θ-term that we neglected earlier. So, effectively we can describe this transformation as $\theta \to \theta + \alpha$.

Even though the θ-term is a boundary term, it has a physical effect. One way to see this in the low-energy theory is with 't Hooft's instanton mechanism [79–81]. 't Hooft showed that instantons generate a new term in the effective Lagrangian which breaks the $U(1)_A$ explicitly,

$$\mathcal{L}_{\text{'tHooft}} = e^{\mathrm{i}\eta'}\det U + \text{h.c.}. \tag{3.17}$$

This new term is called the 't Hooft determinant and it generates a potential for η'. In the dilute instanton gas approximation, the potential is

$$V(\eta') = -\Lambda_{\mathrm{QCD}}^4\cos(N_f\theta_\eta - \theta), \tag{3.18}$$

where $\theta_\eta(x) = \frac{\eta'(x)}{\sqrt{2}f_\eta}$ is the phase degree of freedom of the quark condensate. In a realistic scenario, the number of light quarks is three and the decay constant of the η' is $f_\eta \sim \Lambda_{\mathrm{QCD}}$.

The potential adds a new contribution to the mass of η', $m_\eta \sim \Lambda_{\mathrm{QCD}}^2/f_\eta$. Since the η' now has a mass that is much heavier than the mass if the other Goldstone bosons, the $U(1)_A$ problem is solved.

3.1.3 Instantons and θ-Vacua

Even though we do not discuss all details about instantons, let us say a few more words. We mostly use [74] as a reference.

Instantons [82] are non-perturbative solutions to the euclidean equations of motion and describe the tunneling process between different minima of QCD that have the same energy. In fact, QCD has an infinite number of degenerate classical minima $|\,n\rangle$ that are labeled by an integer n which is the winding number. Because of instantons the amplitude for tunneling between two minima is non-zero.

Thus, the true vacuum in the quantum theory, which we denote by $|\,\theta\rangle$, is a superposition of all these minima

$$|\,\theta\rangle = \sum_{n=-\infty}^{\infty} e^{\mathrm{i}n\theta}\,|\,n\rangle\,. \tag{3.19}$$

The true vacuum is labeled by the parameter θ, called the valuum angle, which has a constant value between 0 and 2π.

Different θ-vacua are orthogonal to each other, since for any operator $\mathcal{O}$ acting on the physical Hilbert space, it can be shown that

$$\langle \theta \,|\, \mathcal{O} \,|\, \theta' \rangle = 0. \tag{3.20}$$

Because the θ-vacua are orthogonal to each other, the Hilbert space can be decomposed into superselection sectors that each correspond to a different value for θ. Thus, QCD has a continuum of vacua which are labeled by θ [83, 84].

This has several physically measurable effects: First, the vacuum energy depends on the global fundamental constant θ. In fact, the vacuum energy is periodic in θ, which is plotted in Figure 3.1. Vafa and Witten [85] showed that the global minimum of the vacuum energy is at $\theta = 0$.

Second, the θ-term in the Lagrangian has physical effects. It violates CP, which is a combined charge and parity transformation. We will discuss the effects of CP violation due to the θ-term on the electric dipole moment of the neutron in the next part about the strong CP puzzle.

Another physical effect of the θ-term was discussed in the previous section. Instantons generate a potential for η', which adds a new mass contribution. In this way, the experimentally measured mass of η' proves that θ vacua exist.

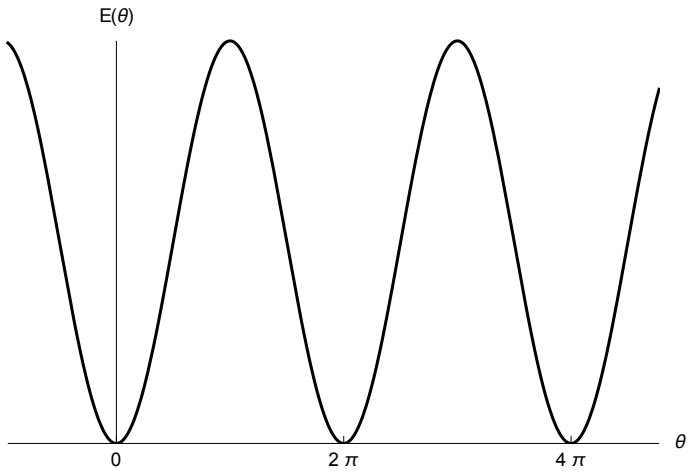

Figure 3.1: A qualitative sketch of the dependence of the vacuum energy of QCD on θ.

3.1.4 Strong CP Puzzle

The θ-term violates CP and, thus, is a measure of CP violation in the strong interaction. Actually, when we include masses for the light quarks, the parameter measuring CP violation is $\bar{\theta} \equiv \theta + \arg(\det M_q)$, where $\arg(\det M_q)$ is defined as the phase of the determinant of the quark mass matrix.

One measurable quantity that is sensitive to the CP violation is the electric dipole moment of the neutron (nEDM) [86, 87]. Theoretical calculations of the nEDM, which we denote as d_n, predict $d_n \approx 10^{-16}\bar{\theta}$e cm [86, 87], while experiments measure $d_n \lesssim 10^{-26}$e cm [88–90]. Therefore, these experiments put a bound on $\bar{\theta}$,

$$|\bar{\theta}| \lesssim 10^{-10}. \tag{3.21}$$

Other contributions to the nEDM coming from CP violation in the weak interaction [91–93] are much smaller than the experimentally measured value and do not affect the bound on $\bar{\theta}$.

This leads us to a small value puzzle: Why do we live in a sector with tiny or even zero $\bar{\theta}$? This is the strong CP puzzle.

3.2 QCD Axion

The axion solves the strong CP problem by promoting θ to a dynamical field. It has a minimum in its potential at $\theta = 0$, such that it relaxes to this value at which there is no CP violation.

We need a new field $a(x)$ that has a $G\tilde{G}$ coupling similar to the theta term,

$$\mathcal{L} \supset \frac{a}{f_a}\frac{g^2}{32\pi^2}G^a_{\mu\nu}\tilde{G}^{\mu\nu,a}. \tag{3.22}$$

It is important that a has a shift symmetry, which means it can only have additional terms depending on $\partial_\mu a$.

The effective vacuum angle, $\theta_{\text{eff}}(x) = a(x)/f_a + \bar{\theta}$, is dynamical and falls into the minimum of its potential which is at $\theta_{\text{eff}} = 0$ [85]. This explains the absence of CP violation in the strong interaction in accordance with nEDM experiments. The axion is also a very promising dark matter candidate, since it is weakly interacting with Standard Model fields.

3.2.1 Peccei-Quinn Solution

In the Peccei-Quinn solution [14, 15], the axion a is the Goldstone boson of a global anomalous $U(1)_{PQ}$ symmetry. In fact, Peccei and Quinn introduced this new symmetry without realizing that their model predicted a new light particle, the axion. This was noticed by Wilczek and Weinberg [12, 13].

For simplicity, we consider a single quark flavor, Ψ, that transforms under this new $U(1)_{PQ}$ symmetry

$$\Psi \to e^{-\frac{i\alpha\gamma_5}{2}}\Psi. \tag{3.23}$$

Just as for the $U(1)_A$ symmetry, the $U(1)_{PQ}$ is anomalous since its current $J^\mu_{PQ} = \bar{\Psi}\gamma_\mu\gamma_5\Psi$ is not conserved,

$$\partial_\mu J^\mu_{PQ} \propto G\tilde{G}. \tag{3.24}$$

Because of the anomaly, the Lagrangian is not invariant under $U(1)_{PQ}$, instead it shifts as

$$\mathcal{L} \to \mathcal{L} + \alpha G\tilde{G} \tag{3.25}$$

Thus, the constant $\bar{\theta}$ can be removed by the appropriate $U(1)_{PQ}$ transformation. Effectively, the shift in the Lagrangian corresponds to a shift in $\bar{\theta}$, so that

$$\bar{\theta} \to \bar{\theta} - \alpha. \tag{3.26}$$

If we choose the transformation with $\alpha = \bar{\theta}$, this term vanishes in the Lagrangian which indicates that it is unphysical.

We assume that the quark Ψ is a new field, so not a Standard Model field. In this case, the Ψ has to get a mass that is much heavier than the mass of Standard Model particles. For this, we introduce a new complex scalar field $\Phi(x) = \rho(x)e^{\mathrm{i}\theta_\phi(x)}$. We call Φ the Peccei-Quinn field and it transforms under the $U(1)_{PQ}$ as

$$\Phi \to e^{\mathrm{i}\alpha}\Phi. \tag{3.27}$$

The Peccei-Quinn field has a potential

$$V(\Phi) = \lambda^2(\Phi^*\Phi - f_\phi^2)^2, \tag{3.28}$$

where the λ is a coupling constant. Thus, the modulus of the scalar field gets a VEV, $\langle\rho\rangle = f_\phi$, and breaks the $U(1)_{PQ}$ spontaneously.

The scalar field couples to the quark through a Yukawa coupling and when it gets a VEV, it gives a mass to the quark. The Lagrangian for the quark is

$$\mathcal{L}_\Psi = i\bar{\Psi}_{L,R}\gamma^\mu D_\mu \Psi_{L,R} - g_\Psi \Phi^*\, \bar{\Psi}_L \Psi_R + \text{h.c.}, \tag{3.29}$$

where we have split the Dirac spinor in left- and right-handed components, $\Psi = \Psi_L + \Psi_R$. The mass of the quark after symmetry breaking is $M_\Psi = g_\Psi f_\phi$, where g_ψ is the Yukawa coupling constant.

The axion is the Nambu-Goldstone phase of the Peccei-Quinn field, θ_ϕ. In terms of the canonically normalized field ϕ, it can be rewritten as $\theta_\phi(x) \equiv \phi(x)/(\sqrt{2}f_\phi)$.

The modulus field that gets a VEV becomes heavy. In the effective theory below the Peccei-Quinn scale, the axion has the following Lagrangian

$$\mathcal{L}_{\text{axion}} = f_\phi^2(\partial_\mu\theta_\phi(x))^2 - \left(\theta_\phi(x) - \bar{\theta}\right) G\tilde{G}. \tag{3.30}$$

Here, we can define the effective vacuum angle $\theta_{\text{eff}}(x) := \theta_\phi(x) - \bar{\theta}$, which becomes dynamical because of the axion. The axion relaxes the effective vacuum angle to its minimum, which is at $\theta_{\text{eff}} = 0$ [85].

That the minimum is at $\theta_{\text{eff}} = 0$ can be seen in the dilute instanton gas approximation. The instantons generate a potential for the axion,

$$V(\theta_\phi) = -\Lambda_{\text{QCD}}^4 \cos\left(\theta_\phi(x) - \bar{\theta}\right), \tag{3.31}$$

In the original Peccei-Quinn model, the quarks that transformed chirally under $U(1)_{PQ}$ as in Eq. (3.23) are the Standard Model quarks. To also keep the Lagrangian invariant under the Standard Model gauge symmetries, it is required to introduce a second Higgs doublet. However, since the Higgs doublets are responsible for electroweak symmetry breaking, the Peccei-Quinn scale, which is the scale at which the $U(1)_{PQ}$ is broken, is the electroweak scale. This is excluded from experiments since the axion would couple too strongly to the Standard Model fields.

Thus, hidden axion models where the Peccei-Quinn scale is much higher, resulting in much weaker interactions of the axion with the Standard Model particles, are more realistic scenarios. The two most common hidden axion models are the KSVZ model, named after Kim, Shifman, Vainshtein and Zakharov [94, 95] and the DFSZ model, after Dine, Fischler,Srednicki and Zhitnitsky [96, 97].

3.2.2 η' as Poor Quality Axion

Let us again consider QCD with massless quarks. In this case, the η' meson of QCD is the axion and the strong CP problem is solved because the θ angle is unphysical. When the quark masses are turned on, we will see that the η' is a poor quality axion and that, to solve the strong CP puzzle, we need an additional QCD axion.

Eq. (3.1) shows the Lagrangian of QCD with massless quarks. The key to the massless quark solution to the strong CP problem is the anomalous axial $U(1)_A$ symmetry.

As discussed in subsection 3.1.2, the instantons generate a potential for η', given in Eq. (3.18). Just like in the PQ solution to the strong CP problem, the effective vacuum angle $\theta_{\text{eff}}(x) = N_f\theta_\eta - \theta$ becomes dynamical. When η' minimizes the potential, the effective vacuum angle is zero. This shows that the η' is nothing but an axion [98–100]!

However, in the real world all quarks are massive [101]. Because the quark masses explicitly break $U(1)_A$, the η' cannot enforce $\theta_{\text{eff}} = 0$.

This can be seen from the effective theory of the η'. For simplicity, we will consider QCD with a single quark that has a mass term

$$m_\psi \bar{\psi}_L \psi_R + \text{h.c.}. \tag{3.32}$$

This adds a new term to the effective potential

$$V(\eta') = -\Lambda_{\text{QCD}}^4 \cos\left(\theta_\eta - \bar{\theta}\right) - \Lambda_m^4 \cos\left(\theta_\eta\right), \tag{3.33}$$

where $\Lambda_m^4 \simeq m_\psi \Lambda_{\text{QCD}}^3$. In the effective potential, we have rotated the phase of the quark mass θ_m into the $\bar{\theta} = \theta + \theta_m$.

When we minimize this effective potential, the minimum is at

$$\theta_\eta = \arctan\left(\tan(\bar{\theta})\left(1 + \frac{\Lambda_m^4}{\Lambda^4 \cos(\bar{\theta})}\right)^{-1}\right). \tag{3.34}$$

Let us assume that the $\bar{\theta}$ is small so that we can approximate $\tan\bar{\theta} \approx \bar{\theta}$. The effective vacuum angle $\theta_{\text{eff}} = \theta_\eta - \bar{\theta}$ is not zero, but

$$\theta_{\text{eff}} \simeq -\frac{|m_\psi|}{\Lambda_{\text{QCD}}}\bar{\theta}. \tag{3.35}$$

Since the light quark mass is only a couple of orders of magnitude smaller than the QCD scale, $m_\psi/\Lambda_{\text{QCD}} \sim 10^{-2}$, the η' cannot explain the smallness of θ_{eff}. This shows that the η' is a poor quality axion. Thus, there has to exist a good-quality axion to solve the strong CP puzzle.

3.2.3 Coupled System

In this section we take a closer look at how the η' and the PQ axion show up together in the low-energy potential. The mixing between the two fields can be seen in a toy model with one light quark ψ and one heavy quark Ψ, which is the simplest example to understand the interplay between the two anomalous symmetries, $U(1)_A$ and $U(1)_{PQ}$.

The light quark ψ is responsible for the global chiral symmetry $U(1)_V \times U(1)_A$. Just like in the more realistic model with three generations of quarks, the $U(1)_A$ is spontaneously broken by the QCD condensate of the light quark, $\langle\overline{\psi}\psi\rangle = \Lambda^3_{\text{QCD}}$. The η' is the Goldstone boson of the $U(1)_A$ symmetry.

The heavy quark gets its mass from the spontaneous breaking of the $U(1)_{PQ}$ symmetry, broken by a PQ scalar field Φ. Thus, we are considering a KSVZ type axion [94, 95]. The PQ axion is the phase of the PQ field Φ.

The Lagrangian for QCD with one light quark ψ with mass m_ψ and one heavy quark Ψ is

$$\begin{aligned}\mathcal{L}_{\text{UV}} =& \partial_\mu\Phi^*\partial^\mu\Phi - \lambda^2(\Phi^*\Phi - f_\Phi^2)^2 + \\ &+ i\bar{\Psi}_{L,R}\gamma^\mu D_\mu\Psi_{L,R} - g_\Psi\Phi^*\bar{\Psi}_L\Psi_R + \text{h.c.} \\ &+ i\bar{\psi}_{L,R}\gamma^\mu D_\mu\psi_{L,R} - m_\psi\bar{\psi}_L\psi_R + \text{h.c.} - \\ &- G_{\mu\nu}G^{\mu\nu} + \bar{\theta}\, G_{\mu\nu}\tilde{G}^{\mu\nu},.\end{aligned} \tag{3.36}$$

For simplicity, we are ignoring irrelevant numberical factors in this expression. The first line is the kinetic term for the PQ field Φ and its potential which leads to a VEV $\langle|\Phi|\rangle = f_\phi$. The second line is the kinetic term for the heavy quark Ψ and a Yukawa type coupling to the PQ field. The third line is the kinetic term for the light quark ψ and its mass term, explicitly breaking the $U(1)_A$ symmetry. The last line is the kinetic term for the gauge bosons and the θ-term.

First, we consider the massless quark case, where $m_\psi = 0$. Second, we discuss the effects of the non-zero mass term.

Massless Quark Case

When the light quark is massless, $m_\psi = 0$, we ignore the explicit breaking of the $U(1)_A$ symmetry from the quark mass term. Thus, the global $U(1)$ symmetries of

the Lagrangian (3.36) are only explicitly broken by their anomalies. Since the $U(1)_V$ is neither explicitly nor spontaneously broken we can neglect it in this discussion and focus on the anomalous $U(1)_A$ and $U(1)_{PQ}$ symmetries.

When we consider both anomalous symmetries together, there is one special combination of both that is anomaly-free,

$$\Phi \to \mathrm{e}^{i\alpha}\Phi\,,\ \Psi \to \mathrm{e}^{i\frac{1}{2}\alpha\gamma_5}\Psi\,,\ \psi \to \mathrm{e}^{-i\frac{1}{2}\alpha\gamma_5}\psi\,. \tag{3.37}$$

For this transformation, the anomaly is canceled because the light and the heavy quark transform oppositely. In the spirit of the vector part of the chiral symmetry being anomaly-free, we will from now on call the symmetry in Eq. (3.37) $U(1)_V$[1].

The orthogonal transformation,

$$\Phi \to \mathrm{e}^{i\alpha}\Phi\,,\ \Psi \to \mathrm{e}^{i\frac{1}{2}\alpha\gamma_5}\Psi\,,\ \psi \to \mathrm{e}^{i\frac{1}{2}\alpha\gamma_5}\psi, \tag{3.38}$$

is anomalous. Thus, we will from now on call this anomalous symmetry $U(1)_A$.

The original $U(1)_A \times U(1)_{PQ}$ are reformulated as the new $U(1)_V \times U(1)_A$ symmetry. The relabeling was necessary to get all explicit breaking due to the anomalous nature of the symmetries into only one $U(1)_A$.

The $U(1)_V$ and $U(1)_A$ are both spontaneously broken by both the VEV of the PQ field $\langle|\Phi|\rangle = f_\phi$ and by the quark condensate $\langle\overline{\psi}\psi\rangle = \Lambda^3_{\mathrm{QCD}}$.

Both the PQ field and the quark condensate have a phase degree of freedom. In the low-energy theory, we expand around the VEVs with $\Phi = f_\phi e^{\mathrm{i}\theta_\phi}$ and $\overline{\psi}\psi = \Lambda^3_{\mathrm{QCD}} e^{\mathrm{i}\theta_\eta}$. The canonically normalized fields are the Nambu-Goldstone bosons ϕ and η', which are related to the phases through their decay constants

$$\theta_\phi = \frac{\phi}{\sqrt{2}f_\phi}\,, \quad \theta_\eta = \frac{\eta'}{\sqrt{2}f_\eta}. \tag{3.39}$$

Let write down the effective low-energy Lagrangian for the Goldstone bosons. Because of the anomaly of $U(1)_A$, there will be a term explicitly breaking this symmetry. Using the dilute instanton gas approximation, the low-energy Lagrangian is

$$\begin{aligned}\mathcal{L}_{\mathrm{eff}} = {} & f_\phi^2(\partial_\mu\theta_\phi\partial^\mu\theta_\phi) + f_\eta^2(\partial_\mu\theta_\eta\partial^\mu\theta_\eta) \\ & + \Lambda^4\cos\left(\theta_\phi + \theta_\eta - \bar{\theta}\right).\end{aligned} \tag{3.40}$$

Because the exact form of the potential is not important for our analysis, we can use the dilute instanton gas approximation, which gives the cosine potential. The important property of the potential is that it is periodic and has a minimum at $\theta_{\mathrm{eff}} = 0$.

Since the quark mass is set to zero, the $U(1)_V$ symmetry is not explicitly broken. Thus, we expect one combination of the Goldstone bosons which is massless, while

[1]The original vector symmetry is still there but since it is not interesting to us we reuse its label $U(1)_V$ as the anomaly free part of $U(1)_A \times U(1)_{PQ}$.

the orthogonal combination of Goldstones gets a mass from the explicit breaking due to the anomaly. This can be seen in the effective potential in Eq. (3.40): The combination $\theta_\phi + \theta_\eta$ gets a mass and therefore is the Goldstone phase belonging to the $U(1)_A$ symmetry.

The canonically normalized Goldstone boson, which we call a_η, is defined as

$$\theta_\phi + \theta_\eta = \frac{a_\eta}{\sqrt{2}\tilde{f}}. \tag{3.41}$$

The corresponding decay constant $\tilde{f}$ is $\tilde{f}^{-2} \equiv f_\phi^{-2} + f_\eta^{-2}$ which can be rewritten using

$$\tilde{f} \equiv \frac{f_\phi f_\eta}{f} \quad \text{and} \quad f = \sqrt{f_\phi^2 + f_\eta^2}. \tag{3.42}$$

With this definition of $\tilde{f}$ the canonically normalized fields are related through a rotation with an angle ξ,

$$a_\eta = \eta' \cos(\xi) + \phi \sin(\xi). \tag{3.43}$$

The rotation is defined by $\sin\xi = f_\eta/f$ and $\cos\xi = f_\phi/f$. From the hierarchy of the decay constants, $f_\phi \gg f_\eta$, it follows that the rotation angle is small, $\xi \simeq f_\eta/f_\phi \ll 1$ so that $f \simeq f_\phi$,$\tilde{f} \simeq f_\eta$, $\cos\xi \simeq 1$ and $\sin\xi \simeq \xi$. Thus, the Goldstone is mostly made up of η', which is why we labeled it with a_η,

$$a_\eta \simeq \eta' + \xi\phi. \tag{3.44}$$

Let us take another look at the cosine potential. Expanding in powers of the Goldstone a_η, this potential has a mass for a_η

$$m_\eta \simeq \frac{\Lambda^2}{f_\eta}. \tag{3.45}$$

Notice that a_η is responsible for canceling the vacuum angle, $\theta_{\text{eff}} = 0$. Thus, in the massless quark case, the axion is the a_η, which is mostly the η'-meson.

The orthogonal combination to a_η we denote as a_ϕ and is made up mostly of the phase of the PQ field ϕ. It is defined as

$$a_\phi \equiv \phi\cos(\xi) - \eta'\sin(\xi) \simeq \phi - \xi\eta'. \tag{3.46}$$

It is the Goldstone boson of the anomaly-free $U(1)_V$ and therefore, as expected, remains massless.

To summarize, in the massless quark case, the η'-meson cancels $\bar{\theta}$ and thus, is the axion. The phase of the PQ field ϕ stays massless and has nothing to do with the effective vacuum angle.

Massive Quark Case

We now investigate what happens when we include a non-zero mass for the light quark, $m_\psi \neq 0$. In this case, both the $U(1)_V$ and $U(1)_A$ are explicitly broken by the quark mass. Hence, the previously massless Goldstone boson gets a mass.

In the low-energy Lagrangian we need to include another term from the quark mass,

$$\begin{aligned}\mathcal{L}_{\text{eff}} = f_\phi^2(\partial_\mu\theta_\phi\partial^\mu\theta_\phi) + f_\eta^2(\partial_\mu\theta_\eta\partial^\mu\theta_\eta) \\ + \Lambda_{\text{QCD}}^4\cos\left(\theta_\phi+\theta_\eta-\bar{\theta}\right) + \Lambda_m^4\cos\left(\theta_\eta\right).\end{aligned} \tag{3.47}$$

Here, the scale in front of the last term is $\Lambda_m^4 \sim m_\psi\Lambda_{\text{QCD}}$.

There are a couple of important things to notice: First, the masses and the mass eigenstates get corrections from the quark mass term. We can diagonalize the mass matrix corresonding to the two fields ϕ and η'

$$\begin{pmatrix} \frac{\Lambda_{\text{QCD}}^4}{f_\phi^2} & \frac{\Lambda_{\text{QCD}}^4}{f_\phi f_\eta} \\ \frac{\Lambda_{\text{QCD}}^4}{f_\phi f_\eta} & \frac{\Lambda_{\text{QCD}}^4+\Lambda_m^4}{f_\eta^2} \end{pmatrix}. \tag{3.48}$$

The previous mass eigenstates a_η and a_ϕ from Eq. (3.44) and (3.46) get modified with $\sim \mathcal{O}(m_\psi/\Lambda_{\text{QCD}})$ corrections. This does not change that the mass eigenstates are mostly given by ϕ and η'. The masses of those states also get contributions proportional to the mass m_ψ, which is a correction for the a_η mass from Eq. (3.45),

$$m_\eta^2 \simeq \frac{\Lambda_{\text{QCD}}^4+\Lambda_m^4}{f_\eta^2}. \tag{3.49}$$

Most crucially, the a_ϕ now also gets a mass,

$$m_\phi \simeq \frac{\Lambda_m^2}{f_\phi}. \tag{3.50}$$

Remember that the mass eigenstate a_ϕ is the Goldstone of the $U(1)_V$ symmetry, which is only broken by the quark mass. Thus it makes perfect sense that its mass is proportional to the amount of explicit breaking, m_ψ.

Second, the effective vacuum angle is zero, since the minimum of the potential is at

$$\theta_\eta = 0\,, \quad \theta_\phi = \bar{\theta}. \tag{3.51}$$

The field responsible for canceling $\bar{\theta}$ and thus the axion is the phase of the PQ field θ_ϕ. So, the axion is a combination of the mass eigenstates, $\theta_\phi \sim a_\phi + \xi a_\eta$.

In the realistic case with nonzero quark masses, the ϕ field is important for solving the strong-CP puzzle. Without it, the η' only reduces the effective vacuum angle to $\theta_{\text{eff}} \sim m_\psi/\Lambda_{\text{QCD}}$, as discussed in Eq. (3.35). This value is still too large compared with the experimental value. Thus, introducing the field ϕ is necessary to reduce the effective vacuum angle to a phenomenologically viable value. When including the ϕ, it takes charge of reducing $\theta_{\text{eff}} = 0$.

3.3 Strings and Walls

In this section, we consider the topological defects that arise in the system of a coupled η' and axion. We first study the case with a massless quark, in which the η' is the axion, and then turn on the quark mass as a deformation of the theory.

In the usual picture, the Peccei-Quinn symmetry breaking gives rise to axionic strings. During the QCD phase transition, since instanton effects break the Peccei-Quinn symmetry explicitly, the axionic strings become the boundaries of domain walls, see for example in [102, 103].

In the coupled system, the spontaneous breaking of the $U(1)_V \times U(1)_A$ leads to cosmic strings. However, explicit breaking of these symmetries can deform these strings and result in domain walls bounded by strings.

3.3.1 Massless Quark Case

In the massless quark case, $m_\psi = 0$, the $U(1)_V$ is an exact symmetry, while the $U(1)_A$ is explicitly broken by the anomaly. If there was no anomaly, there would be no potential relating the two phase degree of freedom and the spontaneous symmetry breaking would allow two unrelated solutions for windings in the phase degree of freedom, i.e. cosmic string solutions.

The non-trivial winding around a straight infinite string in the z-direction can happen in the θ_η- and/or the θ_ϕ-direction. Introducing winding numbers n_η and n_ϕ, we can write these two solutions as

$$\theta_\eta = n_\eta \varphi\,, \quad \theta_\phi = n_\phi \varphi, \tag{3.52}$$

where φ is the angular coordinate in a polar coordinate system r, φ, z. Without the anomaly, the two lowest energy solutions with non-trivial winding would be $n_\eta = \pm 1$ and $n_\phi = \pm 1$.

However, with the $U(1)_A$ being anomalous, the two windings become correlated. This can be seen in the low-energy effective Lagrangian (3.40), where the two phases are linked through the cosine potential. We study the effective theory which describes the winding of the phase degrees of freedom far away from the string. The Lagrangian (3.40) gives the equations of motion

$$\Box\theta_\phi + \frac{\Lambda_{\rm QCD}^4}{2f_\phi^2}\,\sin\left(\theta_\phi + \theta_\eta\right) = 0. \tag{3.53}$$

$$\Box\theta_\eta + \frac{\Lambda_{\rm QCD}^4}{2f_\eta^2}\,\sin\left(\theta_\phi + \theta_\eta\right) = 0, \tag{3.54}$$

which have two lowest energy solutions with non-trivial winding that we discuss in the following.

Axion-η' String of Global $U(1)_V$

Since the $U(1)_V$ is an exact symmetry in the massless quark case, the spontaneous symmetry breaking gives rise to global strings. From the transformation properties

from Eq. (3.37), it is clear that θ_η and θ_ϕ wind oppositely under $U(1)_V$ transformations,

$$\theta_\phi = -\theta_\eta = n_V \varphi, \tag{3.55}$$

where the phases describe the winding far away from the string along the z-direction and n_V is the winding number. The string with one unit of winding number, $n_V = \pm 1$, minimizes the energy functional

$$\sigma = \int_0^{2\pi R} dl\, f_\phi^2 (\partial_l \theta_\phi)^2 + f_\eta^2 (\partial_l \theta_\eta)^2 - \Lambda_{\mathrm{QCD}}^4 \cos\left(\theta_\phi + \theta_\eta\right), \tag{3.56}$$

where $l = R\varphi$ so that we integrate the energy density over a circle with radius R perpendicular to the direction of the string.

The field configuration (3.55) is special because, since $\theta_\phi = -\theta_\eta$, the cosine potential is always in its minimum. Thus, to minimize the energy (3.56), we need to minimize the gradient energy which leads to the phases winding linearly in the polar angle, $\theta_\phi, \theta_\eta \sim \varphi$.

Since it involves winding of both the phase of the PQ field θ_ϕ and the phase of the QCD quark condensate θ_η, we call this string an axion-η' string.

Whenever the phases do not wind oppositely, for example when only one phase winds, the potential energy gives an extra contribution to the energy of the configuration. When minimizing the energy from Eq. (3.56) for only one phase winding, the system will want to jump over the potential energy barrier quickly, i.e. have a nonlinear winding in φ. This non-uniform winding is nothing but a domain wall that attaches to the string. Thus, the solution in (3.55) is the only pure string solution, all other configurations will be string-wall systems.

η' String-Wall System of $U(1)_A$

Since we already found the only string solution, the second solution will be a string-wall system. Any solution involving a $U(1)_A$ transformation will have a non-minimal potential energy. To minimize the energy in the cosine potential, the solution stays at the minimum of the cosine as much as possible and overcome the energy barrier to the adjacent minimum in a small region in the angular coordinate φ. The region where the winding is concentrated is the domain wall.

The $U(1)_A$ transformation from Eq. (3.38) winds both phases identically together, $\theta_\phi = \theta_\eta$. However, when we have to deal with the non-minimal potential energy anyway, there will be one winding which is energetically favorable. Since $f_\eta \ll f_\phi$, the energy cost due to gradient energy of θ_η is less so that the string-wall system with minimal energy will wind around θ_η. A transformation where θ_η winds while θ_ϕ is fixed corresponds to a combination of the $U(1)_A$ and $U(1)_V$ transformation.

The equation of motion for θ_η that we need to solve reduces to the Sine-Gordon Equation. The solution for when l is infinite is well-known and we can use it if the radius of the circle we integrate over in the energy is large. In an infinite dimension, the Sine-Gordon solution describes domain walls, but since we have a

periodic coordinate it describes the string wall system, with the wall located at $l = 0$,

$$\theta_\eta = 4 \arctan(\mathrm{e}^{m_\eta l}), \quad \theta_\phi = 0. \tag{3.57}$$

The mass of η' is defined in Eq. (3.45) and its square is the prefactor of the sine in the equation of motion (3.54). This solution is a good approximation if $m_\eta R \gg 1$.

Let us estimate the energy of this string-wall system. We approximate the Sine-Gordon solution for θ_η with a linear winding concentrated in a small region $2\pi m_\eta^{-1}$,

$$\theta_\eta = m_\eta l \quad \text{for} \quad 0 \leq l \leq 2\pi m_\eta^{-1}. \tag{3.58}$$

Everywhere else the θ_η is in the minimum of the potential. Plugging this into the energy functional (3.56), the energy of the η' string-wall is

$$\sigma_\eta \sim \Lambda^2 f_\eta. \tag{3.59}$$

The analogous calculation for a string-wall in the θ_ϕ gives

$$\sigma_\phi \sim \Lambda^2 f_\phi \gg \sigma_\eta, \tag{3.60}$$

which is much more energy costly than the θ_η string-wall.

So, we have learned that, in the massless quark case, the two types of topological defects are strings invlolving both the axion and the η' winding simultaneously and string-walls of the η'.

3.3.2 Massive Light Quark

We now want to understand what happens when we turn on the mass term for the light quark, $m_\psi \neq 0$. This adds a new term to the potential, as is shown in Eq. (3.47). The last term in this equation is proportional to the light quark mass.

Including the quark mass to the theory has an important consequence: The light quark mass breaks the $U(1)_V$ and the $U(1)_A$ explicitly. The axion-η' string solution of the global $U(1)_V$ that we discussed last section has to be modified. First, we discuss the effect of the mass term on the string-wall system of η', then we focus on the axion-η' string.

η' String-Wall System

Since $m_\psi \ll \Lambda_{\mathrm{QCD}}$, the mass term of the light quark just adds a small correction to the mass of η', as seen in Eq. (3.49). The energy correction to the string-wall system is insignificant, such that, even with a massive light quark, the η' string-wall system is still the lowest energy solution of a defect with winding in the $U(1)_A$ direction.

The solution Eq. (3.57) is slightly modified by the correction to the η' mass.

Axion-η' String-Wall System

Since the mass of the light quark explicitly breaks the $U(1)_V$, there will no longer be a string solution corresponding to the spontaneous breaking of this symmetry. The explicit breaking leads to domain walls attaching to the string. We will show that the lowest energy solution still has both phases θ_η and θ_ϕ winding oppositely around the string-wall.

To see this, we analyze the energy functional similar to Eq. (3.56). Now, there is a new term due to the mass of the light quark

$$\sigma = \int_0^{2\pi R} dl\, f_\phi^2 \left(\partial_l \theta_\phi\right)^2 + f_\eta^2 \left(\partial_l \theta_\eta\right)^2 + \Lambda_{\mathrm{QCD}}^4 \Big(1 - \cos\left(\theta_\phi + \theta_\eta\right)\Big) + \Lambda_m^4 \Big(1 - \cos\left(\theta_\eta\right)\Big). \tag{3.61}$$

As before we take $l = R\varphi$, such that he integral is over a large circle with radius R. Also, we set the potential energy of the vacuum to zero by including constant terms.

Since we have already found a solution with winding in θ_η, the second solution has to involve winding in θ_ϕ, i.e., be an axionic string.

A string that winds only in $\theta_\phi = l/R$ while $\theta_\eta = 0$ minimizes the potential energy from the quark mass term. The energy of this axionic string is $\sigma_R = 2\pi(f_\phi^2/R + R\Lambda_{\mathrm{QCD}}^4)$. Thus, the potential energy from the instanton contribution is linearly divergent in R. This is not the lowest energy solution that involves a winding in θ_ϕ.

Taking $\theta_\eta = -\theta_\phi$, as for the massless light quark, reduces the energy of the string: Since $\Lambda_{\mathrm{QCD}} \gg \Lambda_m$, not minimizing the instanton term costs much more energy than the quark mass term. Still, with the new term proportional to m_ψ the potential energy will be non-zero.

To minimize the cost of the quark mass term, a domain wall will attach to the string. The winding of the phases will be limited to a small region, which is the domain wall. Outside the small region of the domain wall the phases both are in the vacuum.

To explicitly show that the phases wind oppositely and the domain walls attach, we chose an ansatz and minimize the energy. We approximate the winding of both phases as linear in a small region of the circle:

$$\theta_\eta = \begin{cases} \frac{l}{L_\eta} & \text{for} \quad 0 \leqslant l \leqslant 2\pi L_\eta \\ 2\pi & \text{otherwise} \end{cases} \tag{3.62}$$

and

$$\theta_\phi = \begin{cases} -\frac{l}{L_\phi} & \text{for} \quad 0 \leqslant l \leqslant 2\pi L_\phi \\ 2\pi & \text{otherwise} \end{cases}. \tag{3.63}$$

There are several things to notice: The θ_η and θ_ϕ wind linearly in respective arches L_η and L_ϕ. Everywhere else, the phases are in the vacuum, which is periodic at $\theta_\eta, \theta_\phi = 0, 2\pi, \ldots$. The thickness of the domain wall is given by L_η and L_ϕ. From the cost of gradient energy and since $f_\phi > f_\eta$, we expect $L_\phi \geq L_\eta$.

The linear ansatz is only an approximation. The exact solution should be smoothed out and look similar to the Sine-Gordon solution $\sim \arctan(\exp(l/L))$, with $l = L_\eta$ and L_ϕ for θ_η and θ_ϕ respectively. Both functions are plotted in Figure 3.2.

With the linear ansatz, we can integrate over l in the energy functional (3.61) and get

$$\begin{aligned}\sigma(L_\phi, L_\eta) = 2\pi\frac{f_\phi^2}{L_\phi} + 2\pi\frac{f_\eta^2}{L_\eta} + 2\pi\Lambda_m^4\, L_\eta \\ + 2\pi\Lambda_{\rm QCD}^4 L_\phi\left(1 + \frac{L_\phi}{2\pi(L_\phi - L_\eta)}\sin\left(2\pi\frac{L_\eta}{L_\phi}\right)\right).\end{aligned} \tag{3.64}$$

We now estimate the energy of two cases: First, when $L_\phi = L_\eta = L$, such that the phases wind exactly opposite $\theta_\eta = -\theta_\phi$ and second, when $L_\eta \ll L_\phi$, in which case the gradient energy is much smaller that in the first case but the potential energy is higher. The comparison between the two will tell us which is the energetically favorable case.

Let us take $L_\phi = L_\eta = L$ first, which leads to a simplified energy functional

$$\sigma(L) = 2\pi\frac{f^2}{L} + 2\pi\Lambda_m^4 L, \tag{3.65}$$

where the first term is from the gradient energy, using $f^2 = f_\phi^2 + f_\eta^2$, and the second from the quark mass term. Minimizing the energy with respect to L, the winding length with lowest energy is

$$L = \frac{f}{\Lambda_m^2} \sim \frac{1}{m_\phi}, \tag{3.66}$$

where in the last step we used the mass of the PQ phase from Eq. (3.50). Hence, the domain wall in this case has a thickness m_ϕ^{-1}, matching the standard thickness of an axionic domain wall. The energy of this solution is

$$\sigma_1 = 4\pi f\Lambda_m^2 \simeq 4\pi f_\phi\Lambda_m^2. \tag{3.67}$$

Comparing with the energy of a pure axionic string, $\sigma_R = 2\pi(f_\phi^2/R + R\Lambda_{\rm QCD}^4)$, the new solution with a domain wall has less energy.

Second, we compare with the energy in the case $L_\eta \ll L_\phi$. Expanding the energy functional from Eq. (3.64) to leading order in L_η/L_ϕ, we find

$$\sigma(L_\phi, L_\eta) \simeq 2\pi\frac{f_\phi^2}{L_\phi} + 2\pi\frac{f_\eta^2}{L_\eta} + 2\pi\Lambda_m^4 L_\eta + 2\pi\Lambda_{\rm QCD}^4 L_\phi\left(1 + \frac{L_\eta}{L_\phi}\right). \tag{3.68}$$

Minimizing this energy with respect to L_ϕ and L_η, the winding length in this case is

$$L_\phi = \frac{f_\phi}{\Lambda_{\rm QCD}^2}, \quad L_\eta = \frac{f_\eta}{\sqrt{\Lambda_m^4 + \Lambda_{\rm QCD}^4}}. \tag{3.69}$$

This solution corresponds to an energy

$$\sigma_2 = 4\pi f_\phi\Lambda_{\rm QCD}^2 + 4\pi f_\eta\sqrt{\Lambda_m^4 + \Lambda_{\rm QCD}^4}. \tag{3.70}$$

Since $\Lambda_{\mathrm{QCD}} \gg \Lambda_m$, this solution has more energy than the solution in the $L_\phi = L_\eta = L$ case, $\sigma_2 \gg \sigma_1$. Thus, the case where $L_\phi = L_\eta = L$ is energetically favored. The axionic string gets accompanied by opposite winding of the θ_η and axionic domain walls with standard thickness $\sim m_\phi^{-1}$ attach. Compared with the string core size $\sim f_\phi^{-1}$, the domain wall thickness is much larger.

We can now improve our linear ansatz for the field configuration of θ_η and θ_ϕ. Since we learned that $\theta_\eta = -\theta_\phi$ is the lowest energy solution for a configuration that winds in the PQ phase, we can use this condition in the energy functional from Eq. (3.64) and solve the resulting equations of motion. They will be of Sine-Gordon type and for $R \gg m_\phi^{-1}$, the solution to leading order in $m_\psi/\Lambda_{\mathrm{QCD}}$ is

$$\theta_\phi = -\theta_\eta \simeq 4 \arctan(\mathrm{e}^{m_\phi l}). \tag{3.71}$$

To summarize, in the massive light quark case, there are two kinds of lowest energy string-wall systems: The pure η' string-wall system which is unaffected by the light quark mass, and the axion-η' string-wall system, for which the phases wind oppositely and to which the usual axionic domain walls attach. We will now discuss the most important implications of the simultaneous winding of the PQ phase and the phase of the quark condensate.

3.3.3 Implications for Anomaly Inflow

One very interesting property of cosmic strings is that they are superconducting [16]. To understand the superconductivity, we first need to know about zero modes: If a fermion couples to a scalar in a Yukawa type interaction and that scalar field is responsible for the string solution, by the index theorem the fermion deposits a zero mode on the string [31, 32]. For example, as in Eq. (3.36), the scalar field can be the PQ field Φ which has a Yukawa coupling to the heavy quark Ψ, giving mass to the quark. Then the heavy quark deposits a zero mode on the string, i.e., in the $1+1$-dimensional theory on the string, there is a massless Dirac fermion. The number of zero modes is equal to the winding number of the string.

If the fermions carry electric charge, their zero modes can be the charge carriers of a superconducting current on the string [16]. Because of the superconducting current, the string acts as a superconducting wire. This can have important astrophysical consequences, such as changing the behavior of the string in a magnetic field [16] or emitting electromagnetic radiation [104].

For axionic strings, it is important to understand what happens when the spontaneously broken symmetry is anomalous. In this case, the $1+1$-dimensional theory of zero modes on the string also has an anomaly: The sum of the charge of the zero modes is non-zero and this imbalance leads to the anomaly. However, the $1+3$-dimensional theory has no gauge anomaly. This can be explained by an inflow of charge from the $1+3$ dimensions onto the string, which is called anomaly inflow [17].

In the standard picture, axionic strings come from the spontaneous breaking of the anomalous global Peccei-Quinn symmetry, $U(1)_{PQ}$. Thus, axionic strings must

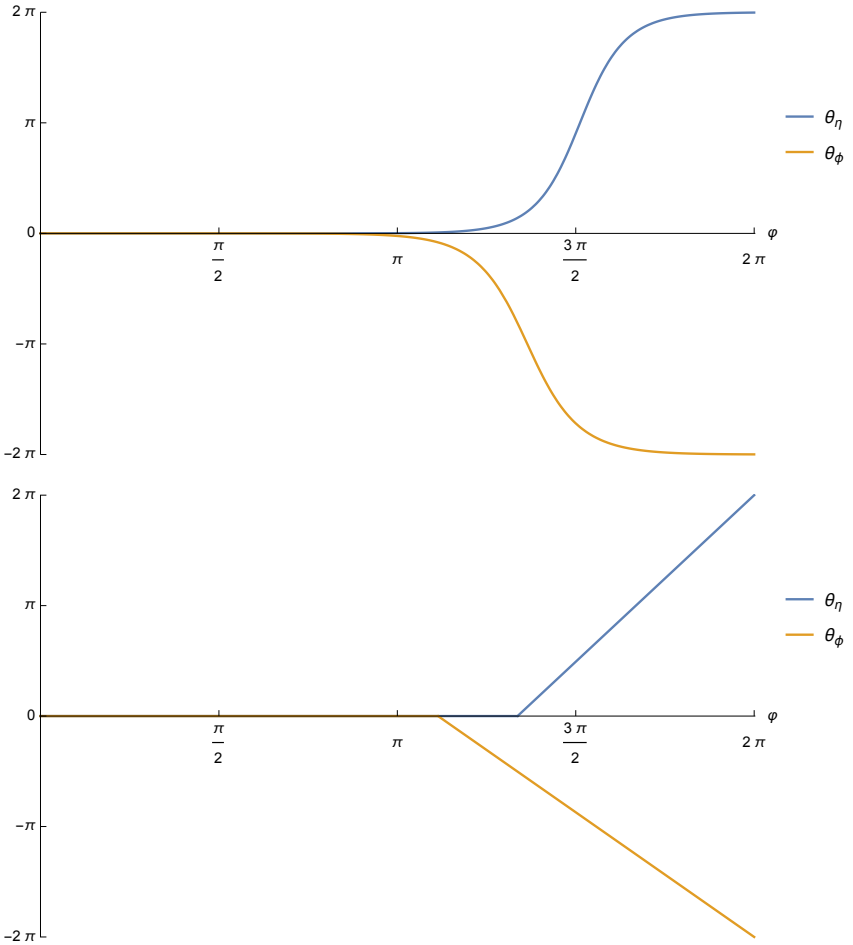

Figure 3.2: Sketch of the wall profiles for the Sine-Gordon ansatz (3.71) in the upper figure and the linear ansatz (3.62) and (3.63) in the lower figure. The opposite winding of θ_η and θ_ϕ is confirmed by numerical analysis [6].

experience anomaly inflow which enters along the domain walls that attach to the string [18, 105, 106].

The anomaly inflow into the axionic string can impact their cosmological evolution and astrophysical properties: The superconducting current on axionic strings can produce large electromagnetic fields around the string and lead to a production of particles surrounding the string [107, 108] and it can increase the density of axion strings in the early universe [109].

Our discussion on axionic strings in the previous section changes the zero-mode composition on the string. We showed that the lowest energy axionic string, around which by definition the PQ phase θ_ϕ winds, is accompanied by opposite winding in the phase of the quark condensate, θ_η. Because of the simultaneous winding in both phases, the axionic string in the toy model with one light quark and one heavy quark exhibits no anomaly inflow.

The scalar field, whose phase winds around the string, is the PQ field Φ, which

has a Yukawa coupling to the heavy quark Ψ, as shown in Eq. (3.36). Hence, the heavy quark deposits a zero mode on the string which on its own makes the $1+1$-dimensional theory anomalous: The heavy quark is electrically charged and carries a color charge. Since it has definite chirality, it moves only in one direction of the string, thus creating the anomaly.

But with the phase of the quark condensate winding oppositely to the PQ phase, the light quark ψ also deposits a zero mode. This can be seen from the effective Yukawa interaction between the PQ field Φ and the light quark

$$\Phi\bar{\psi}_L\psi_R + \text{h.c.}. \tag{3.72}$$

This effective operator is generated through the 't Hooft determinant, as shown in Figure 3.3.

Since the heavy quark couples to Φ^* and the light quark to Φ, their zero modes have opposite chirality on the string. In other words, the PQ string is an anti-string for the light quark.

Since there are two zero modes with opposite chirality they cancel the gauge anomalies. Therefore, the $1+1$-dimensional theory on the string has no anomaly and the string experiences no anomaly inflow.

The fact that the axion string with opposite winding of the phase of the quark condensate is anomaly-free can also be understood from the $U(1)_V$ being the anomaly-free part of the axial symmetry and the Peccei-Quinn symmetry. Since the opposite winding in θ_ϕ and θ_η corresponds exactly to a $U(1)_V$ string, it is clear that this string, originating from an anomaly-free symmetry, has no anomaly inflow. However, we showed only in the toy model with one light quark and one heavy quark that the lowest energy solution corresponds to a $U(1)_V$ string. It would be interesting to study the case with three light quarks in the future, to find the lowest energy defects and to understand the anomaly content.

Let us also comment on the zero mode structure when the fermion has an explicit mass term, i.e., when the mass of the fermion is not only generated by a Yukawa coupling to the string scalar field. This is the case for the explicit mass m_ψ of our light quark. As long as the explicit mass of the fermion is smaller than its mass from the Yukawa coupling to the string field, the zero modes still exist on the string [110]. If the explicit mass term is much smaller than the mass from spontaneous symmetry breaking, the profile of the wave function of the zero mode shows a small deformation [110].

For our axionic strings, this means that since $m_\psi \ll \Lambda_{\text{QCD}}$ the zero modes of the light quark exist on the string, i.e., the zero mode structure is unaffected.

The other string-wall structure in our toy model, which are the pure η' defects, are the result of a spontaneous breaking of the anomalous $U(1)_A$ symmetry. Thus, the η'-string-walls experience anomaly inflow.

The key point is that because of simultaneous winding of the phase of the Peccei-Quinn field and the phase of the quark condensate in an axionic string, the zero mode structure gets altered. This can change the anomaly content of the string and it can even make the axionic string anomaly-free. The details of the zero modes and

anomaly content depend on the number of quark flavors and the winding numbers of the lowest energy defect.

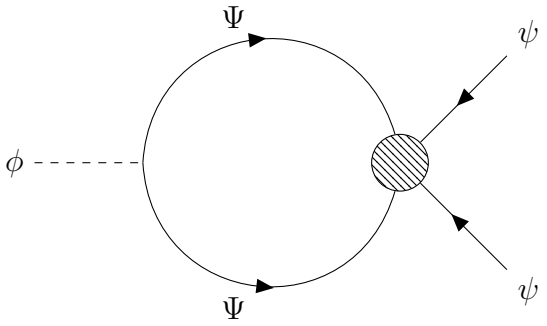

Figure 3.3: A diagram describing how the effective Yukawa coupling (3.72) is generated by the 't Hooft vertex

3.3.4 More Heavy Quark Flavors

So far, we assumed that there is only one heavy quark flavor Ψ. When we introduce multiple heavy quark flavors Ψ_i, where i labels the quark flavor $i = 1, \ldots, N_f$, our analysis changes slightly.

First, we need to redefine the anomaly-free $U(1)_V$ and anomalous $U(1)_A$ symmetries. All heavy quark flavors transform under the Peccei-Quinn symmetry $U(1)_{PQ}$

$$\Psi_i \to e^{\mathrm{i}\frac{1}{2}\alpha\gamma_5}\Psi_i \quad \text{and} \quad \Phi \to e^{\mathrm{i}\alpha}. \tag{3.73}$$

Thus the shift of the Lagrangian by the anomalous Peccei-Quinn symmetry is proportional to the number of flavors N_f.

We can define an anomaly-free symmetry from the combination of $U(1)_{PQ}$ and the original $U(1)_A$, which transforms the light quark as $\psi \to e^{-\mathrm{i}\alpha\gamma_5/2}\psi$, in the following way

$$\Phi \to \mathrm{e}^{i\alpha}\Phi\,, \quad \Psi_i \to \mathrm{e}^{i\frac{1}{2}\alpha\gamma_5}\Psi_i\,, \quad \psi \to \mathrm{e}^{-i\frac{N_f}{2}\alpha\gamma_5}\psi\,. \tag{3.74}$$

Again, we call this anomaly-free symmetry $U(1)_V$.

The new $U(1)_A$ is defined as the orthogonal transformation to $U(1)_V$. To find the orthogonal transformation, we can write the $U(1)_V$ in a matrix form. When we write the fermion fields in a vector, $f = (\Psi_1, \ldots, \Psi_{N_f}, \psi)$, they transform as $f \to e^{\mathrm{i}\alpha A\gamma_5/2}f$, where A is a matrix

$$A = \mathrm{diag}(\underbrace{1, \ldots, 1}_{N_f}, -N_f). \tag{3.75}$$

For the orthogonal transformation, defined by a matrix B acting on the same vector of fermions f, we require that $\mathrm{Tr}(A \cdot B) = 0$. After using the requirement that B is diagonal and transforms the heavy quark flavors equally, the matrix B is

$$A = \mathrm{diag}(\underbrace{1, \ldots, 1}_{N_f}, 1). \tag{3.76}$$

Thus, the transformation $U(1)_A$ is

$$\Phi \to \mathrm{e}^{i\alpha}\Phi\,, \quad \Psi_i \to \mathrm{e}^{i\frac{1}{2}\alpha\gamma_5}\Psi_i\,, \quad \psi \to \mathrm{e}^{i\frac{1}{2}\alpha\gamma_5}\psi\,. \tag{3.77}$$

This $U(1)_A$ symmetry is anomalous, however, it has an anomaly-free subgroup Z_{2N_f} which corresponds to $\alpha = 2\pi k/N_f$ with $k = 1, \ldots, 2N_f$.

The low-energy Lagrangian of the phases is

$$\begin{aligned}\mathcal{L}(\theta_\phi, \theta_\eta) =& f_\phi^2 \left(\partial_\mu\theta_\phi \partial^\mu\theta_\phi\right) + f_\eta^2 \left(\partial_\mu\theta_\eta \partial^\mu\theta_\eta\right) \\ &+ \Lambda_{\mathrm{QCD}}^4 \left(\cos\left(N_f\theta_\phi + \theta_\eta - \bar{\theta}\right) - 1)\right) \\ &+ \Lambda_m^4 \left(\cos\left(\theta_\eta\right) - 1)\right).\end{aligned} \tag{3.78}$$

The phases shift under the $U(1)_V$ symmetry as $\theta_\phi \to \theta_\phi + \alpha$ and $\theta_\eta \to \theta_\eta - N_f\alpha$. Only the quark mass term in the third line is not invariant under $U(1)_V$. The potential is not invariant under $U(1)_A$, transforming the phases as $\theta_\phi \to \theta_\phi + \alpha$ and $\theta_\eta \to \theta_\eta + \alpha$.

Since the Peccei-Quinn phase cancels the $\bar{\theta}$, we can set the effective vacuum angle to zero, so $\bar{\theta} = 0$. To find the lowest energy topological defects, we again consider $m_\psi = 0$ first. Since $U(1)_V$ is not explicitly broken in the massless quark case, there will be a string solution corresonding to the $U(1)_V$

$$n_\eta = \pm N_f \quad \text{and} \quad n_\phi = \mp 1, \tag{3.79}$$

with n_η and n_ϕ the winding numbers for θ_η and θ_ϕ respectively. Thus, around the $U(1)_V$ string, the phases wind linearly with

$$\theta_\eta = \pm N_f\varphi \quad \text{and} \quad \theta_\phi = \mp\varphi. \tag{3.80}$$

When we take into account the light quark mass $m_\psi \neq 0$, the $U(1)_V$ string becomes attached to N_f domain walls. Outside of the walls, the phases are constant and in the vacuum. All winding happens inside the walls, such that across each wall, the phases vary by $\Delta\theta_\eta = 2\pi$ and $\Delta\theta_\phi = 2\pi/N_f$.

The other defect is the pure η' string-wall, which is exactly the same as in the toy model with one heavy quark flavor. Just as explained before, it costs less energy to have only the phase of the quark condensate wind instead of an additional winding in θ_ϕ.

3.4 Axion Models

The toy model we considered with one light and one heavy quark has all important characteristics of a realistic hidden axion model. The KSVZ model [94, 95] is very similar to the toy model we used: It introduces a new heavy quark which gets its mass from the spontaneous symmetry breaking of the Peccei-Quinn symmetry. We only considered one flavor of light quark, which can be the lightest quark in the Standard Model, the up-quark.

Another hidden axion model is the DFSZ type model [96, 97]. These models do not introduce a new heavy quark, but instead there are two Higgs doublets in the Standard Model that also couple to the Peccei-Quinn field. We will now study a DFSZ type toy model that includes the two lightest quarks, the up and the down quark. For simplicity, we take only one generation of the quarks.

The two Higgs doublets have a Yukawa coupling to the quarks. In the low-energy theory, we are in particular interested in the neutral components of the Higgs doublets that aquire a VEV. We call those components $H_u(x) = \rho_u(x)e^{i\chi_u(x)}$ and $H_d(x) = \rho_d(x)e^{i\chi_d(x)}$, where H_u and H_d couple to the up u and the down d respectively. The electrically charged components are unimportant for our following analysis of topologial defects, so that we can leave them out.

Since the Peccei-Quinn field couples to the Higgs doublets, the axionic strings and string-wall systems arising from this symmetry breaking carry flux of the Z-boson.

The Yukawa couplings that generate the masses of the quarks are

$$\mathcal{L}_{\text{Yuk}} = g_u H_u \bar{u}_L u_R + g_d H_d \bar{d}_L d_R + \text{h.c.}, \tag{3.81}$$

where g_u and g_d are the Yukawa coupling constants. The Yukawa couplings are invariant under three $U(1)$ symmetries: The global Peccei-Quinn symmetry $U(1)_{PQ}$ and the local hypercharge $U(1)_Y$ and weak isospin $U(1)_{I_3}$. We can also write the local $U(1)_Y \times U(1)_{I_3}$ as $U(1)_Q \times U(1)_Z$, so the electromagnetic $U(1)_Q$ times the $U(1)_Z$ corresonding to the Z-boson as the gauge field.

The spontaneous breaking of $U(1)_{PQ}$ gives rise to axionic strings, however, when $U(1)_Z$ is also broken at the electroweak scale, the lowest energy defects will involve simultaneous winding of phases shifting under both symmetries. Since, the $U(1)_Q$ is unbroken, we can ignore it in this discussion.

The Peccei-Quinn symmetry transforms the fields as

$$\begin{aligned} &H_u \to \mathrm{e}^{i\alpha} H_u, \quad H_d \to \mathrm{e}^{i\alpha} H_d, \\ &u \to \mathrm{e}^{-i\frac{1}{2}\alpha\gamma_5} u, \quad d \to \mathrm{e}^{-i\frac{1}{2}\alpha\gamma_5} d. \end{aligned} \tag{3.82}$$

So, both Higgs doublets have the same Peccei-Quinn charge. However, they have opposite charges under $U(1)_Z$, under which the fields transform as

$$\begin{aligned} &H_u \to \mathrm{e}^{i\beta} H_u, \quad H_d \to \mathrm{e}^{-i\beta} H_d, \\ &u \to \mathrm{e}^{-i\frac{1}{2}\beta\gamma_5} u, \quad d \to \mathrm{e}^{i\frac{1}{2}\beta\gamma_5} d. \end{aligned} \tag{3.83}$$

When the neutral components of the Higgs doublets gain a VEV, $\langle\rho_u\rangle = v_u$, $\langle\rho_d\rangle = v_d$, the quarks become massive with $m_u = g_u v_u$, $m_d = g_d v_d$. The non-zero VEVs of the Higgs doublets spontaneously break the $U(1)_{PQ}$ and the $U(1)_Z$. The Z-boson gets a mass from eating one combination of Goldstone bosons χ_u and χ_d. The orthogonal combination would be the axion, however, this is not phenomenologically viable. Since the VEVs of the two Higgs doublets are bounded from above by the weak interaction scale, the decay constant of the axion would also be of the same

order. This leads to interactions of the axion with the Standard Model particles that are too strong.

This is why we have invisible axion models: The scale of the breaking of the Peccei-Quinn symmetry can be much higher and thus lead to phenomenologically consistent axion models. We introduce a new scalar field, the Peccei-Quinn field Φ, that transforms under the $U(1)_{PQ}$ as

$$\Phi \to \mathrm{e}^{-i2\alpha}\Phi. \tag{3.84}$$

The $U(1)_{PQ}$ is spontaneously broken when the Φ gets a VEV at a much higher scale than the weak scale. The Peccei-Quinn field interacts with the Higgs doublets

$$\mu\Phi H_u H_d + \text{h.c.}. \tag{3.85}$$

Thus, the phase of the PQ field θ_ϕ mixes with χ_u and χ_d. The Peccei-Quinn symmetry is broken when the Φ gets a VEV, $\langle\Phi\rangle = f_\phi$, which is much higher than the electroweak scale.

Below the QCD scale, the quark condensate forms. We monitor the phases of the quark condensate with the up- and the down-quark separately, $\langle\bar{u}u\rangle = \Lambda_u^3 e^{i\theta_u(x)}$ and $\langle\bar{d}d\rangle = \Lambda_d^3 e^{i\theta_d(x)}$, with scales $\Lambda_u \simeq \Lambda_d \sim \Lambda$. This is useful because the mass of the up- and the down-quark are different.

We get the effective Lagrangian for the phase degrees of freedom by including instanton effects

$$\begin{aligned}
\mathcal{L}_{\text{eff}} &= f_\phi^2 \left(\partial_\mu\theta_\phi\right)^2 && (3.86)\\
&+ v_u^2 \left(\partial_\mu\chi_u - Z_\mu\right)^2 + v_d^2 \left(\partial_\mu\chi_d + Z_\mu\right)^2 && (3.87)\\
&+ f_u^2 \left(\partial_\mu\theta_u + Z_\mu\right)^2 + f_d^2 \left(\partial_\mu\theta_d - Z_\mu\right)^2 && (3.88)\\
&+ \mu f_\phi v_u v_d \cos\left(\theta_\phi + \chi_u + \chi_d\right) && (3.89)\\
&+ m_u\Lambda_u^3 \cos\left(\chi_u + \theta_u\right) + m_d\Lambda_d^3 \cos\left(\chi_d + \theta_d\right) && (3.90)\\
&+ m_d\Lambda_u^3 \cos\left(\theta_u - \chi_d - \bar{\theta}\right) && (3.91)\\
&+ m_u\Lambda_d^3 \cos\left(\theta_d - \chi_u - \bar{\theta}\right) && (3.92)\\
&+ m_u m_d \Lambda_{\text{QCD}}^2 \cos\left(\chi_u + \chi_d + \bar{\theta}\right) && (3.93)\\
&+ \Lambda_{\text{QCD}}^4 \cos\left(\theta_u + \theta_d - \bar{\theta}\right). && (3.94)
\end{aligned}$$

Let us explain this potential line by line. The first line is the kinetic term of the Peccei-Quinn phase, θ_ϕ. It is not charged under the Standard Model gauge symmetry and couples to Standard Model fields only through the interaction (3.85), which is represented in the potential in line (3.89).

The kinetic terms for the phases of the Higgses and for the quark condensates are given in the two lines (3.87) and (3.88). Since the original fields transform under the local $U(1)_Z$ from (3.83), the phases are accompanied by the Z-boson in the Lagrangian. The $U(1)_Z$ is described by transforming $Z_\mu \to Z_\mu + \partial_\mu\beta$ and shifting the phases

$$\chi_u \to \chi_u + \beta,\ \chi_d \to \chi_d - \beta,\ \theta_u \to \theta_u - \beta,\ \theta_d \to \theta_d + \beta. \tag{3.95}$$

Because of the VEVs of the Higgs doublets and also of the quark condensate, the $U(1)_Z$ is spontaneously broken. Thus, the Z-boson becomes massive and eats the following combination of phases,

$$v_u^2\chi_u - v_d^2\chi_d - f_u^2\,\theta_u + f_d^2\theta_d, \tag{3.96}$$

which becomes the longitudinal component of the Z-boson.

The Yukawa coupling from Eq. (3.81) are given in the effective Lagrangian in line (3.90). The three lines (3.91), (3.92) and (3.93) are generated by the combination of the Yukawa couplings with the 't Hooft determinant. The last line (3.94) comes from the instantons.

Notice that the effective Lagrangian respects the local $U(1)_Z$ symmetry, as given in Eq. (3.95). The global $U(1)_{PQ}$, which was defined in Eq. (3.82), shifts the phases as

$$\chi_u \to \chi_u + \alpha,\ \chi_d \to \chi_d + \alpha,\ \theta_u \to \theta_u - \alpha,\ \theta_d \to \theta_d - \alpha,\ \theta_\phi \to \theta_\phi - 2\alpha. \tag{3.97}$$

This symmetry is anomalous and, therefore, explicitly broken by instanton effects, namely by lines (3.91) - (3.94).

The strong CP problem is solved because when we minimize the potential, all CP-odd phases vanish so that we set the effective vacuum angle to zero, $\bar{\theta} = 0$. The combination of phases that cancels $\bar{\theta}$ is what we call the axion but which combination is it?

By the Goldstone theorem, when we break $U(1)_{PQ} \times U(1)_Z$, there should be two Goldstones. The Goldstone for the $U(1)_Z$ is eaten by the Z-boson and we already found it in Eq. (3.96). The other one, the axion, is a would-be Goldstone and has a small mass proportional to the up-quark mass[2]. In other words, in the case of a massless up quark, the axion remains massless. From Eq. (3.85), the combination $\theta_\phi + \chi_u + \chi_d$ gets heavy, while the two orthogonal combinations stay massless. The orthogonal states have to be found from the physical states which are canonically normalized. This leads to the axion being approximately θ_ϕ.

Now axionic strings and walls need to involve winding in the axion phase, θ_ϕ. Even though the θ_ϕ is only transforming under the global $U(1)_{PQ}$, the lowest energy strings that involve winding in the axion will be accompanied by winding in the Higgs phases and thus carry a gauge magnetic flux. This is because of line (3.89), which is the most energy costly term in the potential. To minimize this term, when the θ_ϕ winds, the system will also wind χ_u or χ_d oppositely.

This results in a magnetic flux of the Z-boson in the axionic string, similar to the case in [111]. The Z-boson flux, depending on the winding numbers n_{χ_u}, n_{χ_d}, n_{θ_u} and n_{θ_d} corresponding to winding in the phases χ_u, χ_d, θ_u and θ_d respectively, is given by

$$\text{flux} = \oint dx_\mu Z^\mu = \frac{1}{g_z}\frac{v_u^2 n_{\chi_u} - v_d^2 n_{\chi_d} - f_u^2\, n_{\theta_u} + f_d^2 n_{\theta_d}}{v_u^2 + v_d^2 + f_u^2 + f_d^2}, \tag{3.98}$$

[2]This is similar to subsection 3.2.3

where we integrate around an asymptotic closed path around the string. An accidental cancellation of the flux, which can happen only when the VEVs and winding numbers have very specific values, seems unlikely.

Notice that the string does not carry integer flux of the gauge field in units of the inverse gauge coupling, as is the case for the Nielsen-Olesen string. The fraction on the right-hand-side of the flux is non-integer, so the Z-boson flux is non-integer in units of the inverse gauge coupling $1/g_z$. This also means that the asymptotic pure-gauge form of the gauge field only partially compensates for the gradient energy of the winding phases. Correspondingly, the string has logarithmically divergent energy, similar to a global string.

Since the axionic string carries magnetic flux similar to a local string and has divergent energy similar to a global string, it shares properties of both types of strings. In [111], such types of strings were named "semi-global".

Because the electroweak scale is much higher than the QCD scale, $v_u, v_d \gg f_u, f_d$, we ignore the contributions of the θ_u and θ_d to the Z-flux in Eq. (3.98). In this approximation, the flux depends on the VEVs and winding numbers of the Higgs phases,

$$\text{flux} \simeq \frac{1}{g_z}\left(n_{\chi_u} - \frac{v_d^2(n_{\chi_u}+n_{\chi_d})}{v_u^2+v_d^2}\right). \tag{3.99}$$

In the simplest case where only one Higgs phase winds, e.g., $n_{\chi_u} = \pm 1,\ n_{\chi_d} = 0$, the flux is

$$\text{flux} \simeq \pm\frac{1}{g_z}\frac{v_u^2}{v_d^2+v_u^2}, \tag{3.100}$$

which clearly shows the non-integer and non-zero flux due to the fraction involving the Higgs VEVs.

Next, we discuss the lowest energy topological defects, starting from the case with the lightest quark, the up-quark, being massless. In the case $m_u = 0$, the $\eta' \sim \theta_u + \theta_d$ is responsible for canceling the effective vaccum angle. Then, we turn on the up-quark mass to understand the effects of the up-quark mass on the topological defects.

3.4.1 Massless Up-Quark Case

In this part, we consider the case where the up-quark is massless, $m_u = 0$. This is similar to our analysis in the KSVZ toy-model in subsection 3.3.1. As in the KSVZ case, there is an anomaly-free symmetry that is only exact for $m_u = 0$. To see this, we look at the effective potential with $m_u = 0$,

$$\begin{aligned} V = &-\mu f_\phi v_u v_d \cos(\theta_\phi + \chi_u + \chi_d) \\ &- m_d\Lambda_d^3 \cos(\chi_d + \theta_d) - m_d\Lambda_u^3 \cos(\theta_u - \chi_d) \\ &- \Lambda_{\text{QCD}}^4 \cos(\theta_u + \theta_d)\,. \end{aligned} \tag{3.101}$$

This potential is invariant under shifts of the phases

$$\chi_u \to \chi_u + \alpha\,,\ \chi_d \to \chi_d + \alpha\,, \theta_u \to \theta_u + \alpha\,,\ \theta_d \to \theta_d - \alpha\,,\ \theta_\phi \to \theta_\phi - 2\alpha, \quad (3.102)$$

which is anomaly-free because the θ_u and θ_d shift oppositely. We call this symmetry $U(1)_V$.

We can understand the $U(1)_V$ as the anomaly-free part of the Peccei-Quinn symmetry from Eq. (3.97) and the axial symmetry of the up-quark: Now that $m_u = 0$, there is an anomalous symmetry rotating the up-quark axially, so $\theta_u \to \theta_u + \alpha$.

The massless Goldstone boson corrresponding to the $U(1)_V$ is θ_ϕ with a small admixture $\sim v_{u/d}/f_\phi$ of $\chi_{u/d}$ and an even smaller admixture of the π^0 and the η'. As explained before, in the massless quark solution the η' residing in $\theta_u + \theta_d$ is the axion. Since we have two flavors, there will be another neutral Goldstone, the neutral pion $\pi^0 \sim v_u^2\theta_u - v_d^2\theta_d$, orthogonal to η'.

Since the symmetry is not explicitly broken, there will be $U(1)_V$ strings which include winding in the Peccei-Quinn phase. We call these strings axionic strings even though the Peccei-Quinn phase becomes the axion only when the up-quark is massive.

So, an axionic string winds around the phase of the Peccei-Quinn field θ_ϕ at least by one unit. To minimize the effective potential (3.101), other phases will simultaneously wind around the axionic string.

In the case of minimal winding in θ_ϕ, so that the winding number is unit one $n_\phi = \pm 1$, a pure $U(1)_V$ string is impossible. This is because when θ_ϕ winds by one unit, a $U(1)_V$ transformation makes the other fields wind fractionally. Since the winding number in each phase has to be integer, a pure $U(1)_V$ string cannot have minimal winding in θ_ϕ.

However, if the string also includes a $U(1)_Z$ transformation, we can find a string solution with minimal winding. The configuration that keeps the potential in its minimum everywhere is $n_\phi = \pm 1$ and $n_{\chi_u} = \mp 1$. All other phase do not wind around the string, $n_{\chi_d} = 0$, $n_{\theta_u} = 0$ and $n_{\theta_d} = 0$. The simultaneous winding in θ_u and χ_u corresponds to combination of a $U(1)_V$ transformation from Eq. (3.102) and a $U(1)_Z$ tranformation from Eq. (3.95). As explained above, a string solution of a combination of a global and a local $U(1)$ leads to semi-global strings with non-integer magnetic Z-flux in the core of the string [111].

We can also consider a configuration where the other Higgs phase winds, so $n_\phi = \pm 1$ and $n_{\chi_d} = \mp 1$, while $n_{\chi_u} = 0$. This also minimizes the first term in the potential. In this case, the phases of the quark condensate will also wind around the string to minimize the other terms in the potential, so $n_{\theta_u} = \mp 1$ and $n_{\theta_d} = \pm 1$. This corresponds to a winding in the π^0. We expect that this configuration will have slightly more energy than the one winding only in θ_ϕ and χ_u since the quark phases also contribute to the energy in the kinetic terms and in the gauge flux. However, which configuration has lower energy also depends on the parameters v_u and v_d.

There can also be configurations with higher winding numbers which are more energy costly due to the higher winding numbers contributing more to the kinetic energy and gauge flux. Whenever the phase χ_d winds, so do the phases of the

quark condensate to minimize the potential. Their winding numbers are related by $n_{\chi_d} = n_{\theta_u} = -n_{\theta_d}$.

There are several important results from this analyis: If there is more than one light quark flavor, axionic strings can require windings of the neutral pion π^0. Compared to the KSVZ toy model from the earlier section, in the DFSZ toy model the Peccei-Quinn field does not couple directly to the quarks. Instead, it couples to the Higgs fields, which results in the Higgs phases winding in the axionic strings and thus, a magnetic Z-flux in the core of the string. Unlike in the KSVZ case, a simultaneous winding of the phases of the quark condensate around the axionic string may or may not be necessary, depending on the parameters of the theory.

3.4.2 Massive Up Quark Case

Now we deform the theory by switching on the mass term for the up quark, $m_u \neq 0$. This introduces back the terms proportional to m_u in the effective potential,

$$\begin{aligned} V_{m_u} \equiv & - m_u \Lambda_u^3 \cos(\chi_u + \theta_u) - m_u \Lambda_d^3 \cos(\theta_d - \chi_u) \\ & - m_u m_d \Lambda^2 \cos(\chi_u + \chi_d) . \end{aligned} \tag{3.103}$$

This explicitly breaks the $U(1)_V$ symmetry from Eq. (3.102). Thus, domain walls attach to the axionic strings.

Let us take a closer look at axionic strings with minimal winding $n_\phi = \pm 1$. Since the first term in the potential (3.101) costs more energy than the other terms, the system will always minimize this cosine and require $n_\phi + n_{\chi_u} + n_{\chi_d} = 0$. Thus, just like in the massless up quark case, the axionic string will be accompanied by simultaneous winding of one of the Higgs phases.

However, the new terms due to up-quark mass can change the lowest energy windings in θ_u and θ_d. Specifically, it can be energetically favorable, additionally to winding in χ_u, to stimulate windings in the phases of the quark condensates. The exact dependence on the parameters has to be determined by minimizing the energy in detail and can be studied in future work.

To summarize, also in the DFSZ toy model the lowest energy configuration of axionic string-wall systems can be accompanied by windings in the phases of the quark condensate. Additionally, in the DFSZ case the axionic string carries magnetic Z-flux in the core of the string.

3.5 Internal Structure of QCD Walls

In the previous sections we showed that because of the topological structure of the QCD vacuum there exist 2π-domain walls. The 2π in front of the domain wall stands for the fact that the phase of the quark condensate winds by 2π across the wall. If there are several flavors of light quarks that condense, the winding in the 2π-domain walls can have different patterns in flavor space. Assuming that the quark condensate

consists of the up- and the down-quark, $\langle\bar{u}u\rangle$ and $\langle\bar{d}d\rangle$, the winding can go in two basic flavor directions.

For $n_{\theta_u} = -n_{\theta_d} \neq 0$, there is no involvement of the η' and the direction of the winding is in the π^0. In the opposite case, i.e., $n_{\theta_u} + n_{\theta_d} \neq 0$, the winding involves the η'-meson.

The 2π-domain walls can form structures like closed bubbles of a certain radius, membranes bounded by strings, or planar (infinite) walls. These structures are unstable, i.e., quantum tunneling effects can punch a hole through it whose edge is a cosmic string. Therefore, in each direction of 2π-domain walls in the flavor space (π^0 or η') there needs to exist a corresponding string that bounds it.

In this section we are concerned with the internal structure of these walls. More specifically, we want to study whether the quark condensate, which is the order parameter at which the symmetry leading to the 2π-domain walls is broken, remains non-zero throughout the wall. If this were not the case, then the phase that winds around the 2π-domain wall would not be well-defined. As long as the absolute value of the quark condensate stays non-zero when passing through a wall, the winding of the phases is well-defined and the existence of the 2π-domain wall is required by topology.

This question is crucial for pure η'-domain walls that do not invlove winding in the Peccei-Quinn phase θ_ϕ. Since the Peccei-Quinn phase θ_ϕ is well-defined everywhere, for axionic domain walls, the Peccei-Quinn phase guides the phases of the quark condensates.

Across the η'-domain wall, the effective vaccum angle θ_{eff} changes by 2π. Thus, the QCD backreaction to the order parameter might be important, for example, if the dilute instanton gas approximation breaks down. Notice that the analogous question does not emerge for domain walls with π^0 winding because the potential of the π^0 orgiginates only from the quark masses and not from the anomaly.

Inside the η'-domain wall, the effective theory of the order parameter breaks down, which makes it difficult to resolve the internal structure of the domain wall. Nevertheless, we can ensure that the quark condensate is non-zero across the wall without finding an exact solution. Instead, we can use the domain walls in $\mathcal{N} = 1$ supersymmetric QCD (SQCD) [22] as a guideline since they are the closest cousins to our η'-domain walls.

The closely related theory with similar domain walls is an $\mathcal{N} = 1$ supersymmetrized version of $SU(N)$ Yang-Mills (SYM). In this theory, the fermionic partners of the gauge bosons, which we call gauginos and denote with λ, play the role of the quarks. Even though the gauginos transform in the adjoint representation of $SU(N)$ while the quarks of QCD transform in the fundamental representation, we do not expect this to be essential for our discussion.

The supersymmetrized model has an anomalous chiral symmetry, the $U(1)_R$-symmetry, under which the gauginos transform as

$$\lambda \to \mathrm{e}^{i\alpha}\lambda\,. \tag{3.104}$$

The $U(1)_R$ has an anomaly-free subgoup Z_N because the gauginos are in the adjoint

representation of $SU(N)$.

Analogous to the quark condensate in QCD, in the supersymmetric $SU(N)$ the theory confines and the gauginos condense. The gaugino condensate $\langle\bar{\lambda}\lambda\rangle \neq 0$ breaks the anomalous $U(1)_R$ symmetry. The instantons generate the 't Hooft determinant which is represented as a $2N$-gaugino vertex.

The breaking of the anomaly-free subgroup of $U(1)_R$, the Z_N-symmetry,

$$\langle\bar{\lambda}\lambda\rangle \to \mathrm{e}^{i\frac{2\pi}{N}}\langle\bar{\lambda}\lambda\rangle, \tag{3.105}$$

produces domain walls [22]. Since these domain walls have BPS properties, it is possible to compute the tension of the domain walls exactly in terms of the gaugino condensate.

Witten [112] suggested that in the large N limit, the wall behaves like a D-brane for large-N QCD string theory. Many subsequent papers strengthened this conjecture, for example the analysis of [113, 114].

Across each domain wall the phase of the gaugino condensate changes by $2\pi/N$, while at the same time the effective phase of the 't Hooft determinant varies by 2π. Therefore, across the domain wall the effective vacuum angle θ_{eff} changes by 2π. This is very similar to the η'-domain walls in ordinary QCD. We conclude that the two cases of domain walls in the phase of the gaugino and the quark condensate are similar, including whether or not the phase degree of freedom is well-defined.

To understand the validity of the phase of the gaugino condensate in large N supersymmetric QCD, we study the exact solution of the domain wall derived in [113]. This solution shows that, since the gaugino condensate is non-zero across the wall, the phase degree of freedom is well-defined everywhere. We conjecture that this also holds in our case, so that the quark condensate remains non-zero across the wall and that η' is well-defined everywhere.

As a result, pure QCD can support the existence of at least two types of string-wall systems, which are determined by the winding of π^0 and η' respectively.

3.6 Cosmology

In this section, we explore the effects of our findings about the axionic and pure η' string-wall systems on cosmology. We showed that axionic strings are accompanied by windings of the phases of the quark condensate and that there exist pure QCD topologial defects of the η' and the π^0. This permits an entirely new perspective on the cosmology of the θ-vacuum.

For the cosmic strings to be relevant for cosmology, the phase transition that forms the strings has to happen after (or towards the end of) inflation. Otherwise, the strings will be inflated away during the inflationary period of the universe and have no relevance for comology.

If the reheating temperature after inflation is larger than the present day QCD scale Λ_{QCD}, then QCD effects are unimportant for the early cosmology of the θ-vacuum. Since this is the case for most inflationary scenarios, it is usually assumed that QCD plays no role in the early universe.

However, this standard picture of cosmology does take into account the effect of axionic strings: It is usually assumed that axionic strings, involving winding in the phase of the Peccei-Quinn field, dominate the early string cosmology. Additionally, it is assumed that the axion potential vanishes at the moment when the strings form and thus, there are no domain walls attached to the axionic strings at the moment of formation.

The point of this section is that the above picture is true only in a small region of the parameter space of scenarios. In general, early cosmology of the θ-vacuum can be dominated by string-wall systems of the QCD condensate and, therefore, can be drastically different. In the following discussion, we will refer to the defects in the early universe as θ-defects, instead of limiting ourselves to Peccei-Quinn strings.

To understand why generic scenarios allow for a different picture in the early universe, let us study the above assumptions of the standard scenario more carefully. The standard assumptions are based on the large hierarchy between the Peccei-Quinn and the QCD scale at the present day

$$\left.\frac{f_\phi}{\Lambda_{\rm QCD}}\right|_{\rm today} \gg 1. \tag{3.106}$$

The assumption now is that one can extrapolate this hierarchy of scales to the post-inflationary epoch, namely that we can use the same scales for when the phase transitions happen in the early cosmology. This hypothesis has been challenged in [115], since it is not supported by any well-established understanding of the early cosmology. To see that this hierarchy can in fact be different, let us explain how gauge couplings and symmetry breaking scales can be affected after inflation using effective field theory.

First, notice that the formation of θ-defects after inflation does not have to correspond directly with the reheating temperature. This is because the phase transition could have taken place non-thermally, through direct interactions with the inflaton field Σ.

Using effective field theory, we expect the potential of the Peccei-Quinn field Φ to depend on couplings to the inflaton (or other fields)

$$\mathcal{U}\left(\frac{\Sigma}{M}\right)\Phi^*\Phi\,, \tag{3.107}$$

where $\mathcal{U}$ is a generic function of Σ and M is a scale. Through such couplings, the VEV of the Peccei-Quinn field depends on Σ. Thus, such couplings to Σ can change the moment in time when the phase transition occurs and also change the tension of the Peccei-Quinn strings.

Let us now focus on the value of the QCD scale during the spontaneous breaking of the axial $U(1)_A$-symmetry, at which the θ-defects form. If the QCD gauge coupling becomes strong during or towards the end of inflation, it produces a potential for $\theta_{\rm eff}$ [115]. The QCD gauge coupling can strongly depend on the inflaton or other fields (which themselves can strongly depend on the inflaton) through effective operators

coupling to the Σ. As a result, the effective coupling strength of QCD can change significantly throughout the (post)inflationary epoch, for example, because of large modifications of the expectation value of the inflaton (and its subsequent decay) or through other fields whose VEVs depends on the inflaton (see e.g. (3.107)). Even if such a field-dependence is not included by tree-level renormalizable operators (which has no a priory justification), we expect them to be generated both by loops and by higher-dimensional operators (for earlier discussions on this topic see [116]).

This situation is common in inflationary scenarios emerging from string theory, such as e.g., brane inflation [117, 118]. In string theory, gauge couplings depend on fields, for example the dilaton. During inflation, these fields become easily displaced because of their interactions with the inflaton. As a result, the values of the gauge couplings are also considerably different from the present day values [115].

The dependence of the QCD gauge coupling on the inflaton can be understood without making any assumptions about the UV structure of the theory: In the effective field theory, we naturally expect the appearance of operators like

$$\mathcal{W}\left(\frac{\Sigma}{M}\right) \mathrm{tr} G_{\mu\nu} G^{\mu\nu} \,, \tag{3.108}$$

where $\mathcal{W}$ is a generic function of Σ and M is a scale. The value of the QCD gauge coupling is set by

$$\frac{1}{g^2} = \mathcal{W}\left(\frac{\Sigma}{M}\right) \,. \tag{3.109}$$

Because of this relation, it is most sensible to expect the gauge coupling to depend on the inflaton, either directly or through other fields. Moreover, it is reasonable to assume the value of the QCD gauge coupling during inflation differed significantly from its current value.

At the moment of symmetry breaking and string formation, the gauge coupling could have been shifted towards stronger or weaker values, depending on the model. The likelihood of realizing an early epoch of strong QCD [115] appears rather high, in view of the large variety and parameter space of inflationary models.

Thus, the hierarchy between f_ϕ and Λ in an early epoch can be drastically different from its present day value (3.106). In fact, it is even possible for the Peccei-Quinn scale to be much smaller than the QCD scale at an early time,

$$\left.\frac{f_\phi}{\Lambda_{\mathrm{QCD}}}\right|_{\mathrm{early}} \ll 1 \,. \tag{3.110}$$

If this is the case, the potential of θ_{eff} is generated at this early epoch and the cosmology of θ-defects is fully dominated by QCD dynamics[3].

[3]This has immediate implication of lifting out the previous cosmological bound on the axion scale, $f_\phi > 10^{12}$ GeV [119–121], since in the scenario of [115], the axion's coherent oscillations start way before the ordinary QCD temperatures. Correspondingly, even for a maximal initial amplitude, the axion energy gets efficiently red-shifted in the early epoch. For more recent implementations of this scenario, see [122] and references therein. CHANGE FOOTNOTE

In particular, a strong early epoch has several important implications: First, the cosmic strings from the spontaneous breaking of the axial $U(1)_A$ (or $U(1)_{PQ}$), either formed by the Peccei-Quinn field or the QCD condensate, are immediately attached to domain walls. More importantly, it is possible that the string dynamics was dominated not by the Peccei-Quinn hidden axion but entirely by the phase of the QCD condensate. If the hierarchy (3.110) was so extreme that, at the moment of quark condensation, the PQ field was still in the symmetric vacuum, $\Phi = 0$, the the quark composites, such as η' or π^0, were the main driving force of the string-wall dynamics.

3.6.1 Pion Strings

So far we have focused mostly on η' defects arising from chiral symmetry breaking. However, if we assume two light quark flavor there can also be defects in the neutral pion π^0 direction. While the η'-strings would always attach to domain walls, the properties of pion strings are more subtle and deserve special attention.

The precise nature of the pion strings depends on the VEV of the Higgs field when the quarks condense. Since the pion strings are pure QCD defects, we do not need a hidden axion to describe them. Thus, we restrict the model to pure SM with a single Higgs field. Since only the neutral component of the Higgs, which we denote by $H = \rho(x)\mathrm{e}^{i\chi(x)}$, is important for this discussion, we leave out the charged component. To understand various regimes, consider the Yukawa couplings of the two flavors of quarks, u and d,

$$g_u H \bar{u}_L u_R + g_d H^* \bar{d}_L d_R + \text{h.c.}. \tag{3.111}$$

For simplicity, we restrict ourselves to only one generation of quarks. There is only one exact chiral symmetry respected by these couplings, which is the local symmetry $U(1)_Z$ gauged by the Z-boson, $Z_\mu \to Z_\mu + \partial_\mu \beta$. Under this $U(1)_Z$, the phases of the Higgs and the quark condensates shift as

$$\chi \to \chi + \beta\,,\ \theta_u \to \theta_u - \beta\,,\ \theta_d \to \theta_d + \beta. \tag{3.112}$$

The Goldstone boson that gets eaten by the Z-boson is the following combination of the phases.

$$v^2\chi - f_u^2\theta_u + f_d^2\theta_d\cdot, \tag{3.113}$$

The ordinary SM vacuum at the present day has a much larger VEV of the Higgs, v, than the absolute value of the quark condensate. Therefore, the longitudinal component of the Z-boson consists mostly of the Higgs phase, with a very small admixture from the phases of the quark condensate. The π^0 is orthogonal to the longitudinal component of the Z-boson and it gets a mass from the Yukawa couplings.

If the early universe is subject to a strong epoch, the story can be very different. In the epoch of early quark condensation, the VEV of the Higgs boson can be smaller than the QCD scale and the quark condensate is the dominant source for electroweak symmetry breaking. The longitudinal component of the Z-boson would be the

neutral pion π^0, with a small admixture from χ. In this case, the phase transition produces local cosmic strings with magnetic Z-boson flux in the core of the string,

$$\text{flux} = \frac{1}{g_z} \frac{v^2 n_\chi - f_u^2\, n_{\theta_u} + f_d^2 n_{\theta_d}}{v^2 + f_u^2 + f_d^2}. \tag{3.114}$$

This flux will be integer around the string because the winding of the phases corresponds to a $U(1)_Z$ transformation from Eq. (3.112). For instance, the string with minimal winding number, so $n_{\theta_u} = -n_{\theta_d} = -n_\chi = \pm 1$, carries a magnetic Z-boson flux flux $= \mp 1/g_z$, whose value is one in units of the inverse gauge coupling.

Such pion strings are very similar to semi-local electroweak strings [123] in many aspects, for example the integer Z-flux. However, the phases that wind around the pion string are the phases of the QCD quark condensate, which is different to the electroweak strings.

Let us also discuss the case in which, at the moment of quark condensation, we have the same hierarchy as today, $v \gg f_u, f_d$. Then, the low-energy theory of π^0 has an approximate global symmetry, under which the Higgs phase χ does not transform. When this symmetry is spontaneously broken, global strings form. The minimal winding around a string corresponding to this global symmetry is $n_{\theta_u} = -n_{\theta_d} = \pm 1$ and $n_\chi = 0$. Since only the phases of the quark condensate wind around the string, the magnetic flux of the Z-boson in the string core is negligible. Because the symmetry is explicitly broken by the quark masses, the strings become boundaries of 2π-domain walls.

A priori, both scenarios are equally possible. Due to interactions with the inflaton and other fields, the QCD gauge coupling can become strong, as described by the effective operator (3.108). At the same time, the VEV of the Higgs can be dynamically changed by interactions with the inflaton of type (3.107). Therefore, the hierarchy between the Higgs VEV and the value of the quark condensate is model-dependent and so is which of the two scenarios is correct.

If such string-wall systems of π^0 or η' are formed in an epoch of early strong QCD [115], their cosmology would be very different from the standard one. For example, their wall tension would be much higher because the value of the quark condensate would have to be much larger. This means that the string-walls would collapse much faster, resulting in intense radiation, including gravitational waves.

The important point about this section is that the string-wall systems of η' and the pion an be the main driving force of the early cosmology of the θ-vacuum.

Because the early QCD scale can be much larger than the explicit breaking of $U(1)_A$ due to the quark masses from the Yukawa couplings, other, heavier mesons than the η could be equally (or more) important for the winding. Actually, in scenarios with $\Lambda_{\rm QCD}/v|_{early} \gg 1$ heavy quarks (those with $m_Q \gtrsim 1$ GeV) might also condense during the phase transition. Then, the number of flavors could be more than $N_f = 3$, and it is possible that there is a much higher number of mesons involved compared to the minimal picture.

3.6.2 Implications for the QCD Phase Transition

We discuss now what implications the string-wall systems of the phases of the quark condensate have on the ordinary, thermal QCD phase transition. In the standard picture, the QCD condensate forms when the inflaton and other heavy VEVs have already settled to their vacua.

Since the order parameter that is responsible for the formation of the strings, $\Lambda_{\rm QCD}$, and the parameter leading to the domain walls, i.e., the explicit breaking proportional to the light quark mass m_ψ, have no significant hierarchy of scales, the formation of the strings and of the walls happens essentially at the same time. When the value of the quark condensate falls into its minimum, the potential is already slightly shifted so that the phase has a well-defined minimum. Thus, when we reach the critical temperature, the value of the quark condensate increases to find a minimum in the radial direction and simultaneously, the phase reaches its minimum.

The phases θ_u, θ_d become well-defined modulo 2π only after the onset of the transition. Thus, at the start of the transition, each phase aquires an initial value and relaxes towards the minimum. As a result, 2π-domain walls can form, where the 2π stands for the change of the phases.

Of course, with a more precise understanding of the phase transition, we can predict the characteristic size of the wall in greater detail. If we apply the intuition coming from previous work on domain walls in weakly-coupled scalar theories [124–126], we expect their size to reach Hubble scale. Since the upper limit on the correlation length is given by the Hubble scale, at larger scales, the walls are bounded by strings.

When those strings attached to the domain walls enter the horizon, which happens soon after their formation because the Hubble scale gradually expands, the walls will collapse. During their collapse, they release energy in the form of hadrons and gravitational waves.

3.7 Implications for Heavy Ion Colliders

From the perspective of the low-energy theory of mesons, the string-wall-systems formed by the QCD condensate describe solitonic states. An important question is if it is possible to observe them in high-energy collisions. In general, when a small number of high-energy quanta collides, the formation of solitons or other non-perturbative states is exponentially suppressed [127–139].

We can think of the formation of a soliton as a $2 \to N$ transition in the S-matrix. A soliton has some characteristic size L and mass $M \gg 1/L$ and, in a weakly interacting theory, can be considered a coherent state. The coherent state consists of constituent quanta with characteristic energy $E \sim 1/L$ and occupation number $N \sim (ML) \gg 1$. Hence, when we collide two particles, so two hard quanta, in a high-energy process, they have to scatter into a state with N soft quanta (of energy $\sim 1/L$). It was shown [138] that the matrix element of such a $2 \to N$ transition is

bounded from above by a factor e^{-N}.

However, if the final state soliton has a maximal microstate degeneracy, it is possible to overcome this suppression. For a coherent bound state with N-particles, the maximal possible degeneracy is proportional to $\sim e^N$ [138]. Those states with maximal degeneracy have maximal microstate entropy $S \sim N$. Examples of states with maximal microstate entropy are certain multi-gluon states called the "color glass condensate" [140]: In [141] it was suggested that such a compensation due to maximal microstate energy takes place for the color glass condensate. Still, for the present work investigating the string-wall solitons of the quark condensate, the degeneracy factor needs to be studied in detail.

As for trying to experimentally produce these defects, heavy ion collision are promising candidates, for example at the LHC [142, 143] and at the RIHC [144, 145]. The size of the solitons produced in heavy ion collisions cannot be much larger than the QCD length. Nevertheless, any chance of experimentally producing string-wall resonances would be of extraordinary importance.

3.8 Comment on the Gauge Axion

The axion can be formulated in an alternative way [98], which is not based on any anomalous global symmtery. Instead, the axion transforms non-trivially under the QCD gauge symmetry, which is why we call it the "gauge axion".

The gluons are the gauge fields of QCD, transforming in the adjoint representation

$$A_\mu \to U(x) A_\mu U^\dagger(x) + U \partial_\mu U^\dagger \text{ with } U(x) \equiv e^{-i\omega(x)^a T^a}, \tag{3.115}$$

Under the same QCD gauge transformation, now also the gauge axion $B_{\mu\nu}$, which is a 2-form, transforms as

$$B_{\mu\nu} \;\to\; B_{\mu\nu} \;+\; \frac{1}{f}\Omega_{\mu\nu}\,, \tag{3.116}$$

where $\Omega_{\mu\nu} = \mathrm{Tr} A_{[\mu}\partial_{\nu]}\omega$ and f is the gauge axion scale.

To form a gauge invariant operator in the Lagrangian, the the gauge axion $B_{\mu\nu}$ partners up with the Chern-Simons 3-form of QCD, $C_{\mu\nu\alpha} \equiv \mathrm{Tr}\left(A_{[\mu}\partial_\nu A_{\alpha]} + \frac{2}{3} A_{[\mu} A_\nu A_{\alpha]}\right)$. Together, they form a unique gauge invariant combination

$$C_{\mu\nu\alpha} - f\partial_{[\mu} B_{\nu\alpha]}. \tag{3.117}$$

This is because the Chern-Simons 3-form transforms under the QCD gauge transformation as

$$C_{\mu\nu\alpha} \to C_{\mu\nu\alpha} + \partial_{[\mu}\Omega_{\nu\alpha]}. \tag{3.118}$$

It can be shown [98, 146] that the gauge axion solves the Strong CP Problem to all orders in the operator expansion because the gauge redundancy of the two-form makes $\bar{\theta}$ unphysical.

At low-energies, the gauge axion is dual to a pseudo-scalar phase, i.e. the axion: They have the same number of degrees of freedom, namely one, and their Lagrangians are related by a dualization procedure. Since their low-energy theories are the same, the previously discussed axionic domain walls also exist in the gauge axion formulation.

However, while the axion is UV-completed into a complex scalar field, the Peccei-Quinn field, this is not the case for the gauge axion [98, 146, 147]. Thus, the structure of cosmic strings of the gauge axion is different and will be discussed in upcoming work [5].

The structure of pure QCD defects such as the η' or π^0 string-wall systems are unrelated to the nature of the axion. For these defects, regardless of the origin of the axion, the previous discussion remains valid.

3.9 Summary and Outlook

In this chapter, we have studied field configurations that involve winding in the phases of the QCD quark condensate. These configurations are 2π-domain walls that are bounded by cosmic strings. Across such domain walls, the phases of the QCD quark condensate, which correspond to the η' or π^0 mesons, change by 2π. We have demonstrated that, if we inlcude a hidden axion to solve the strong CP problem, the topologial defects involving the axion also wind in the phases of the quark condensate.

The simultaneous winding of the axion and the quark condensate phases can change the properties of axionic strings: the structure of fermionic zero modes and the anomaly content on the string, the anomaly inflow and superconductive properties of the string.

The pure QCD string-wall systems, which only involve winding in the phases of the quark condensate, are not contingent on the hidden axion. The string-wall systems of pure QCD form in the QCD phase transition and soon after their formation they collapse during which they send off gravitational waves and electromagnetic radiation. They can even be the dominant topologial defects in early cosmology, if the universe went though a strong epoch of QCD.

The string-wall systems formed by the QCD condensate are solitonic states from the point of view of the low-energy theory of mesons. We discussed the possibility to produce these solitons in heavy ion collisions.

In a future work, we will present numerical results that support the discussed winding configurations of the phases of the quark condensate [6].

Lastly, we point out that it is possibe that there are string-wall structures formed by other fermion condensates from other gauge sectors of the Standard Model or gravity. For example, the string-wall systems of the neutrino condensate [100], which can lead to a neutrino mass [148], have been studied in [149]. These defects form when the neutrino condensate spontaneously breaks the non-abelian neutrino-flavor symmetry.

Furthermore, it would be interesting to investigate the string-wall systems of the η_w, which is a new pseudo-scalar meson in the electroweak sector, whose existance was suggested recently [150].

Chapter 4

Conclusion

In this thesis we have discussed two main topics: neutron oscillations with an extra-dimensional fermion and string-wall systems of the QCD quark condensate. Let us summarize the results of both projects.

In the first part, we have proposed a new way to look for large extra dimensions in low-energy neutron experiments.

The ADD model [7, 8] was first introduced to solve the hierarchy problem. Additionally, it offers a natural way to explain the smallness of the neutrino mass. The right-handed neutrino is a Standard Model singlet and, thus, is a good candidate for an extra-dimensional fermion. Since the interactions of extra-dimensional particles with Standard Model fields are suppressed by the volume of the extra dimensions, also the Dirac mass of the neutrino is suppressed in this way [9, 10].

This motivated us to investigate the interactions of an extra-dimensional fermion with other Standard Model fields. Besides the neutrino, the neutron is also a good candidate to interact with hidden dimensions. This is because the neutron carries no conserved gauge charges and, thus, can serve as a "portal" to the extra dimensions.

We have found that, even though the mixing between the neutron and the bulk fermion is volume suppressed, neutron experiments can put bounds on the parameters of the ADD model. First of all, the disappearance of bound neutrons in nuclei, followed by de-excitation of the nucleus and sending out a hard photon, constrains the parameters of the theory. However, if the bulk fermion has a mass in the extra dimensions which is higher than the bound neutron energy, the bound neutron cannot oscillate away and the bounds are lifted.

If the bulk fermion mass is between the bound and free neutron energy, the free neutron experiments become most constraining. The interesting feature of free neutron experiments is that we can change the neutron energy by a magnetic field. By increasing the magnetic field in small steps over a large range we expect to observe a unique pattern of recurring resonant transitions in the neutron disappearance amplitude. Thus, free neutron experiments offer a new possiblility to perform a scanning of the Kaluza-Klein tower and to put bounds on the parameters of extra dimensions.

Recent experiments are already testing an interesting parameter range of the

theory and, in this way, impose bounds on the parameters of the ADD model. In the future, with a finer scanning and a wider range of the magnetic field, experiments can test a larger parameter space. Thus, free neutron experiments have an exciting opportunity to carry out a spectroscopy of the Kaluza-Klein tower.

In the second project, we have investigated winding configurations of the QCD quark condensate. We found that, during the QCD phase transition, 2π-domain walls bounded by strings of the η' or π^0-mesons are produced. These pure QCD defects are unstable and collapse soon after their formation. In that process, they send out gravitational waves and electromagnetic radiation. If the universe experiences a strong early epoch, the pure QCD defects can even play a dominant role in cosmology.

We also analyzed the topological defects in a coupled system with a hidden axion [12, 13]. When the QCD potential becomes important, axionic strings, that involve winding in the phase of the Peiccei-Quinn field [14, 15], are accompanied by windings in the quark condensate. The simultaneous winding of the phases changes the properties of axionic strings, for example their superconductivity [16] and anomaly inflow properties [17, 18].

Numerical results on the string-wall structures that fully support the presented resuls will be discussed in future work [6].

Bibliography

[1] G. Dvali, M. Ettengruber, and A. Stuhlfauth, "Kaluza-Klein spectroscopy from neutron oscillations into hidden dimensions", Phys. Rev. D **109**, 055046 (2024), arXiv:2312.13278 [hep-ph].

[2] G. Dvali, L. Komisel, and A. Stuhlfauth, "Cosmic strings and domain walls of the QCD quark condensate with and without a hidden axion", (2025), arXiv:2505.03542 [hep-ph].

[3] G. Dvali, O. Sakhelashvili, and A. Stuhlfauth, "TeV Window to Grand Unification: Higgs's Light Color Triplet Partner", (2024), arXiv:2411.14051 [hep-ph].

[4] A. Alexandre, G. Dvali, and A. Stuhlfauth, in progress.

[5] G. Dvali, L. Komisel, and A. Stuhlfauth, in progress.

[6] M. Bachmaier, G. Dvali, L. Komisel, and A. Stuhlfauth, in progress.

[7] N. Arkani-Hamed, S. Dimopoulos, and G. Dvali, "The Hierarchy problem and new dimensions at a millimeter", Phys. Lett. B **429**, 263–272 (1998), arXiv:hep-ph/9803315.

[8] N. Arkani-Hamed, S. Dimopoulos, and G. Dvali, "Phenomenology, astrophysics and cosmology of theories with submillimeter dimensions and TeV scale quantum gravity", Phys. Rev. D **59**, 086004 (1999), arXiv:hep-ph/9807344.

[9] N. Arkani-Hamed, S. Dimopoulos, G. R. Dvali, and J. March-Russell, "Neutrino masses from large extra dimensions", Phys. Rev. D **65**, 024032 (2001), arXiv:hep-ph/9811448.

[10] G. Dvali and A. Y. Smirnov, "Probing large extra dimensions with neutrinos", Nucl. Phys. B **563**, 63–81 (1999), arXiv:hep-ph/9904211.

[11] G. Ban et al., "Search for Neutron-to-Hidden-Neutron Oscillations in an Ultracold Neutron Beam", Phys. Rev. Lett. **131**, 191801 (2023), arXiv:2303.10507 [hep-ph].

[12] S. Weinberg, "A New Light Boson?", Phys. Rev. Lett. **40**, 223–226 (1978).

[13] F. Wilczek, "Problem of Strong P and T Invariance in the Presence of Instantons", Phys. Rev. Lett. **40**, 279–282 (1978).

[14] R. D. Peccei and H. R. Quinn, "CP Conservation in the Presence of Instantons", Phys. Rev. Lett. **38**, 1440–1443 (1977).

[15] R. D. Peccei and H. R. Quinn, "Constraints Imposed by CP Conservation in the Presence of Instantons", Phys. Rev. D **16**, 1791–1797 (1977).

[16] E. Witten, "Superconducting Strings", Nucl. Phys. B **249**, 557–592 (1985).

[17] C. G. Callan Jr. and J. A. Harvey, "Anomalies and Fermion Zero Modes on Strings and Domain Walls", Nucl. Phys. B **250**, 427–436 (1985).

[18] G. Lazarides and Q. Shafi, "Superconducting Strings in Axion Models", Phys. Lett. B **151**, 123–126 (1985).

[19] E. G. Adelberger, J. H. Gundlach, B. R. Heckel, S. Hoedl, and S. Schlamminger, "Torsion balance experiments: A low-energy frontier of particle physics", Prog. Part. Nucl. Phys. **62**, 102–134 (2009).

[20] J. G. Lee, E. G. Adelberger, T. S. Cook, S. M. Fleischer, and B. R. Heckel, "New Test of the Gravitational $1/r^2$ Law at Separations down to 52 μm", Phys. Rev. Lett. **124**, 101101 (2020), arXiv:2002.11761 [hep-ex].

[21] W.-H. Tan, S.-Q. Yang, C.-G. Shao, J. Li, A.-B. Du, B.-F. Zhan, Q.-L. Wang, P.-S. Luo, L.-C. Tu, and J. Luo, "New Test of the Gravitational Inverse-Square Law at the Submillimeter Range with Dual Modulation and Compensation", Phys. Rev. Lett. **116**, 131101 (2016).

[22] G. Dvali and M. A. Shifman, "Domain walls in strongly coupled theories", Phys. Lett. B **396**, [Erratum: Phys.Lett.B 407, 452 (1997)], 64–69 (1997), arXiv:hep-th/9612128.

[23] G. Aad et al., "Search for new phenomena in events with an energetic jet and missing transverse momentum in pp collisions at $\sqrt{s}$ =13 TeV with the ATLAS detector", Phys. Rev. D **103**, 112006 (2021), arXiv:2102.10874 [hep-ex].

[24] A. Tumasyan et al., "Search for new particles in events with energetic jets and large missing transverse momentum in proton-proton collisions at $\sqrt{s}$ = 13 TeV", JHEP **11**, 153 (2021), arXiv:2107.13021 [hep-ex].

[25] T. Kaluza, "Zum Unitätsproblem der Physik", Sitzungsber. Preuss. Akad. Wiss. Berlin (Math. Phys.) **1921**, 966–972 (1921), arXiv:1803.08616 [physics.hist-ph].

[26] O. Klein, "Quantum Theory and Five-Dimensional Theory of Relativity. (In German and English)", Z. Phys. **37**, edited by J. C. Taylor, 895–906 (1926).

[27] K. R. Dienes, E. Dudas, and T. Gherghetta, "Neutrino oscillations without neutrino masses or heavy mass scales: A Higher dimensional seesaw mechanism", Nucl. Phys. B **557**, 25 (1999), arXiv:hep-ph/9811428.

[28] G. Dvali and G. Gabadadze, "Nonconservation of global charges in the brane universe and baryogenesis", Phys. Lett. B **460**, 47–57 (1999), arXiv:hep-ph/9904221.

[29] I. Antoniadis, N. Arkani-Hamed, S. Dimopoulos, and G. Dvali, "New dimensions at a millimeter to a Fermi and superstrings at a TeV", Phys. Lett. B **436**, 257–263 (1998), arXiv:hep-ph/9804398.

[30] R. Jackiw and C. Rebbi, "Solitons with Fermion Number 1/2", Phys. Rev. D **13**, 3398–3409 (1976).

[31] R. Jackiw and P. Rossi, "Zero Modes of the Vortex - Fermion System", Nucl. Phys. B **190**, 681–691 (1981).

[32] E. J. Weinberg, "Index Calculations for the Fermion-Vortex System", Phys. Rev. D **24**, 2669 (1981).

[33] I. Antoniadis, "A Possible new dimension at a few TeV", Phys. Lett. B **246**, 377–384 (1990).

[34] V. A. Rubakov and M. E. Shaposhnikov, "Do We Live Inside a Domain Wall?", Phys. Lett. B **125**, 136–138 (1983).

[35] M. Shifman, "Large Extra Dimensions: Becoming acquainted with an alternative paradigm", Int. J. Mod. Phys. A **25**, edited by M. Peloso and A. Vainshtein, 199–225 (2010), arXiv:0907.3074 [hep-ph].

[36] G. Dvali and M. Redi, "Phenomenology of 10^{32} Dark Sectors", Phys. Rev. D **80**, 055001 (2009), arXiv:0905.1709 [hep-ph].

[37] G. Dvali, "Black Holes and Large N Species Solution to the Hierarchy Problem", Fortsch. Phys. **58**, 528–536 (2010), arXiv:0706.2050 [hep-th].

[38] G. Dvali and M. Redi, "Black Hole Bound on the Number of Species and Quantum Gravity at LHC", Phys. Rev. D **77**, 045027 (2008), arXiv:0710.4344 [hep-th].

[39] S. Hannestad and G. Raffelt, "New supernova limit on large extra dimensions", Phys. Rev. Lett. **87**, 051301 (2001), arXiv:hep-ph/0103201.

[40] N. Arkani-Hamed, S. Dimopoulos, and J. March-Russell, "Stabilization of submillimeter dimensions: The New guise of the hierarchy problem", Phys. Rev. D **63**, 064020 (2001), arXiv:hep-th/9809124.

[41] G. F. Giudice, R. Rattazzi, and J. D. Wells, "Quantum gravity and extra dimensions at high-energy colliders", Nucl. Phys. B **544**, 3–38 (1999), arXiv:hep-ph/9811291.

[42] T. Han, J. D. Lykken, and R.-J. Zhang, "On Kaluza-Klein states from large extra dimensions", Phys. Rev. D **59**, 105006 (1999), arXiv:hep-ph/9811350.

[43] J. L. Hewett, "Indirect collider signals for extra dimensions", Phys. Rev. Lett. **82**, 4765–4768 (1999), arXiv:hep-ph/9811356.

[44] S. B. Giddings and S. D. Thomas, "High-energy colliders as black hole factories: The End of short distance physics", Phys. Rev. D **65**, 056010 (2002), arXiv:hep-ph/0106219.

[45] S. Dimopoulos and G. L. Landsberg, "Black holes at the LHC", Phys. Rev. Lett. **87**, 161602 (2001), arXiv:hep-ph/0106295.

[46] G. Hardy, E. Wright, D. Heath-Brown, and J. Silverman, *An introduction to the theory of numbers*, Oxford mathematics (OUP Oxford, 2008).

[47] M. D. Schwartz, *Quantum Field Theory and the Standard Model* (Cambridge University Press, Mar. 2014).

[48] S. Weinberg, *The Quantum theory of fields. Vol. 1: Foundations* (Cambridge University Press, June 2005).

[49] F. Wilczek and A. Zee, "Families from Spinors", Phys. Rev. D **25**, 553 (1982).

[50] A. Zee, *Group Theory in a Nutshell for Physicists* (Princeton University Press, USA, Mar. 2016).

[51] P. A. N. Machado, H. Nunokawa, and R. Zukanovich Funchal, "Testing for Large Extra Dimensions with Neutrino Oscillations", Phys. Rev. D **84**, 013003 (2011), arXiv:1101.0003 [hep-ph].

[52] D. V. Forero, C. Giunti, C. A. Ternes, and O. Tyagi, "Large extra dimensions and neutrino experiments", Phys. Rev. D **106**, 035027 (2022), arXiv:2207.02790 [hep-ph].

[53] T. Araki et al., "Search for the invisible decay of neutrons with KamLAND", Phys. Rev. Lett. **96**, 101802 (2006), arXiv:hep-ex/0512059.

[54] E. Tiesinga, P. J. Mohr, D. B. Newell, and B. N. Taylor, "CODATA recommended values of the fundamental physical constants: 2018*", Rev. Mod. Phys. **93**, 025010 (2021).

[55] C. Abel et al., "A search for neutron to mirror-neutron oscillations using the nEDM apparatus at PSI", Phys. Lett. B **812**, 135993 (2021), arXiv:2009.11046 [hep-ph].

[56] M. Ettengruber, "Neutrino physics in TeV scale gravity theories", Phys. Rev. D **106**, 055028 (2022), arXiv:2206.00034 [hep-ph].

[57] G. Dvali, I. Sawicki, and A. Vikman, "Dark Matter via Many Copies of the Standard Model", JCAP **08**, 009 (2009), arXiv:0903.0660 [hep-th].

[58] N. Arkani-Hamed, S. Dimopoulos, G. Dvali, and N. Kaloper, "Many fold universe", JHEP **12**, 010 (2000), arXiv:hep-ph/9911386.

[59] Z. Berezhiani and L. Bento, "Neutron - mirror neutron oscillations: How fast might they be?", Phys. Rev. Lett. **96**, 081801 (2006), arXiv:hep-ph/0507031.

[60] Z. Berezhiani, "More about neutron - mirror neutron oscillation", Eur. Phys. J. C **64**, 421–431 (2009), arXiv:0804.2088 [hep-ph].

[61] R. L. Workman et al., "Review of Particle Physics", PTEP **2022**, 083C01 (2022).

[62] F. M. Gonzalez et al., "Improved neutron lifetime measurement with UCNτ", Phys. Rev. Lett. **127**, 162501 (2021), arXiv:2106.10375 [nucl-ex].

[63] V. F. Ezhov et al., "Measurement of the neutron lifetime with ultra-cold neutrons stored in a magneto-gravitational trap", JETP Lett. **107**, 671–675 (2018), arXiv:1412.7434 [nucl-ex].

[64] A. T. Yue, M. S. Dewey, D. M. Gilliam, G. L. Greene, A. B. Laptev, J. S. Nico, W. M. Snow, and F. E. Wietfeldt, "Improved Determination of the Neutron Lifetime", Phys. Rev. Lett. **111**, 222501 (2013), arXiv:1309.2623 [nucl-ex].

[65] Z. Berezhiani, "Neutron lifetime puzzle and neutron–mirror neutron oscillation", Eur. Phys. J. C **79**, 484 (2019), arXiv:1807.07906 [hep-ph].

[66] W. Tan, "Neutron oscillations for solving neutron lifetime and dark matter puzzles", Phys. Lett. B **797**, 134921 (2019), arXiv:1902.01837 [physics.gen-ph].

[67] B. Fornal and B. Grinstein, "Dark Matter Interpretation of the Neutron Decay Anomaly", Phys. Rev. Lett. **120**, [Erratum: Phys.Rev.Lett. 124, 219901 (2020)], 191801 (2018), arXiv:1801.01124 [hep-ph].

[68] G. K. Karananas and A. Kassiteridis, "Small-scale structure from neutron dark decay", JCAP **09**, 036 (2018), arXiv:1805.03656 [hep-ph].

[69] A. Czarnecki, W. J. Marciano, and A. Sirlin, "Neutron Lifetime and Axial Coupling Connection", Phys. Rev. Lett. **120**, 202002 (2018), arXiv:1802.01804 [hep-ph].

[70] E. Gonzalo, M. Montero, G. Obied, and C. Vafa, "Dark dimension gravitons as dark matter", JHEP **11**, 109 (2023), arXiv:2209.09249 [hep-ph].

[71] E. Koutsangelas, "How the axion paves the way beyond the standard model", PhD thesis (Munich U., 2023).

[72] A. Hook, "TASI Lectures on the Strong CP Problem and Axions", PoS **TASI2018**, 004 (2019), arXiv:1812.02669 [hep-ph].

[73] M. Srednicki, *Quantum field theory* (Cambridge University Press, Jan. 2007).

[74] M. Shifman, *Advanced topics in quantum field theory.: A lecture course* (Cambridge Univ. Press, Cambridge, UK, Feb. 2012).

[75] S. Weinberg, "The U(1) Problem", Phys. Rev. D **11**, 3583–3593 (1975).

[76] S. L. Adler, "Axial vector vertex in spinor electrodynamics", Phys. Rev. **177**, 2426–2438 (1969).

[77] J. S. Bell and R. Jackiw, "A PCAC puzzle: $\pi^0 \to \gamma\gamma$ in the σ model", Nuovo Cim. A **60**, 47–61 (1969).

[78] W. A. Bardeen, "Anomalous Ward identities in spinor field theories", Phys. Rev. **184**, 1848–1857 (1969).

[79] G. 't Hooft, "Symmetry Breaking Through Bell-Jackiw Anomalies", Phys. Rev. Lett. **37**, edited by M. A. Shifman, 8–11 (1976).

[80] G. 't Hooft, "Computation of the Quantum Effects Due to a Four-Dimensional Pseudoparticle", Phys. Rev. D **14**, edited by M. A. Shifman, [Erratum: Phys.Rev.D 18, 2199 (1978)], 3432–3450 (1976).

[81] G. 't Hooft, "How Instantons Solve the U(1) Problem", Phys. Rept. **142**, 357–387 (1986).

[82] A. A. Belavin, A. M. Polyakov, A. S. Schwartz, and Y. S. Tyupkin, "Pseudoparticle Solutions of the Yang-Mills Equations", Phys. Lett. B **59**, edited by J. C. Taylor, 85–87 (1975).

[83] C. G. Callan Jr., R. F. Dashen, and D. J. Gross, "The Structure of the Gauge Theory Vacuum", Phys. Lett. B **63**, edited by J. C. Taylor, 334–340 (1976).

[84] R. Jackiw and C. Rebbi, "Vacuum Periodicity in a Yang-Mills Quantum Theory", Phys. Rev. Lett. **37**, edited by J. C. Taylor, 172–175 (1976).

[85] C. Vafa and E. Witten, "Parity Conservation in QCD", Phys. Rev. Lett. **53**, 535 (1984).

[86] V. Baluni, "CP Violating Effects in QCD", Phys. Rev. D **19**, 2227–2230 (1979).

[87] R. J. Crewther, P. Di Vecchia, G. Veneziano, and E. Witten, "Chiral Estimate of the Electric Dipole Moment of the Neutron in Quantum Chromodynamics", Phys. Lett. B **88**, [Erratum: Phys.Lett.B 91, 487 (1980)], 123 (1979).

[88] C. A. Baker et al., "An Improved experimental limit on the electric dipole moment of the neutron", Phys. Rev. Lett. **97**, 131801 (2006), arXiv:hep-ex/0602020.

[89] J. M. Pendlebury et al., "Revised experimental upper limit on the electric dipole moment of the neutron", Phys. Rev. D **92**, 092003 (2015), arXiv:1509.04411 [hep-ex].

[90] B. Graner, Y. Chen, E. G. Lindahl, and B. R. Heckel, "Reduced Limit on the Permanent Electric Dipole Moment of Hg199", Phys. Rev. Lett. **116**, [Erratum: Phys.Rev.Lett. 119, 119901 (2017)], 161601 (2016), arXiv:1601.04339 [physics.atom-ph].

[91] J. R. Ellis, M. K. Gaillard, and D. V. Nanopoulos, "Lefthanded Currents and CP Violation", Nucl. Phys. B **109**, 213–243 (1976).

[92] E. P. Shabalin, "Electric Dipole Moment of Quark in a Gauge Theory with Left-Handed Currents", Sov. J. Nucl. Phys. **28**, 75 (1978).

[93] J. R. Ellis and M. K. Gaillard, "Strong and Weak CP Violation", Nucl. Phys. B **150**, 141–162 (1979).

[94] J. E. Kim, "Weak Interaction Singlet and Strong CP Invariance", Phys. Rev. Lett. **43**, 103 (1979).

[95] M. A. Shifman, A. I. Vainshtein, and V. I. Zakharov, "Can Confinement Ensure Natural CP Invariance of Strong Interactions?", Nucl. Phys. B **166**, 493–506 (1980).

[96] M. Dine, W. Fischler, and M. Srednicki, "A Simple Solution to the Strong CP Problem with a Harmless Axion", Phys. Lett. B **104**, 199–202 (1981).

[97] A. R. Zhitnitsky, "On Possible Suppression of the Axion Hadron Interactions. (In Russian)", Sov. J. Nucl. Phys. **31**, 260 (1980).

[98] G. Dvali, "Three-form gauging of axion symmetries and gravity", (2005), arXiv:hep-th/0507215.

[99] G. Dvali, R. Jackiw, and S.-Y. Pi, "Topological mass generation in four dimensions", Phys. Rev. Lett. **96**, 081602 (2006), arXiv:hep-th/0511175.

[100] G. Dvali, S. Folkerts, and A. Franca, "How neutrino protects the axion", Phys. Rev. D **89**, 105025 (2014), arXiv:1312.7273 [hep-th].

[101] Y. Aoki et al., "FLAG Review 2024", (2024), arXiv:2411.04268 [hep-lat].

[102] A. Vilenkin and E. P. S. Shellard, *Cosmic Strings and Other Topological Defects* (Cambridge University Press, July 2000).

[103] P. Sikivie, "Of Axions, Domain Walls and the Early Universe", Phys. Rev. Lett. **48**, 1156–1159 (1982).

[104] J. P. Ostriker, A. C. Thompson, and E. Witten, "Cosmological Effects of Superconducting Strings", Phys. Lett. B **180**, 231–239 (1986).

[105] S. G. Naculich, "Axionic Strings: Covariant Anomalies and Bosonization of Chiral Zero Modes", Nucl. Phys. B **296**, 837–867 (1988).

[106] J. A. Harvey and O. Ruchayskiy, "The Local structure of anomaly inflow", JHEP **06**, 044 (2001), arXiv:hep-th/0007037.

[107] P. Agrawal, A. Hook, J. Huang, and G. Marques-Tavares, "Axion string signatures: a cosmological plasma collider", JHEP **01**, 103 (2022), arXiv:2010.15848 [hep-ph].

[108] P. Agrawal, A. Hook, and J. Huang, "A CMB Millikan experiment with cosmic axiverse strings", JHEP **07**, 138 (2020), arXiv:1912.02823 [astro-ph.CO].

[109] H. Fukuda, A. V. Manohar, H. Murayama, and O. Telem, "Axion strings are superconducting", JHEP **06**, 052 (2021), arXiv:2010.02763 [hep-ph].

[110] H. Bagherian, K. Fraser, S. Homiller, and J. Stout, "Zero modes of massive fermions delocalize from axion strings", JHEP **05**, 079 (2024), arXiv:2310.01476 [hep-th].

[111] G. R. Dvali and G. Senjanovic, "Topologically stable electroweak flux tubes", Phys. Rev. Lett. **71**, 2376–2379 (1993), arXiv:hep-ph/9305278.

[112] E. Witten, "Branes and the dynamics of QCD", Nucl. Phys. B **507**, 658–690 (1997), arXiv:hep-th/9706109.

[113] G. R. Dvali and Z. Kakushadze, "Large N domain walls as D-branes for N=1 QCD string", Nucl. Phys. B **537**, 297–316 (1999), arXiv:hep-th/9807140.

[114] G. R. Dvali, G. Gabadadze, and Z. Kakushadze, "BPS domain walls in large N supersymmetric QCD", Nucl. Phys. B **562**, 158–180 (1999), arXiv:hep-th/9901032.

[115] G. R. Dvali, "Removing the cosmological bound on the axion scale", (1995), arXiv:hep-ph/9505253.

[116] G. R. Dvali, "Inflation induced SUSY breaking and flat vacuum directions", Phys. Lett. B **355**, 78–84 (1995), arXiv:hep-ph/9503375.

[117] G. R. Dvali and S. H. H. Tye, "Brane inflation", Phys. Lett. B **450**, 72–82 (1999), arXiv:hep-ph/9812483.

[118] G. R. Dvali, Q. Shafi, and S. Solganik, "D-brane inflation", in 4th European Meeting From the Planck Scale to the Electroweak Scale (May 2001), arXiv:hep-th/0105203.

[119] J. Preskill, M. B. Wise, and F. Wilczek, "Cosmology of the Invisible Axion", Phys. Lett. B **120**, edited by M. A. Srednicki, 127–132 (1983).

[120] M. Dine and W. Fischler, "The Not So Harmless Axion", Phys. Lett. B **120**, edited by M. A. Srednicki, 137–141 (1983).

[121] L. F. Abbott and P. Sikivie, "A Cosmological Bound on the Invisible Axion", Phys. Lett. B **120**, edited by M. A. Srednicki, 133–136 (1983).

[122] E. Koutsangelas, "Removing the cosmological bound on the axion scale in the Kim-Shifman-Vainshtein-Zakharov and Dine-Fischler-Srednicki-Zhitnitsky models", Phys. Rev. D **107**, 095009 (2023), arXiv:2212.07822 [hep-ph].

[123] A. Achucarro and T. Vachaspati, "Semilocal and electroweak strings", Phys. Rept. **327**, 347–426 (2000), arXiv:hep-ph/9904229.

[124] A. Vilenkin and A. E. Everett, "Cosmic Strings and Domain Walls in Models with Goldstone and PseudoGoldstone Bosons", Phys. Rev. Lett. **48**, 1867–1870 (1982).

[125] W. H. Press, B. S. Ryden, and D. N. Spergel, "Dynamical Evolution of Domain Walls in an Expanding Universe", Astrophys. J. **347**, 590–604 (1989).

[126] A. M. M. Leite and C. J. A. P. Martins, "Scaling Properties of Domain Wall Networks", Phys. Rev. D **84**, 103523 (2011), arXiv:1110.3486 [hep-ph].

[127] L. S. Brown, "Summing tree graphs at threshold", Phys. Rev. D **46**, R4125–R4127 (1992), arXiv:hep-ph/9209203.

[128] M. B. Voloshin, "Estimate of the onset of nonperturbative particle production at high-energy in a scalar theory", Phys. Lett. B **293**, 389–394 (1992).

[129] E. N. Argyres, R. H. P. Kleiss, and C. G. Papadopoulos, "Amplitude estimates for multi - Higgs production at high-energies", Nucl. Phys. B **391**, 42–56 (1993).

[130] A. S. Gorsky and M. B. Voloshin, "Nonperturbative production of multiboson states and quantum bubbles", Phys. Rev. D **48**, 3843–3851 (1993), arXiv:hep-ph/9305219.

[131] M. V. Libanov, V. A. Rubakov, D. T. Son, and S. V. Troitsky, "Exponentiation of multiparticle amplitudes in scalar theories", Phys. Rev. D **50**, 7553–7569 (1994), arXiv:hep-ph/9407381.

[132] M. V. Libanov, D. T. Son, and S. V. Troitsky, "Exponentiation of multiparticle amplitudes in scalar theories. 2. Universality of the exponent", Phys. Rev. D **52**, 3679–3687 (1995), arXiv:hep-ph/9503412.

[133] D. T. Son, "Semiclassical approach for multiparticle production in scalar theories", Nucl. Phys. B **477**, 378–406 (1996), arXiv:hep-ph/9505338.

[134] G. Dvali, C. Gomez, R. S. Isermann, D. Lüst, and S. Stieberger, "Black hole formation and classicalization in ultra-Planckian 2→N scattering", Nucl. Phys. B **893**, 187–235 (2015), arXiv:1409.7405 [hep-th].

[135] A. Addazi, M. Bianchi, and G. Veneziano, "Glimpses of black hole formation/evaporation in highly inelastic, ultra-planckian string collisions", JHEP **02**, 111 (2017), arXiv:1611.03643 [hep-th].

[136] G. Dvali, "Classicalization Clearly: Quantum Transition into States of Maximal Memory Storage Capacity", (2018), arXiv:1804.06154 [hep-th].

[137] A. Monin, "Inconsistencies of higgsplosion", (2018), arXiv:1808.05810 [hep-th].

[138] G. Dvali, "Entropy Bound and Unitarity of Scattering Amplitudes", JHEP **03**, 126 (2021), arXiv:2003.05546 [hep-th].

[139] G. Dvali and L. Eisemann, "Perturbative understanding of nonperturbative processes and quantumization versus classicalization", Phys. Rev. D **106**, 125019 (2022), arXiv:2211.02618 [hep-th].

[140] F. Gelis, E. Iancu, J. Jalilian-Marian, and R. Venugopalan, "The Color Glass Condensate", Ann. Rev. Nucl. Part. Sci. **60**, 463–489 (2010), arXiv:1002.0333 [hep-ph].

[141] G. Dvali and R. Venugopalan, "Classicalization and unitarization of wee partons in QCD and gravity: The CGC-black hole correspondence", Phys. Rev. D **105**, 056026 (2022), arXiv:2106.11989 [hep-th].

[142] G. Aad et al., "The ATLAS Experiment at the CERN Large Hadron Collider", JINST **3**, S08003 (2008).

[143] K. Aamodt et al., "The ALICE experiment at the CERN LHC", JINST **3**, S08002 (2008).

[144] M. Harrison, T. Ludlam, and S. Ozaki, "RHIC project overview", Nucl. Instrum. Meth. A **499**, 235–244 (2003).

[145] S. Ozaki, "The Relativistic heavy ion collider at Brookhaven", Nucl. Phys. A **525**, edited by J. P. Blaizot, C. Gerschel, B. Pire, and A. Romana, 125C–132C (1991).

[146] G. Dvali, "Strong-CP with and without gravity", (2022), arXiv:2209.14219 [hep-ph].

[147] O. Sakhelashvili, "Consistency of the dual formulation of axion solutions to the strong CP problem", Phys. Rev. D **105**, 085020 (2022), arXiv:2110.03386 [hep-th].

[148] G. Dvali and L. Funcke, "Small neutrino masses from gravitational θ-term", Phys. Rev. D **93**, 113002 (2016), arXiv:1602.03191 [hep-ph].

[149] G. Dvali, L. Funcke, and T. Vachaspati, "Time- and Space-Varying Neutrino Mass Matrix from Soft Topological Defects", Phys. Rev. Lett. **130**, 091601 (2023), arXiv:2112.02107 [hep-ph].

[150] G. Dvali, A. Kobakhidze, and O. Sakhelashvili, "Electroweak ηw meson", Phys. Rev. D **111**, 113002 (2025), arXiv:2408.07535 [hep-th].

Acknowledgments

There are many people whose support was crucial for the completion of this thesis.

First of all, I would like to thank Gia Dvali for giving me the opportunity to work with him and his outstanding group. Because of him, I had the chance to explore so many different topics in particle physics and cosmology.

I also want to thank my collaborators Gia Dvali, Manuel Ettengruber, Lucy Komisel and Otari Sakhelashvili.

I want to send out a special thanks to Otari Sakhelashvili for supervising my Master's thesis and, from that point on, for patiently answering the many questions I had.

It is a pleasure to thank my fellow (past and current) PhD students of the group, Ana Alexandre, Maximilian Bachmaier, Philipp Bakauov, Giordano Cintia, Giacomo Contri, Manuel Ettengruber, Anna Jankowsky, Lucy Komisel, Emmanouil Koutsangelas, Juan Sebastian Valbuena Bermudez, Tong Zhang. Our discussions have made the past 3 years an absolute blast.

I would also like to thank Lasha Berezhiani, Lucy Komisel and Giacomo Contri for proofreading my thesis.

I am grateful to Gia Dvali, Goran Senjanovic and Lasha Berezhiani for writing reference letters for my postdoc applications.

Many thanks go out to the Max Planck Institute for Physics and especially Frank Steffen for the great PhD program.

I am grateful to Allen Caldwell, Jan von Delft and Georg Raffelt for agreeing to be part of my doctoral committee. I would also like to thank Goran Senjanovic for being part of my adivsory panel.

I would like to thank Ali-Dzhan Ali who I was lucky to co-supervise as my first Master student.

I also would like to thank Gonzalo Villa for discussions on dimensional reduction of spinors.

I want to thank my family and friends for all their support. I am grateful for having a big brother who was my role model when I was young. I want to thank my dad for always being there for me and mom for supporting my interest in science since when I was young.

Most importantly, I would like to thank my wonderful husband. I cannot express in words how grateful I am for his endless support during these last years.